Assembly, characterization and evaluation of a 3rd generation nanoparticle based drug carrier for metastatic breast cancer treatment

Wei Huang

Dissertation submitted to the faculty of Virginia Polytechnic Institute and State University in partial fulfillment of the requirements for the degree of

Doctorate of Philosophy

In

Biological Systems Engineering

Chenming Zhang, Chair

Xiangjin Meng

Ryan S. Senger

Harry C. Dorn

Iuliana Lazar

May 07, 2013

Blacksburg, VA

Keywords: metastatic breast cancer, nanohorn, immunoliposome, nanoparticle based drug carrier, double controlled release

Abstract

Cancer is one of the leading causes of death in the world. For women in the U.S. and the European countries, breast cancer is the most common type and it continuously threatens the lives of the patients and causes huge economic losses. Chemotherapy and endocrine therapy are the common treatments for recurrence prevention and metastatic cancer symptom palliation. However, the uses of these therapies are meanwhile largely limited because their toxic side effects and non-specificity usually lead to low quality lives of the patients. Low aqueous solubility, multi-drug resistance, degradation of drug, limited intra-tumor diffusion and etc. are other limitations of conventional chemotherapies and endocrine therapies.

Nanoparticle based drug carriers were extensively studied for therapeutic drug delivery. Many carriers could be loaded with high dose of hydrophobic and hydrophilic drugs, protect the drug from the surrounding *in vivo* environment during the transportation, specifically target and enter the tumor cells and slowly release the drug thereafter. Advanced nanoparticle drug carriers are studied driven by the need of a more efficient drug delivery. The 3rd generation of nanoparticle based drug carriers are recently developed. They usually consist of more than one type of nanoparticles. Different part of the particle has more specialized functions. Therefore, by carefully selecting from the conventional nanoparticle carriers, a 3rd generation particle could have the properties such as high loading capacity of multiple drugs, prolonged half-life in circulation, higher tendency of accumulating at the tumor site, improved specificity to the tumor cells, higher cell uptake rate and accurately triggered controlled release, and combination of the above-mentioned properties.

In our study, a paclitaxel loaded nanoparticle supported immunoliposome was assembled for metastatic breast cancer drug delivery. Functionalized single walled carbon nanohorn or

poly(lactic-co-glycolic acid) was encapsulated in the polyethylene glycol (PEG) coated liposome for high drug loading and controlled release. Anti-Her2 antibody or Herceptin® was grafted onto the surface of the liposome for a higher affinity to the Her2 overexpressing breast cancer cells.

Firstly, the conjugation of protein to the surface of liposome and PEGylated liposomes were investigated. Proteins with or without membrane binding domain were conjugated to liposome and PEGylated liposomes through covalent and non-covalent binding for comparison. A modified enzyme-linked immune sorbent assay was developed for surface grafted protein quantification.

Secondly, the encapsulation of solid nanoparticle into PEGylated immunoliposome was investigated. Results showed a new structure of solid nanoparticle in PEGylated immunoliposome at a 1:1 ratio was formed during the repeated freeze-thawing process. Supported immunoliposomes with high homogeneity in size and structure were purified by sucrose density gradient centrifugation.

Thirdly, the drug loading, triggered release, cell binding, cell uptake and cell toxicities of the supported immunoliposome were studied. Release results showed a minimum drug leakage in serum at body temperature from the particle. The release was initiated with a minor burst trigged by low pH inside the tumor cell and followed with a long term linear pattern. Cell assay results showed the highest binding affinity of the antibody or Herceptin® grafted nanoparticles to Her2 overexpressing cell lines and a lysosomal intracellular distribution of the endocytosised particles.

In the final study, a fabrication process for polymeric material nanoparticles was established. The process was capable of providing accurate control of the particle size with significant

high output rates, thus largely extends the scope of materials for supporting the immunoliposome.

Dedication

I dedicated this dissertation to my parents, Xiaohua Huang and Aiyun Liu.

Acknowledgements

I would like to give my greatest thanks to my advisor, Dr. Chenming Zhang, for the generous support on all my research work, for the enlightening guidance on becoming a better researcher and writer, and for setting up a perfect model for all his students on how to be a strong, confident man with love.

I am grateful for my committee members, Dr. X.J. Meng, Dr. Harry C. Dorn, Dr. Ryan S. Senger, and Dr. Iuliana Lazar for their kind guidance and support.

I give my special thanks to Xiaoling Wang. Thank you for being here when I needed you the most. Thank you for your best support and company during 2008 to 2012 as my wife.

I enjoyed all the days working with my colleagues, Dr. Jianzhong Hu, Dr. Somayesadat Badieyan, Andrew Fulton, Carolyn Hey, Dr. Chong Liu, Dr. Hong Zheng, Yun Hu and Ambika M.V. Murthy. I am thankful for the help provided by Amy Egan, Teresa Cox, Susan Rosebrough, Barbara Wills, Denton Yoder and Ling Li.

I am grateful for all the assistances kindly provided by Kathy Lowe and Melissa Makris on transmission electronic microscopes and flow cytometer.

TABLE OF CONTENTS

List of Figures

List of Tables

Chapter I: Introduction

Cancer is one of the top leading causes of death that continuously threatens the life of the patients and causes huge economic losses all over the world. In the U.S., cancer is the second leading cause of death only after heart disease. Due to the huge population and the high cancer incidence rate, the U.S. was reported to have the world's highest cancer death count per year [1].

Breast, lung, colorectal and prostate cancer were categorized as the four major types of all since they constitute for over half of the newly diagnosed cases [1]. For women in the U.S., breast cancer has led to the second most cancer death counts after lung cancer [2]. In 2006, 212,920 women in the U.S. were diagnosed to carry breast cancer and 40,000 is the estimated yearly death rate [3-5]. The total annual spending on initial treatment of metastatic breast cancer is estimated to be $370 million nationwide, with a per-person cost of $28,000 [6].

Although many risk factors for breast cancer such as family history, carcinogens, smoking, certain virus infections and lack of DNA repair have been identified, direct causes of the disease are still unclear. Treatment of the disease is relying on surgery, radiation therapy, endocrine therapy and chemotherapy used in combinations depending on the metastatic stage. Early diagnosis is the key for a successful first-line treatment. A tumor is initially formed in the duct or lobules, of groups of mutated immortal cells [7]. It is detectable by self-body examine and mammogram. Local treatments such as surgery and radiation therapy are used at this stage at the tumor site. Some tumor cells have the ability to detach from the original tumor and intravasate into the surrounding tumor blood vessels [8,9]. These cells would spread through the circulation, incubate and start new tumors at other locations. Systematic

treatments such as endocrine therapy and chemotherapy that have better global effect are used to inhibit the growth of these mobilized tumor cells.

So far, the elimination and treatment of recurrence are relying on endocrine therapy and chemotherapy. The therapy agents attack rapid dividing cells by interfering with DNA replication and transcription, interrupting incoming signals that can promote the proliferation, or interfere with the cell dividing cycle. However, the use and efficacy of these therapies have been largely limited by their non-specificity and toxic side effects [10]. In fact, the available treatments of metastatic breast cancer would only palliate the symptom and extend the life. In many cases, the treatment will have to be terminated at a predetermined end point, where the patients develop too much pain from the treatment itself.

Nanoparticle based anti-cancer drug carriers have attracted much attention for their potential use in metastatic cancer treatment [11]. As reported, with modified structure, nanoparticles could have high dose of drug loading, targeted delivery and controlled release inside the tumor cells [11]. The goal of this study was to develop a 3rd generation nanoparticle with accurately triggered controlled release and solve the basal drug leakage associated with conventional drug carriers. A second nanoparticle was encapsulated into PEGylated (polyethylene glycol) immunoliposome. The major function of the nanoparticle was for high dose drug loading, immunoliposome stabilization and controlled release. Herceptin or anti-HER2 monoclonal antibodies were attached to the surface of PEGylated liposomes to increase their affinity and uptake rate to the HER2 overexpressing breast cancer cells.

Grafting of different types of protein based targeting ligand to the surface of liposome will be discussed in chapter III. A modified enzyme linked immunosorbent assay was established for accurate liposome surface ligand concentration quantification. In chapter IV, methods of nanohorn encapsulated immunoliposome assembly and purification will be described. Size

distribution, drug loading capacity, drug release profile, specific cell binding, cell uptake, toxicity of the nanohorn supported immunoliposome will be discussed in chapter V. Polymeric nanoparticles are a family of new materials that possess many desirable properties for drug delivery. The incorporation of polymeric nanoparticles into the supported immunoliposome platform would largely extend the application area. In chapter VI, a systematic study of polymeric nanoparticle fabrication parameters effect on particle size and charge will be described. Chapter VII is the general conclusion of the work.

Reference

[1] Airley, R., Cancer epidemiology. Cancer chemotherapy, 2009, John Wiley & Sons Ltd.

[2] CDC, US Cancer Statistics Working Group. Top 10 Causes of Death for Women in the United States (2003). CDC Statistics: 2007.

[3] American Cancer S. Cancer Facts & Figures 2007. Atlanta: American Cancer Society: 2007.

[4] Jemal A., Siegel R., Ward E., et al. Cancer statistics, 2008. CA Cancer J Clin 58 (2008) 71-96.

[5] Foster T. S., Miller J. D., Boye M. E., Blieden M. B., Gidwani R., Russell M. W. The economic burden of metastatic breast cancer: A systematic review of literature from developed countries. Cancer treatment reviews, 37 (2011) 405-415.

[6] Shih, Y.C., Elting, L.S., Pavluck, A.L., Stewart, A., Halpern, M.T. Immunotherapy in the initial treatment of newly diagnosed cancer patients: utilization trend and cost projections for non-Hodgkin's lymphoma, metastatic breast cancer, and metastatic colorectal cancer. Cancer Invest 28 (2010) 46-53.

[7] Miller, K.D. What is breast cancer? Choices in breast cancer treatment, Miller, K.D., 2008, The Johns Hopkins University Press, 132-152.

[8] Airley, R., Tumour metastasis: a convergence of many theories, Cancer chemotherapy, 2009, John Wiley & Sons Ltd. 37-48.

[9] Yamaguchi, H., Wyckoff, J., Condeelis, J., Cell migration in tumors, Current Opinion in Cell Biology, 17 (2005) 559-564.

[10] I. Brigger, C. Dubernet, P. Couvreur, Nanoparticles in cancer therapy and diagnosis, Advanced Drug Delivery Reviews 54 (2002) 631-651

[11] S. Parveen, R. Mistra, S. K. Sahoo, Nanoparticles: a boon to drug delivery, therapeutics, diagnostics and imaging, Nanomedicine: Nanotechnology, Biology and Medicine 8 (2012) 147-166.

Chapter II: Literature Review

3rd generation nanoparticle based drug carrier for metastatic breast cancer treatment

Overview of breast cancer epidemiology

Metastatic cancer remains a leading cause of death. Globally, it has led to 7.9 million case of death in 2007 [1]. An average of more than 10 million people were diagnosed bearing cancer each year and 15 million new cases are the estimated annual increase till 2020 [2,3]. The U.S. was reported to have the world's highest cancer mortality count [4]. Breast cancer is the most commonly seen cancer type in woman [5]. In the U.S. about 40,000 lives were taken away by metastatic breast cancer (MBC) each year along with huge economic losses [6,7]. Extensive work is still undergoing attempting to understand the disease and to find a cure. However, the up-to-date treatments could only palliate the symptoms and prolong the survival [8]. Nonetheless, the efforts were gradually turning the tide. Statistic results have shown a 1.7% yearly reduction of the mortality rate in the U.S. since 1990 [9-12]. This reduced mortality rate can be attributed to the improvement of screening program, adjuvant therapies and novel therapeutic agents that have been constantly developed during the period and a better common awareness of the disease.

Along with biopsies, radiotherapy and chemotherapy are used as a first line treatment to help eliminate the chance of metastasis and recurrence. It is of worth to point out that the severe side effects of the therapies and the hospitalization can sometimes bring as much pain to the patient as the cancer itself, and result in low quality lives of the patients despite the extended survival. Thanks to the cancer drug screening programs (i.e. combinatorial and rational drug

design and development) [13,14], new chemotherapy agents or new modifications of old ones are coming out each year to have higher specificity, lower toxicity and thus improve the overall therapeutic potency. Instead of using high dose of single agent, multiple chemotherapies with minimum doses are now given in combinations at intervals in pulsed doses or in cycles to have even better therapeutic effect and less severe side effects [15,16]. Other adjuvant therapy (i.e. endocrine therapy, immunotherapy) is given as a single agent or in combination with chemotherapies. It has been shown very effective against estrogen receptor (ER) or human epidermal growth factor receptor 2 (Her2) positive cancer cells [17]. For further improvement, nanoparticle (NP) based drug carriers are used in order to achieve goals such as lower toxicity, targeted delivery and controlled release [18-21]. The emergence of NP based drug carriers has brought fresh air to the traditional chemotherapy treatment area by solving problems such as the low solubility and high toxicity of the drug, the low permeability across the cell membrane and the strong drug resistance from the cell [22]. NPs are also used to deliver gene therapies [23]. In cancer treatment, the goal of current gene therapy is to silence the oncogene or the other genes related to cancer progression. Gene therapy is of great potential, but the specific targeting and the protection from degradation are still relying on the NP carriers [22].

Breast cancer biology

Contact with carcinogens, family history, smoking, certain virus infections and lack of DNA repair are the known risk factors for genetic mutations to occur and preserve. Some cells gradually gain survival advantages through the accumulation of amplifications of oncogenes or dysfunctions of tumor suppressor genes. Cancer cells are formed from such normal cells through accumulating the genetic mutations that lead to immortality [24]. The cell proliferation and death become non-regulated. Instead of functioning and behaving normally, the cells will go through rapid, anchorage-independent growth and form a tumor. For breast

cancer, the tumors are originated mostly from the duct and in some cases inside the lobules [25].

A tumor is tightly packed with cancerous cells, connective tissue and blood vessels with a higher density close to the center. This creates an outward convective interstitial fluid flow and largely limits the inward diffusion of small molecules such as chemotherapy agents [22]. The extensive angiogenesis is promoted by the tumor and is highly non-regulated. Researches showed the gaps between the vascular endothelial cells could be as large as a few hundred nanometers and render the tumor vascular hyperpermeable [26]. Also due to the lack of lymphatic draining network, intravenously injected NPs will have a long retention time at the tumor and thus have high chances to be uptake by the cancer cells. This is called the enhanced permeability and retention effect (EPR) and considered to be the key of NP targeting to the tumor [26].

The disease is highly treatable if the tumor is localized in the duct or lobules [25]. However, some of the tumor cells could produce proteolytic enzymes such as the matrix metalloproteinase and invadolysin, which digests the collagen fibers through the extracellular matrix (ECM) [27]. These tumor cells could intravasate into local blood vessels through invadopodia and macrophage-induced penetration [28]. The tumor cells will then spread from the original position following the blood and lymphatic circulation and start new growth at other parts of the body. Fluid samples are usually taken from the closest lymph node, the one under the arm in the case of breast cancer, to check traces of cancer cell biomarkers, which can provide the information of the metastasis stage [25]. A well accepted standard to describe breast cancer stage is the TNM (tumor node metastasis) system. The three letters stand for the size of the tumor, the degree of lymph node involvement and the stage of metastasis respectively [25]. Large numbers of TNM results indicate advanced stages of the cancer. 90% survival rate was reported for patients having early awareness of the tumor if appropriate

treatments were taken. However, bone marrow, blood and lymph nodes are the known reservoirs for residual cancer cells. Recurrences could occur a few years post the first line treatment [27]. Usually, the cancer is found spread to the lungs and bones for metastatic breast cancer [25]. At this stage, the current available treatments are aimed to extend the patient a short period of life and to reduce the pain.

Breast cancer treatment

A diagnose is given at the first place in order to acquire information such as the amount, location, size, the major specific subtype of the cancer and the stage of progression. A decision of treatment will be made in discussion with the patient to clarify the final goal of the treatment. Usually, surgically removing of the tumor is unavoidable. Depending on the tumor size and stage, a lumpectomy or mastectomy will be performed along with radiation therapy and sentinel node biopsy [29]. Nausea, fatigue, low white blood cell count and skin irritation are the side effects associated with radiotherapy. However, it helps eliminate most of the chance of recurrence [30].

Chemotherapies are usually taken orally or intravenously. They can be used to reduce the tumor size before the surgery; however, it is more importantly a follow up treatment to lower the risk of recurrence. A list of commonly used chemotherapy agents can be found from the National Comprehensive Cancer Network (NCCN) guidelines for breast cancer. The most frequently used ones include 5 fluorouracil, doxorubicin, cyclophosphamide, epirubicin, paclitaxel and docetaxel. Different types of chemotherapy agents inhibit the cancer cells differently. By choosing combinations of chemotherapy agents, multiple pathways for the surviving and progression of the cancer cells could be blocked, thus to achieve higher therapeutic outcomes and meanwhile lower the toxic side effects.

5 Fluorouracil is a pyrimidine antagonist belonging to the antimetabolite family, which interferes normal DNA synthesis. It functions either as an inhibitor of thymidylate synthase that blocks the formation of pyrimidine nucleotide or an analog to the pyrimidine nucleotide and incorporates into a growing DNA [31]. Doxorubicin and epirubicin are well known for the applications in solid tumor treatment. They are anthracyclines belonging to the antitumor antibiotics family. The general function is to block DNA replication as a topoisomerase IIalfa inhibitor [32,33]. Cyclophosphamide is an alkylating agent, which possesses the nitrogen mustard motif upon activation by P450 cytochrome enzymes. The nitrogen mustard motif causes cross-linking of intrastrand and interstrand of DNA and results in interruptions of transcription [34-37]. Paclitaxel and docetaxel are taxane drugs from the antimicrotubule agent family. The taxane drugs can target the beta-tubulin in the microtubule polymer and inhibit the depolymerization. This will lead to a mitotic block and cause the cancer cells to stay in the G1-phase and stop dividing [38,39]. Another common chemotherapy family is the platinum drugs. An example is cisplatin, which is used in treating advanced stage of the disease. Cisplatin can cause cross-linking of intrastrand and interstrand of DNA, thus result in inhibition of DNA replication and transcription [40].

Another two agents clinically used for adjuvant therapy are tamoxifen and herceptin. They are provided to the patients post-surgery and -radiotherapy depending on the caner subtype. They can be used as a single agent or more frequently in combination with chemotherapy. The goal is to reduce the risk of recurrence [41]. Some breast cancer cells were found to over-express characteristic molecular markers such as estrogen receptors (ER), progesterone receptor (PR) and Her2. Identification of these subtypes provides valuable information on the evolution, propensity of metastasis as well as making a proper treatment decision [42]. Immunohistochemistry and fluorescence in situ hybridization are performed for subtype diagnosis [43]. An ER+ result indicates the cancer cells will be sensitive to endocrine

therapies such as tamoxifen, which blocks the estrogen induced cell proliferation pathway by competitively binding to the estrogen receptors [41,44]. Her2 receptor is over-expressed in 20-30% of human breast cancer cells. This type of cell is very aggressive with high cell proliferation and propensity to early metastatization, and it usually leads to bad prognosis [45,46]. Herceptin is used in combination with other chemotherapy in Her2 positive cases to block the Her2 encoded transmembrane tyrosine kinase receptor and shut down the related PI3K/Akt and MAPK pathways that lead to cell invasion, survival and angiogenesis [47].

Metastatic breast cancer tumors are most frequently found in the liver, bone and lung. Local therapies and systemic therapies are used for the treatment. Local therapies refer to surgery and radiotherapy, which is not recommended unless the position of the tumor is life threatening. This is because, at this stage, multiple metastases at different position are usually seen simultaneously. A systemic therapy, including chemotherapy and other adjuvant therapies, will have an overall global effect on all the metastatic tumors. The treatment will start with low dose of less toxic drugs since a shrinking tumor, prolonged life and relieved patient will be the best outcome [48].

NP based drug carrier

The use of traditional chemotherapy and other adjuvant therapy are largely limited by many intrinsic problems such as poor solubility, side effect, non-specificity, *in vivo* degradation. NP based anti-cancer drug carriers are being extensively studied and reported to have largely improved the overall pharmacokinetics, bioavailability, *in vivo* distribution and controlled release of the drug content [49,50].

The so-called NPs are commonly seen as colloid particles with an average size up to a few hundred nanometers. NPs with different shape, hydrophobicity, material and modification are made to address different needs [50]. Examples of materials include polymer, ceramic and

other metallic materials, lipid, proteins, sugar and other synthetic carbon, silicon particles such as dendrimer, fullerene, nanotube and nanohorns [50, 51]. The most commonly used structures are nanospheres or nanocapsules. Poly (D,L-lactide-co-glycolide) (PLGA) [52] and silica NPs [53] are examples of solid and porous nanospheres. Drugs are embedded inside the NP during the particle formation. There were some issues with drug loading capacity when polar drugs are to be embedded into nonpolar NPs or *vice versa*. However, this problem has been solved by using special synthesis processes such as the double emulsion method [54]. A good example of nanocapsule is liposome. The lipid bilayer serves as the capsule and limits the movement of encapsulated drug across the boundary [55]. Moreover, the lipid bilayer itself mimics the cell membrane system, and therefore, it can harbor protein based anti-cancer therapies such as antibodies (i.e. Herceptin) [56].

Drug loading of NP drug carrier

Many chemotherapy and other adjuvant therapy agents have very low aqueous solubility, such as paclitaxel, doxorubicin and tamoxifen. High dose of these agents were conventionally given to the patients through daily oral administrations [57]. Unfortunately, very little drug was sent into the tumor cells due to the insoluble form resulted low intra-tumor diffusion and low cell uptake [16]. Liposome formulated paclitaxel (Taxol®) and doxorubicin (Doxil®, Caelyx® and Myocet®) are currently available for the patients. Although the formulation of tamoxifen with NP drug carriers is still under development [58], high dosage of another antiestrogen agent RU 58668 has been shown to incorporate into polyethylene glycol (PEG) coated poly (lactic acid) [59]. Other attempts have been made to encapsulate docetaxel [60], Ionidamine [61], Rapamycin [62] into PLGA, and curcumin into solid lipid NP [63].

Multiple agents inhibiting different cell proliferation pathways are used in combination to improve the therapeutic efficiency [15,16]. A particle based cell uptake will theoretically guarantee a synchronized delivery of the drugs of choice in the designated ratio. Therapeutic

cocktails loaded NPs have been assembled and tested. Zhao et al. tested a co-delivery of doxetaxel and polo-like kinase 1 siRNA to SK-BR-3 cells and the result showed the lowest amount of drug needed for the co-delivery to kill 50% of the cells compared to all other control groups [64]. In Wang et al.'s work, doxorubicin and paclitaxel were co-delivered by PEG-PLGA NP [65]. The highest anti-tumor activity was found for a 2:1 doxorubicin paclitaxel co-delivery [65].

The use of NP drug carriers seemed to overcome another problem, the multidrug resistance. Researches showed that an overexpression of a plasma membrane P-glycoprotein can increase the resistance to the drug by rapidly pumping them out across the membrane [66]. Some theory believes the efflux only occurs in the plasma membrane. Therefore, the NP carriers could solve the problem because they ship the drugs into the cytoplasm. Successful examples were also reported when poly(alkyl cyanoacrylate) NP was used to deliver doxorubicin [67]. This is however not always true as evidenced by some other works in which adriamycin with poly(methacrylate) [68], or other cell lines [69] were used. The results of which showed a rather drug, carrier and cell dependent inhibition of the P-glycoprotein induced drug resistance. Another strategy is to co-deliver anti-drug resistance agents in the NP. For example, in Patil et al.'s work, tariquidar was delivered together with paclitaxel and results showed an inhibited efflux of the drug [70]. A simultaneous delivery is still crucial since the blocking of P-glycoprotein by tariquidar is temporary [71].

Targeting of NP drug carrier

As discussed earlier, the anti-cancer therapies usually inhibit the cell proliferation *via* disruptions of DNA replication and transcription, interrupting incoming signals that can promote the proliferation, or interfere with the cell dividing cycle. The 'specificity' of these therapies is really relying on the fact that actively dividing cells (i.e. tumor cells) would be more affected by those agents. NP can protect both the drug and the surrounding tissue

during the delivering. Targetable NPs are being developed to have high specificity to the tumor cells.

As mentioned previously, intravenously administrated NPs have a tendency to extravasate and accumulate at the tumor side as a result of the EPR effect. However, on the other hand, a very broad *in vivo* distribution is more often observed [72]. In a few hours post-administration, the NPs were found mostly in the liver, spleen and kidney and with a few in the lung, skin and the tumor site [73,74]. This is mostly resulted from the active uptake by the mononuclear phagocyte system (MPS) located mainly in the liver and spleen. NPs inside the bloodstream undergo rapid opsonization process, within which blood serum proteins such as laminin, fibronectin, C-reactive protein and type I collagen etc. quickly adsorb onto the NP surface and make it more susceptible to the MPS clearance [75,76]. To overcome this, NPs are currently coated with amphiphilic polymeric materials to create a 'cloudy' layer around the NPs and render them less 'invisible' to the MPS. PEG and poly(ethylene oxide) (PEO) are the most common ones used for this purpose [77,78]. Besides the coating, a high curvature, low hydrophobicity, small size and negative charge can help reduce the MPS uptake [79-81]. These surface modified NPs are referred to as the second generation of NP drug carriers [22]. The modifications have resulted in prolonged circulation time and a more significant EPR effect [82].

Some immunotherapy agents inhibit the cell growth by binding on the surface receptors such as Herceptin. However, many more other therapies require an internalization of the carrier into the cytoplasm (chemotherapies) or the nucleus (gene therapies). In this case, intra tumor diffusion and cell uptake of the NPs will be involved. NPs are found to diffuse inside the tumor with great difficulty. Florence pointed out that the diffusion rate through the extracellular matrix (ECM) has to be considered when studying the in tumor drug distribution [83], based on a finding by Goodman et al. that only 20-40 nm particles were found

penetrated into an enzyme treated tumor spheroid (i.e. enzyme treatment degrade ECM inside the tumor) [84]. In Perche et al.'s work, 14 nm NPs were found spread through the entire *in vitro* tumor spheroid model [85]. NPs get internalized by the cells via receptor mediated endocytosis or phagocytosis generally depending on the size and surface chemistry [86]. NPs with a slight negative charge and average diameter around 150 nm were found most efficient in the cell uptake by many [87-89]. Targeting ligands are shown beneficial for the targeting specificity and cell uptake rate. Park et al. showed increased uptake of folate-conjugated polymeric micelles by the folate receptor overexpressing MCF7 cells [90]. Avastin®, an anti-vascular endothelial growth factor, was used to target the tumor and showed anti-angiogenesis effect [91]. Lee et al. showed a Her2 overexpression level dependent uptake by MCF7, T47D, BT474 and HEK293 cell lines with Herceptin conjugated NPs [92]. Anti-ErbB2 (another name for Her2) Fab grafted liposomes were found internalized with high efficacy of cancer kill [93]. scFv antibodies (anti Her2 antibody) were used to deliver doxorubicin-loaded immunoliposomes and resulted in higher internalization efficacy [94]. Many other types of targeting ligands including antibody fragments, vitamins, glycoproteins, peptides and oligonucleotides aptamers have also been utilized in tumor targeting [57]. It is noteworthy to point out that although the targeting ligands have been shown to improve the specificity and cell uptake rate when compared to non-grafted NPs, they are found (1) to only function when NPs have direct contact with the cells and (2) to increase the chance of non-specific binding, on the other hand [95,96]. The targeting ligand is modified and conjugated to the surface of the NP or more frequently to the distal terminal of the PEG through covalent or non-covalent binding, or through affinity bound when metallic NPs are used [97]. To improve the targeting efficiency, more tumor-specific antigens [98] are still to be discovered.

Drug release of NP drug carrier

The term controlled release describes a prolonged release of drug in response to stimuli or time. A controlled release is beneficial because it provides longer and steadier blood drug concentration within the therapeutic limits, which would lead to the same therapeutic outcome as a peak-like release, but with less dose requirement and side effect [99]. It also has higher user compliance due to the less need of the hospitalization and repeatedly administrations of drug [100,101].

A typical drug release from NPs is usually initiated with a burst phase (up to 50% of total loading) within the first few hours post exposure, and followed with a slow release phase [102]. The burst phase corresponds to the release of drug molecules that are loosely associated with the particle, mostly located on the surface of the NPs. The slow release phase results from the drug release from the inner core via diffusion and erosion (for biodegradable particles) [102]. However, the transportation time needed for the NPs from injection to tumor cell internalization usually exceeds the burst phase release. Zhang et al. described a 3.5 hours *in vitro* cell uptake rate using 30 nm quantum dots [103]. In the experiment, NPs were directly added into the cell culture. Longer duration of the delivery is expected since the time for transportation in the blood, extravasation and the diffusion through the tumor are to be included. The leakage will lead to efficacy loss of the drug and cause toxic side effects to the health tissue [104].

An advanced release scenario referred to as trigged bust release was described by Huang et al. [99]. Briefly, a trigged bust release profile has three stages. Before the nanoparticle reach the tumor cell, there should be no or very limited release. Triggered by certain types of agitation, such as pH, temperature change inside the tumor cell, the release will start with a burst release and followed by a zero-order controlled release. Finally, the NPs are fully degraded and drug release stops. A more sophisticated drug delivery system is needed for the

release scenario. The 3rd generation of NP based drug carriers were developed recently [105-107]. These new drug carriers are assembly of multi-types of NPs in a manner that improves the overall drug delivery (i.e. one encapsulated in another). Different parts of the carrier are usually responsible for more specialized functions (i.e. drug loading, drug releasing, MPS evading, targeting). Mal et al. described an end-capped mesoporous silica NP for stimuli-responsive drug release [108]. Proteins, polymers and inorganic NPs were used to cap the pores post drug loading and stimuli such as pH [109], temperature [110], redox potential, enzymes [111,112], glucose or antigens [113], light, ultrasounds or voltage [114] could be applied to open and close the cap. In our work, a paclitaxel loaded carbon nanohorn was encapsulated into an immunoliposome. Results showed an elimination of basal drug release in serum at 37 ºC and a high SK-BR-3 cell uptake rate.

Conclusion

Despite the difficulties in treating metastatic breast cancer, progresses have been made in the recent a few years as evidenced by a constant declining of the mortality rate since 1990. Chemotherapy and endocrine therapy are used for first-line and metastatic breast cancer treatment. Factors limiting the use include the strong side effects, low solubility of most chemotherapies, non-specificity to tumor cells, multi-drug resistance of the cells, and etc. The therapies are strong enough to inhibit the growth of the cell and the progression of the cancer especially when used in combinations by interrupting processes such as DNA replication and transcription, cell dividing, angiogenesis and etc. However, advanced drug delivering method is strongly needed.

The NP based drug carriers have developed their 3rd generation. The new NPs are assembled with multi-types of NPs and thus possess combined advantages. Different parts of the particle are assigned with more specialized functions. As a result, the 3rd generation of NP based drug

carriers usually have improved drug loading, tumor-specific targeting and more accurately controlled drug release.

References

[1] Jemal, A., Bray, F., Center, MM., Ferlay J., Ward, E., Forman, D., "Global cancer statistics", CA: a cancer journal of clinicians 61 (2011) 69-90.

[2] Brannon-Peppas, L., Blanchette J.O. Nanoparticle and targeted systems for cancer therapy. Adv. Drug Delivery Rev. 56 (2004) 1649-1659.

[3] Feng, S.S. Nanoparticles of biodegradable polymers for new-concept chemotherapy. Expert Rev. Med. Devices 1 (2004) 115-125.

[4] CANCERMondial http://www-dep.iarc.fr. Accessed October 2002.

[5] CDC, US Cancer Statistics Working Group. Top 10 Causes of Death for Women in the United States (2003). CDC Statistics; 2007.

[6] Jemal, A., Siegel, R., Ward, E., et al. Cancer statistics, 2008. CA Cancer J Clin 58 (2008) 71-96.

[7] Foster, T.S., Miller, J.D., Boye, M.E., Blieden, M.B., Gidwani, R., Russell, M.W. The economic burden of metastatic breast cancer: A systematic review of literature from developed countries. Cancer treatment reviews, 37 (2011) 405-415.

[8] Greenberg, P.A., Hortobagyi, G.N., Smith, T.L., Ziegler, L.D., Frye, D.K., Buzdar, A.U., Long term follow-up of patients with complete remission following combination chemotherapy for metastatic breast cancer. J Clin Oncol, 14 (1996) 2197-2205.

[9] Cronin, K.A., Feuer, E.J., Clarke, L.D., Pleveritis, S.K., Impact of adjuvant therapy and mammography on U.S. mortality from 1975 to 2000: comparision of mortality results from the cisnet breast cancer base case analysis. J Natl Cancer Inst Monogr, 36 (2006) 112-121.

[10] Verry, D.A., Cronin, K.A., Plevritis, S.K., et al. Effect of screening and adjuvant therapy on mortality from breast cancer. N Engl J Med, 353 (2005) 1782-1792.

[11] Giordano, S.H., Buzdar, A.U., Smith, T.L., Kau, S.W., Yang, Y., Hortobagyi, G.N., Is breast cancer survival improving? Cancer, 100 (2004) 44-52.

[12] Chia, S.K., Speers, C.H., D'yachkova Y., et al. The impact of new chemotherapeutic and hormone agents on survival in a population based cohort of women with metastatic breast cancer. Cancer, 110 (2007) 973-979.

[13] Missailidis, S., Combinatorial approaches to anticancer drug design. Anticancer therapeutics. Missailidis, S., 2008, John Wiley & Sons, Ltd. 17-28.

[14] Alcaro, S., Artese, Anna, Ortuso, F., Rational approaches to anticancer drug design/in silico drug development. Missailidis, S., 2008, John Wiley & Sons, Ltd. 29-47.

[15] Andreetta, C., Minisini, A. M., Miscoria, M., Puglisi, F., First-line chemotherapy with or without biologic agents for metastatic breast cancer. Critical Reviews in Oncology/Hematology, 76 (2010) 99-111.

[16] Reddy, L. H. Drug delivery to tumors: recent strategies, J. Pharm. Pharmacol. 37 (2005) 1231-1242.

[17] Wolff, A.C., Davidson, N.E. Beyond local therapy, hormonal therapy and chemotherapy, Choices in breast cancer treatment, Miller, K.D., 2008, The Johns Hopkins University Press, 132-152.

[18] Minisini, A.M., Andreetta, C., Fasola, G., Puglisi, F., Pegylated liposomal doxorubicin in elderly patients with metastatic breast cancer. Expert Rev Anticancer Ther, 8 (2008) 331-342.

[19] Singh, R., Lillard, J. W., Jr. Nanoparticle-based targeted drug delivery. Exp. Mol. Pathol. 86 (2009) 215-223.

[20] Yang, T., Choi, M., Cui, F., Kim, J.S., Chung, S., Shim, C., Kim, D. Preparation and evaluation of paclitaxel-loaded PEGylated immunoliposome. Journal of Controlled Release, 120 (2007) 169-177.

[21] Xu, J., Yudasaka, M., Kouraba, S., Sekido, M., Yamamoto, Y., Iijima, S. Single wall carbon nanohorn as a drug carrier for controlled release. Chem. Phys. Lett. 461 (2008) 189-192.

[22] Serpe, L. Conventional chemotherapeutic drug nanoparticles for cancer treatment. Kumar, C.S.S.R. Nanomaterials for cancer therapy, 2006, WILEY-VCH Verlag GmbH & Co. KGaA, Weinheim, 1-39.

[23] Lacroix, M. MicroRNAs in Breast Cancer. Romero, M.E., Dashek, L.M., Breast cancer causes, diagnosis and treatment. 2010, Nova Science Publishers, Inc. 1-52.

[24] Airley, R., Carcinogenesis, carcinogenesis, malignant transformation and progression, Cancer chemotherapy, 2009, John Wiley & Sons Ltd.

[25] Miller, K.D. What is breast cancer? Choices in breast cancer treatment, Miller, K.D., 2008, The Johns Hopkins University Press, 132-152.

[26] Maeda, H., The enhanced permeability and retention (EPR) effect in tumor vasculature: The key role of tumor-selective macromolecular drug targeting, Adv. Enzyme Regul. 2001, 41, 189-207.

[27] Airley, R., Tumour metastasis: a convergence of many theories, Cancer chemotherapy, 2009, John Wiley & Sons Ltd. 37-48.

[28] Yamaguchi, H., Wyckoff, J., Condeelis, J., Cell migration in tumors, Current Opinion in Cell Biology, 17 (2005) 559-564.

[29] Deckers, P.J., Tsangaris, T.N. Choices in breast cancer treatment, Miller, K.D., 2008, The Johns Hopkins University Press, 86-102.

[30] Recht, A. Radiation therapy for breast cancer. Choices in breast cancer treatment, Miller, K.D., 2008, The Johns Hopkins University Press, 110-124.

[31] Scaife, J., Kerr, D., Antimetabolites in cancer therapy, Missailidis, S., Anticancer therapeutics. 2008, John Wiley & Sons, Ltd. 91-110.

[32] Paz, M.M. Antitumour antibiotics, Missailidis, S., Anticancer therapeutics. 2008, John Wiley & Sons, Ltd. 111-132.

[33] Gewirtz, D.A., A critical evaluation of the mechanisms of action proposed for the antitumour effects of the anthracycline antibiotics Adriamycin and daunorubicin. Biochem Pharmacol 1999, 57, 727-741.

[34] Balcome, S., Park, S., Dorr, D.R., Hafner, L., Philips, L., Tretyakova, N., Adenine-containing DNA-DNA cross-links of antitumor nitrogen mustards. Chem Res Toxicol, 2004 17, 950-962.

[35] Dronkert, M.L.G., Kanaar, R., Repair of DNA interstrand cross-links. Mutation Research/DNA Repair 486 (2001) 217-247.

[36] Bauer, G.B., Povirk, L.F., Specificity and kinetics of interstrand and intrastrand bifunctional alkylation by nitrogen mustards at a G-G-C sequence. Nucl Acids Research 25 (1997) 1211-1218.

[37] Masta, A., Gray, P.J., Philips, R., Molecular basis of nitrogen mustards effects on transcription processes: role of depurination. Nucl Acid Research 22 (1994) 3880-3886.

[38] Bharadwaj R., Yu H. The spindle checkpoint, aneuploidy, and cancer. Oncogene, 23 (2004) 2016-2027.

[39] Brito, D.A., Yang, Z., Rieder, C.L. Microtubules do not promote mitotic slippage when the spindle assembly checkpoin cannot be satisfied. J. Cell Biol. 182 (2008) 623-629.

[40] Boulikas, T., Pantos, A., Bellis, E., Christofis, P., Platinum drugs. Missailidis, S., Anticancer therapeutics. 2008, John Wiley & Sons, Ltd. 55-78.

[41] Wolff, A.C., Davidson, N.E., Beyond local therapy, Miller, K.D., 2008, The Johns Hopkins University Press, 132-151.

[42] Henry, N.L., Hayes, D.F., Uses and abuses of tumor markers in the diagnosis monitoring, and treatment of primary and metastatic breast cancer. Oncologist, 11 (2006) 541-552.

[43] Madarnas, Y., Trudeau, M., Franek, J.A., McCready, D., Pritchard, K.I., Messersmith, H., Adjuvant/neoadjuvant trastuzumab therapy in women with HER-2/neu-overexpressing breast cancer: A systematic review. Cancer treatment reviews, 34 (2008) 539-557.

[44] Tran-Thanh, D., Done, S.J., The evolving role of molecular markers in the diagnosis of breast cancer. Romero, M.E., Dashek, L.M., Breast cancer causes, diagnosis and treatment. 2010, Nova Science Publishers, Inc. 89-116.

[45] Slamon, D.J., Clark, G.M., Wong, S.G., Levin, W.J., Ullrich, A., McGuire, W.L., Human breast cancer: correlation of relapse and survival with amplification of the HER-2/neu oncogene. Science, 235 (1987) 177-182.

[46] Hynes, N.E., Stern, D.F., The biology of erbB-2/neu/HER-2 and its role in cancer, Biochim. Biophys, Acta, 1198 (1994) 165-184.

[47] Belimezi, M., Cancer Immunotherapy. Missailidis, S., Anticancer therapeutics. 2008, John Wiley & Sons, Ltd. 283-304.

[48] Hayes, D.F., Treatment options for metastatic breast cancer. Miller, K.D., 2008, The Johns Hopkins University Press, 186-200.

[49] Brigger, I., Dubernet, C., Couvreur, P., Nanoparticles in cancer therapy and diagnosis, Advanced Drug Delivery Reviews 54 (2002) 631-651.

[50] Parveen, S., Mistra, R., Sahoo, S.K., Nanoparticles: a boon to drug delivery, therapeutics, diagnostics and imaging, Nanomedicine: Nanotechnology, Biology and Medicine 8 (2012) 147-166.

[51] Naahidi, S., Jafari, M., Edalat, F., Raymond, K., Khademhosseini, A., Chen, P., Biocompatibility of engineered nanoparticles for drug delivery. Journal of Controlled Release 166 (2013) 182-194.

[52] Koopaei, M.N., Dinarvand, R., Amini, M., et al. Docetaxel immunonanocarriers as targeted delivery systems for HER 2-positive tumor cells: preparation, characterization and cytotoxicity studies. Int J Nanomed 6 (2011) 1903-1912.

[53] Li, X., Chen, Y., Wang, M., Ma, Y., Xia, W., Gu, H., A mesoporous silica nanoparticle-PEI-Fusogenic peptide system for siRNA delivery in cancer therapy. Biomaterials 34 (2013) 1391-1401.

[54] Carlos, E., Sabliov, M., Synthesis and characterization of PLGA nanoparticles. J. Biomater. Sci. Polymer Edn 17 (2006) 247-289.

[55] Theresa, M.A., Pieter, R.C., Liposomal drug delivery systems: From concept to clinical applications. Advanced Drug Delivery Reviews 65 (2013) 36-48.

[56] Yang, T., Choi, M., Cui, F., Kim, J. S., Chung, S., Shim, C., Kim, D. Preparation and evaluation of paclitaxel-loaded PEGylated immunoliposome. *J. Control. Release* 120 (2007) 169-177.

[57] Maillard, S., Fattal, E., Marsaud, V., Sola, B., Colloidal systems for the delivery of anticancer agents in breast cancer and multiple myeloma, Kumar, C.S.S.R. Nanomaterials for cancer therapy, 2006, WILEY-VCH Verlag GmbH & Co. KGaA, Weinheim, 371-403.

[58] Brigger, I., Chaminade, P., Marsaud, V., Appei, M., Besnard, M., Gurny, R., Renoir, M., Couvreur, R., Tamoxifen encapsulation within polyethylene glycol-coated nanospheres. A new antiestrogen formulation, Int. J. Pharm. 214 (2001) 37-42.

[59] Amelier, T., Marsaud, V., Legrand, P., Gref, R., Barratt, G., Renoir, J.M., Polyester-poly(ethylene glycol) nanoparticles loaded with the pure antiestrogen RU 58668, physic-chemical and opsonization properties, Pharm. Res., 20 (2003) 1063-1070.

[60] Murphy, E.A., Majeti, B.K., Mukthavaram, R., Acevedo, L.M., Barnes, L.A., Cheresh, D.A., Targeted nanogels: a versatile platform for drug delivery to tumors. Mol. Cancer. Ther. 10 (2011) 972-82.

[61] Milane, L., Duan, Z., Amiji, M., Development of EGFR-targeted polymer blend nanocarriers for combination paclitaxel/lonidamine delivery to treat multi-drug resistance in human breast and ovarian tumor cells. Mol. Pharm. 8 (2011) 185-203.

[62] Acharya, S., Dilnawaz, F., Sahoo, S.K., Targeted epidermal growth factor receptor nanoparticle bioconjugates for breast cancer therapy. Biomaterials 30 (2009) 5737-5750.

[63] Mulik, R.S., Monkkonen, J., Juvonen, R.O., Mahadik, K.R., Paradkar, A.R.,

Transferrin mediated solid lipid nanoparticles containing curcumin: enhanced in vitro anticancer activity by induction of apoptosis. Int. J. Pharm. 398 (2010) 190-203.

[64] Zhao, J., Mi, Y., Feng, S., Targeted co-delivery of docetaxel and siPlk1 by Herceptin-conjugated vitamin E TPGS based immunomicelles. Biomaterials 34 (2013) 3411-3421.

[65] Wang, H., Zhao, Y., Wu, Y., Hu, Y., Nan, K., Nie, G., Chen, H., Enhanced anti-tumor efficacy by co-delivery of doxorubicin and paclitaxel with amphiphilic methoxy PEG-PGLA copolymer nanoparticles. Biomaterials 32 (2011) 8281-8290.

[66] Larsen, A.K., Escargueil, A.E., Skladanowski, A., Resistance mechanisms associated with altered intracellular distribution of anticancer agents, Pharmacol. Ther. 88 (2000) 217-229.

[67] Vauthier, C., Dubernet, C., Chauvierre, C., Brigger, I., Couvreur, P., Drug delivery to resistant tumors: The potential of poly(alkyl cyanoacrylate) nanoparticles. J. Control. Release, 93 (2003) 151-160.

[68] Astier, A., Doat, B., Ferrer, M.J., Benoit, G., Fleury, J., Rolland, A., Leverge, R., Enhancement of Adriamycin antitumor activity by its binding with an intracellular sustained-release form, polymethacrylate nanospheres, in U-937 cells, Cancer Res. 48 (1988) 1835-1841.

[69] Bennis, S., Chapey, C., Couvreur, P., Robert, J., Enhanced cytotoxicity of doxorubicin encapsulated in polyisohexylcyanoactylate nanospheres against multi-drug-resistant tumour cells in culture, Eur. J. Cancer 30A (1994) 889-893.

[70] Ptail Y, Sadhukha T, Ma L, Panyam J. Nanoparticle-mediated simultaneous and targeted delivery of paclitaxel and tarquidar overcomes tumor drug resistance. *J. Control. Release* 136 (2009) 21-29.

[71] Fougere, C.L., Boning, G., Bartmann, H., Wangler, B., Nowak, S., Just, T., Wagner, E., Winter, P., Rominger, A., Forster, S., Gildehaus, F., Rosa-Neto, P., Minuzzi, L., Bartenstein, P., Potschka, H., Cumming, P., Uptake and binding of the serotonin 5-HT_{1A} antagonist [^{18}F]-MPPF in brain of rats: Effects of the novel P-glycoprotein inhibitor tariquidar. Neurolmage 49 (2010) 1406-1415.

[72] Dufort, S., Sancey, L., Coll, J.L., Physico-chemical parameters that govern nanoparticles fate also dictate rules for their molecular evolution. Adv. Drug Deliv. Rev. 64 (2012) 179-189.

[73] Xiao, K., Li, Y., Li, J., Xiao, W., Gonik, A.M., Agarwal, R.G., Lam, K.S., The effect of surface charge on in vivo biodistribution of PEG-oligocholic aid based micellar nanoparticles. Biomaterials 32 (2011) 3435-3446.

[74] Kennel, S.J., Woodward, J.D., Rondinone, A.J., Wall, J., Huang, Y., Mirzadeh, S., The fate of MAb-targeted Cd125^{m}Te/ZnS nanoparticles in vivo. *Nucl. Med. Biol.* 35 (2008) 501-514.

[75] Frank, M., Fries, L., The role of complement in inflammation and phagocytosis. Immunol. Today 12 (1991) 322–326.

[76] Johnson, R.J., The complement system. In: Ratner, B.D., Hoffman, A.S., Schoen, F.J., Lemons, J.E. (Eds.), Biomaterials Science: An Intro-duction to Materials in Medicine. Elsevier Academic Press, Amsterdam, 2004, pp. 318–328.

[77] Boulikas, T., Stathopoulos, G.P., Volakakis, N., Vougiouka, M., Systemic lipoplatin infusion results in preferential tumor uptake in human studies. Anticancer Res. 25 (2005) 3031-3039.

[78] Chawla, J.S., Amiji, M.M., Biodegradable poly(epsilon-caprolactone) nanoparticles for tumor targeted delivery of tamoxifen. Int. J. Pharm. 249 (2002) 127-138.

[79] Storm, G., Belliot, S.O., Daemen, T., Lasic, D.D., Surface modification of nanoparticles to oppose uptake by the mononuclear phagocyte system. Adv. Drug Deliv. Rev. 17 (1995) 31-48.

[80] Xu, F., yuan, Y., Shan, X., Liu, C., Tao, X., Sheng, Y., Zhou, H., Long-circulation of hemoglobin-loaded polymeric nanoparticles as oxygen carriers with modulated surface charges. International Journal of Pharmaceutics, 377 (2009) 199-206.

[81] Jong, W.H.D., Hagens, W.I., Krystek, P., Burger, M.C., Sips, A.J.A.M., Geertsma, R.E. Particle size-dependent organ distribution of gold nanoparticles after intravenous administration. Biomaterials 29 (2008) 1912-1919.

[82] Matsumura, Y., Maeda, H., A new concept for macromolecular therapeutics in cancer thermotherapy: Mechanism of tumoritropic accumulation of proteins and the antitumor agent smancs. Cancer Res. 46 (1986) 6387-6392.

[83] Florence, A.T., "Targeting" nanoparticles: The constraints of physical laws and physical barriers. J. Control. Release 164 (2012) 115-124.

[84] Goodman, T.T., Chen, J., Matveev, K., Pun, S.H., Spatio-temporal modeling of nanoparticle delivery to multicellular tumor spheroids. Biotechnol. Bioeng. 101 (2008) 388-396.

[85] Perche, F., Patel, N.R., Torchinlin, V.P., Accumulation and toxicity of antibody-targeted doxorubicin-loaded PEG-PE micelles in ovarian cancer cell spheroid model. Journal of Controlled Release 164 (2012) 95-102.

[86] Rabinovitch, M., Professional and non-professional phagocytes: an introduction, Trens Cell Biol. 5 (1995) 85-87.

[87] Chung, T., Wu, S., Yao, M., Lu, C., Lin, Y., Hung, Y., Mou, C., Chen, Y., Huang, D., The effect of surface charge on the uptake and biological function of mesoporous silica nanoparticles in 3T3-L1 cells and human mesenchymal stem cells. Biomaterials 28 (2007) 2959-2966.

[88] Foged, C., Brodin, B., Frokjaer, S., Sundblad, A., Particle size and surface charge affect particle uptake by human dendritic cells in an in vitro model. International Journal of Pharmaceutics. 298 (2005) 315-322.

[89] He, C., Hu, Y., Yin, L., Tang, C., Yin, C., Effects of particle size and surface charge on cellular uptake and biodistribution of polymeric nanoparticles. Biomaterials. 31 (2010) 3657-3666.

[90] Park, E.K., Kim, S.Y., Lee, S.B., Lee, Y.M., Folate-conjugated methoxy poly(ethylene glycol)/poly(ε-caprolactone) amphiphilic block copolymeric micelles for tumor-targeted drug delivery. Journal of Controlled Release. 109 (2005) 158-168.

[91] Hood, J.D. et al., Tumor regression by targeted gene delivery to the neovasculature. Science, 296 (2002) 2404-2407.

[92] Lee, A.L.Z., Wang, Y., Cheng, H., Pervaiz, S., Yang, Y., The co-delivery of paclitaxel and Herceptin using cationic micellar nanoparticles. Biomaterials. 30 (2009) 919-927.

[93] Park, J.W. et al. Anti-HER2 immunoliposomes for targeted therapy of human tumors, Cancer Lett. 118 (1997) 153-160.

[94] Schier, R. et al. Isolation of picomolar affinity anti-c-erbB-2 single-chain Fv by molecular evolution of the complementarity determining regions in the center of the antibody binding site, J. Mol. Biol. 263 (1996) 551-567.

[95] Lammers, T., Kiessling, F., Hennink, W.E., Storm, G., Drug targeting to tumors: Principles, pitfalls and (pre-) clinical progress. Journal of Controlled Release, 161 (2012) 175-187.

[96] Grobmyer, S.R., Zhou, G., Gutwein, L.G., Iwakuma, N., Sharma, P., Hochwald, S.N., Nanoparticle delivery for metastatic breast cancer. Maturitas 73 (2012) 19-26.

[97] Manjappa, A.S., Chaudhari, K.R., Venkataraju, M.P., Dantuluri, P., Nanda, B., Sidda, C., Sawant, K.K., Murthy R.S.R., Antibody derivatization and conjugation strategies: Application in preparation stealth immunoliposome to target chemotherapeutics to tumor. Journal of Controlled Release 150 (2011) 2-22.

[98] Browning, M., The cancer cell and the immune system, ed. 1995, Vile, R.G. John Wiley & Sons, New York,.

[99] Huang, X., Brazel, C. S., On the importance and mechanisms of burst release in matrix-controlled drug delivery systems. J. Control. Release 73 (2001) 121-136.

[100] Matschke, C., Isele, U., Van Hoogevest, P., Fahr, A., Sustained-release injectables formed in situ and their potential use for veterinary products. J. Control. Release 85 (2002) 1-15.

[101] Brazel, C. S., Peppas, N. A., Termperature- and pH-sensitive hydrogels for controlled release of antithrombotic agents. Mater. Res. Soc. Symp. Proc. 331 (1994) 211-216.

[102] Fredenberg, S., Wahlgren, M., Reslow, M., Axelsson, A., The mechanisms of drug release in poly(lactic-co-glycolic acid)-based drug delivery systems-A review. Int. J. Pharm. 415 (2011) 34-52.

[103] Zhang, Y., Chatterjee, D.K., Liposomes, dendrimers and other polymeric nanoparticles for targeted delivery of anticancer agents – A comparative study. Kumar, C.S.S.R. Nanomaterials for cancer therapy, 2006, WILEY-VCH Verlag GmbH & Co. KGaA, Weinheim, 338-370.

[104] Singh, R., Lillard, L. W. Jr., Nanoparticle-based targeted drug delivery. Exp. Mol. Pathol. 86 (2009) 215-223.

[105] Dufort, S., Sancey, L., Coll, J., Physico-chemical parameters that govern nanoparticles fate also dictate rules for their molecular evolution. Advanced Drug Delivery Reviews 64 (2012) 179-189.

[106] Liu, J., Stace-Naughton, A., Jiang, X., Brinker, C.J., Porous nanoparticle supported lipid bilayers (protocells) as delivery vehicles, J. Am. Chem. Soc. 131 (2009) 1354-1355.

[107] Ashley, C.E., Carnes, E.C., Phillipos, G.K., Padilla, D., Durfee, P.N., Brown, P.A., Hanna, T.N., Liu, J., Phillips, B., Carter, M.B., Carroll, N.J., Jiang, X., Dunphy, D.R., Willman, C.L., Petsev, D.N., Evans, D.G., Parikh, A.N., Chackerian, B., Wharton, W., Peabody, D.S., Brinker, C.J., The targeted delivery of multicomponent cargos to cancer cells by nanoporous particle-supported lipid bilyers, Nat. Mater. 10 (2011) 389-397.

[108] Mal, N.K., Fujiwara, M., Tanaka, Y., Photocontrolled reversible release of guest molecules from coumarin-modified mesoporous silica, Nature 421 (2003) 350-353.

[109] Muhammad, F., Guo, M., Qi, W., Sun, F., Wang, A., Guo, Y., Zhu, G., pH-triggered controlled drug release from mesoporous silica nanoparticles via intracellular dissolution of ZnO nanolids, J.Am. Chem. Soc. 133 (2011) 8778-8781.

[110] Tian, B.S., Yang, C., Thermo-sensitive poly(N-isopropylacrylamide)/mesoporous silica nanocomposites as controlled delivery carriers: loading and release behaviors for drug ibuprofen, J. Nanosci. Nanotechnol. 11 (2011) 1871-1879.

[111] Patel, K., Angelos, S., Dichtel, W.R., Coskun, A., Yang, Y.W., Zink, J.I., Stoddart, J.F., Enzyme-responsive snap-top covered silica nanocontainers, J. Am. Chem. Soc. 130 (2008) 2382-2383.

[112] Schlossbauer, A., Kecht, J., Bein, T., Biotin-avidin as a protease-responsive cap system for controlled guest release from colloidal mesoporous silica, Angew. Chem. Int. Ed. Engl. 48 (2009) 3092-3095.

[113] Climent, E., Bernardos, A., Martinez-Manez, R., Maquieira, A., Marcos, M.D., Pastor-Navarro, N., Puchades, R., Sancenon, F., Soto, J., Amoros, P., Controlled delivery systems using antibody-capped mesoporous nanocontainers, J., Am. Chem. Soc. 131 (2009) 14075-14080.

[114] Zhao, Y., Vivero-Escoto, J.L., Slowing, I.I., Trewyn, B.G., Lin, V.S., Capped mesoporous silica nanoparticles as stimuli-responsive controlled release systems for intracellular drug/gene delivery, Expert Opin. Drug Deliv. 7 (2010) 1013-1029.

Chapter III: Assembly and characterization of lipid-lipid binding protein particles

Wei Huang and Chenming Zhang*

Department of Biological Systems Engineering

Virginia Polytechnic Institute and State University

Blacksburg, VA 24061

Journal of Biotechnology, 2011, 154, 60-67

Reuse permission acquired from Elsevier

Abstract

Lipid-protein complexes, lipoplexes, are currently of great interest because of their immunogenic, gene free, and low cost properties. For their applications as potential vaccines, it is critical to display a target protein on the surface of lipoplex particles to allow external interactions to take place. However, how to effectively assemble lipoplexes with target proteins externally accessible is a constant challenge. In this study, human liver fatty acid binding protein 1 (hl-FABP1) was used as a model protein in lipoplex assembly with a non-lipid binding protein, bovine serum albumin (BSA), serving as a comparison. The protein-lipid particles were assembled by four different processes and characterized by dynamic light scattering (DLS), transmission electron microscope (TEM), flow cytometry (FCM), and a modified ELISA. Results indicate that by incubating the target protein with pre-formed liposomes at a temperature higher than all transition temperatures (T_m) of the lipids used through an extended period of time, 1.48×10^{-6} nmol per lipoplex of incorporated proteins can be detected by ELISA and are externally accessible. Additional experiments showed that most of those externally accessible proteins are likely embedded in the lipid bilayer structure and are not subject to dissociation from the lipoplex particles at elevated salt concentrations.

Key words: Liposomes; Lipid binding Proteins; Lipoplexes; Vaccines; Particle Characterization.

1. Introduction

First studied in the 1970s (Curman et al., 1978; Manesis et al., 1978; Strejan et al., 1979; Burakoff et al., 1980; Hale et al., 1981), liposome associated with antigens has attracted much attention especially in the past few years as liposomal vaccines (Ivanoff et al., 1996; Galdiero et al., 1995; Idanpaan-Heikkila et al., 1995; Baca-Estrada et al., 2000; Nagata et al., 2007; Humphries et al., 2006; Gupta et al., 2010; Mohammed et al., 2010) and virus-like particles for viral vaccines (Noad and Roy, 2003). Besides their immunogenic nature and low associated cost, liposomal vaccines and virus-like particles are more importantly gene free. Consequently, they are free of those problems often associated with virus-based vaccines, such as reverting to pathogenic phenotype and causing diseases in vaccinated individuals or even mutating the host gene by insertion, reverse transcription and genetic exchanging (Noad and Roy, 2003). Moreover, due to their high density display of epitopes and protection to embedded antigens, liposomal vaccines often have an enhanced efficiency in boosting both the humoral and cellular immune systems than antigens injected alone (Galdiero et al., 1995; Grgacic and Anderson, 2006). A group of liposomal drug delivery systems, referred to as immunoliposomes, have been shown to navigate themselves to pathological cells due to the specific interaction between antibodies that has been attached to the surface of liposomes and antigen epitopes that are presented by the targeted cells (Wright and Huang, 1989; Park et al., 2004). Similarly, antigens, such as virus envelope proteins, have been assembled with liposomes to help boost their immunogenicity and elicit antibody production in immunized individuals (Parmar et al., 1997; Orellana et al., 1999; Steers et al., 2009).

The assembly of liposomal based vaccines shares much similarity with the assembly of liposomes used as drug delivery vehicles, in which liposomes have been successfully loaded with DNAs, proteins, or other ligands (Kaneda, 2000). However, it is paramount for liposome based particles as vaccines to have exposed immune-eliciting epitopes, and failing to do so could hamper the recognition of the particles by immunocyte-surface receptors and cause a reduction in their immunogenic activities to the host (Pellequer et al., 2004). Studies showed that, unlike antigens encapsulated in liposomes which could only be presented by marcrophages, antigens exposed at the surface could also be presented by B cells to T cells (Szoka, 1992).

So far, many methods have been studied to incorporate liposome with proteins, either before or after the formation of liposomes. In the former case, proteins and lipids mixtures are allowed to go through dialysis (Torchilin et al., 1980) or a size exclusion column (Idanpaan-Heikkila et al., 1995) to form lipoplexes. In the latter case, proteins are coupled to pre-formed liposomes through incubation (Galdiero et al., 1995), some special linkages (Oja et al., 2000), or even transferred directly from tumor cells when the cells and liposomes are incubated together (Sunamoto et al, 1992). However, how effectively proteins are incorporated in lipoplexes and more importantly how effectively the protein is incorporated in the lipid bilayer to be externally accessible have not been well studied. Here we compared four methods to investigate the effect of (1) adding protein prior to or after the formation of liposome and (2) incubation temperature and duration on assembling lipoplexes with externally accessible proteins. A lipid binding protein, recombinant human liver fatty acid binding protein 1 (hl-FABP1, MW ~18.3 kDa) was used in this study with bovine serum albumin (BSA, MW ~66 kDa) as a reference. Size distribution and morphology study of lipoplexes were studied by dynamic light scattering (DLS) and transmission electron microscopy (TEM). Total protein association rate were determined by SDS-PAGE. The externally accessible hl-FABP1 in the lipoplexes was quantified by the combination of flow cytometry (FCM) and a modified ELISA.

2. Materials and Methods

2.1 Materials

All lipid and extrusion system were purchased from Avanti Polar Lipids (Alabaster, AL). hl-FABP1 and BSA were purchased from Cayman Chemical (Ann Arbor, MI) and Jackson ImmunoResearch (West Grove, PA), respectively. Monoclonal anti-hl-FABP1 mouse IgG_1 and horseradish peroxidase conjugated anti-mouse IgG antibody were purchased from R&D systems (Minneapolis, MN). Monoclonal anti-bovine serum albumin in mouse and anti-mouse IgG2a HRP conjugate were purchased from Sigma-Aldrich (St. Louis, MO) and Alpha Diagnostic Intl. (San Antonio, TX) respectively. All SDS gels, sample buffers, running buffers and silver staining kits were purchased from Invitrogen (Carlsbad, CA). Sepharose CL 4B size exclusion resin and XK 16/20 column were purchased from GE Healthcare (Piscataway, NJ). All other chemicals were purchased from Fisher Scientific (Houston, TX) unless otherwise specified.

2.2 Liposomes preparation

Homogeneous unilamellar liposomes were formed by extruding hydrated lipids through a polycarbonate membrane with 100 nm pores 41 times at 60 °C with a mini-extruder system. 1, 2-distearoyl-sn-glycero-3-phosphocholine (DSPC), 1, 2-dioleoyl-sn-glycero-3-phosphoethanolamine (DOPE), and 1, 2-dioleoyl-sn-glycero-3-phospho-L-serine sodium salt (DOPS) were mixed at a mass ratio of 2:5:3 in chloroform. A thin layer of lipid was formed by eliminating chloroform in a fume hood overnight. 0.25 mg lipid cake was fully hydrated with 100 µl hydration buffer at 60 °C with shaking for 1 hour. The hydration buffer contained Tris-HCl (0.05 M, pH 7.8), 0.9% Sodium Chloride, 5% dextrose and 10% sucrose. 1.8 ml glass vials with teflon-lined caps (Wheaton, Millville, NJ) were used as containers for all steps handling with lipid materials.

2.3 Protein-lipid particle assembly

Four different processes were used to prepare the lipoplexes for each protein. The process flow charts are illustrated in Figure 1. Briefly, lipoplexes were assembled by incorporating proteins either before or after the formation of liposomes. In method A, lipid cake was hydrated in 100 µl buffer and extruded through membranes with 100 nm pores to form liposomes. 20 µl protein (50 µg/ml), either hl-FABP1 or BSA, was added to the liposome suspension and incubated for 4 hours at room temperature. Free proteins were eliminated by sepharose CL 4B size exclusion chromatography (SEC) with an XK 16/20 column packed to a bed height of 16 cm on an AKTA explorer 100 system controlled by a UNICORN 3.1 software (GE Healthcare, Uppsala, Sweden). Ultrapure water was used as the mobile phase. Flow rate was 2 ml/min. In method B, 20 µl protein was added to the lipid within the hydration buffer. Extrusion was carried out after 1 hour incubation at 60 °C. Lipoplexes were purified by SEC. Method M is modified from method A, wherein the pre-formed liposome and protein were allowed to incubate overnight at 60 °C. Method N is modified from method B, wherein lipid mixture and protein were incubated overnight at 37 °C. Subscript 'f' and 'b' are used to represent lipoplexes prepared with hl-FABP1 or BSA, respectively, and 'l' represents bare liposome samples. For example, M_f is an hl-FABP1 lipoplex sample prepared by method M. Unless otherwise mentioned, all lipoplex samples were purified by SEC prior to analyses. All experiments were repeated multiple times.

2.4 Characterization of lipoplex size by DLS

Size distributions of all lipoplexes were analyzed on a Zetasizer Nano ZS (Malvern Instruments, Southborough, MA). Samples were freshly made before use by adding aliquots of lipoplexes to 0.01 M sodium chloride buffer to make a solution with a lipid concentration of 0.01 mg/ml. During the test, samples were injected into a disposable capillary cell DTS1060 (Malvern Instruments, MA) and loaded onto the analyzer. Measurements were taken at 25 °C with a material refraction index of 1.33, and a viscosity of 0.8872 cp. For each sample, three measurements were taken, and each measurement contains fifteen counts.

2.5 Characterization of liposome morphology by TEM

Lipoplex morphology was studied by TEM. 100 µl of a lipoplex sample was fixed in osmium tetroxide three days before the following steps. Samples were embedded in water soluble melamine resin, so an approximately 90 nm ultrathin sectioning could then be performed. Negative staining was conducted with 2% uranyl acetate. Images were taken by a Zeiss 10CA Transmission Electron Microscope equipped with AMT Advantage GR/HR-B CCD Camera System at Virginia-Maryland Regional College of Veterinary Medicine.

2.6 Protein-liposome association efficiency analysis

Unattached free proteins in crude lipoplex samples were detected by SDS-PAGE analyses. It is worth nothing that lipoplexes will not disintegrate with the presence of up to 5% of SDS in the SDS running buffer (data not shown). Similar experiments by Pappalardo et al. (2009) also showed the stability of lipoplexes with the presence of Tween-20. Therefore, during SDS-PAGE (1% of SDS in the sample buffer), proteins integrated into lipoplexes will not be able to migrate into the gels, and only the unassociated protein can. Briefly, crude sample M_f, N_f, A_f, B_f, M_b, N_b, A_b and B_b were ran

on a 4-12% Bis-Tris gel (Invitrogen, Carlsbad, CA). Silver staining was performed, and the intensities of the protein bands were determined by a Bio-Rad ChemiDoc XRS imager and analyzed by the software Quantity One (Bio-Rad, Hercules, CA). A standard curve was generated by running different dilutions of a respective protein on the same gel to assist with protein quantification. The concentration of lipoplex particles was determined by a FCM test with the assistance of countbright absolute counting beads (Invitrogen, Carlsbad, CA). Lipoplexes was labeled by integrating 15% (lipid mass) nitrobenzoxadiazole (NBD) labeled DOPE into the lipid mixture.

2.7 Characterization of externally accessible proteins in lipoplexes by ELISA assay

The external accessibility of a target protein incorporated in lipoplexes was determined by a modified ELISA test. Briefly, 96 well microtiter plates (Greiner bio-one, Monroe, NC) were coated with duplicated samples of blank control, hl-FABP1, BSA, purified samples and bare liposomes, all in 0.05 M carbonate-bicarbonate, pH 9.6; each well was blocked with Tris buffered saline with Tween 20 (TBST, 50mM Tris, 0.14 M NaCl, 0.05% Tween 20, pH 8.0) containing 5% blotting grade blocker non-fat dry milk (Bio-Rad, Hercules, CA); diluted monoclonal anti-hl-FABP1 mouse IgG_1 (R&D systems, Minneapolis, MN) and monoclonal anti-bovine serum albumin produced in mouse (Sigma-Aldrich, St. Louis, MO) were added to incubate with hl-FABP1 and BSA attached lipoplexes, respectively; then horseradish peroxidase conjugated anti-mouse IgG antibody (R&D systems, Minneapolis, MN) and anti-mouse IgG_{2a} HRP conjugate (Alpha Diagnostic intl, San Antonio, TX) were added as a secondary antibody for hl-FABP1 and BSA attached lipoplexes, respectively; finally, tetramethyl benzidine (TMB) peroxidase (Bethyl, Montgomery, TX) was used as the substrate. Between every two steps, each well was gently washed 5 times with TBST. Absorbances were measured on a Synergy HT Multi-Mode Microplate Reader (Bio Tek, Winooski, VT) at 450 nm and converted to protein concentrations using a standard curve developed from dilutions of hl-FABP1 or BSA samples, respectively.

3. Results and Discussion

3.1 Size distribution of lipoplexes

The size distribution of lipoplexes assembled by the four processes (Fig. 1) was analyzed by DLS. Size distributions of all samples seem identical regardless of the assembly method or protein used. Result of freshly made M_f and M_f after 30 days of storage at room temperature were shown in Figure 2A and 2B as a pair of representatives. Narrow distributions with mean diameters of 96 nm and 67.5 nm were observed respectively. The decrease in size after storage is likely due to hydrolytic degradation of phospholipids (Grit et al., 1993). Moreover, purification by SEC clearly reduced the particle size distribution of each sample by removing very large and small particles, which were present in the crude samples (Fig. 2C). Aggregation (Chapman, 1984) and hydrolytic degradation (Grit et al., 1993) are likely responsible for the broad size distribution of the crude samples.

3.2 Morphology study of lipoplexes by TEM

TEM images of negatively stained lipoplexes were taken for morphology study. In Fig. 3A, lipoplexes are shown as gray spheres in contrast to the background. Fig. 3B shows the corss-section view of a liposome particle through an ultrathin sectioning process, which cuts a liposome particle in the middle. The particle shows a gray lipid bilayer ring with dark inside background. No difference was observed between samples prepared by different methods. Proteins could not be resolved at this magnification level.

3.3 Study of protein-liposome association efficiency

Unattached free proteins in lipoplex samples were detected by SDS PAGE. The silver stained gel is shown in Fig. 4A. The unassociated protein concentrations in various samples and the standard curves are shown in Fig. 4B and 4C. The calculated associated protein concentrations are shown in Table 1. Despite the error associated with this method for protein concentration determination, data in Table 1 can be used qualitatively to compare the protein association efficiency between the two proteins and among the different methods used for lipoplex assembly. As expected, hl-FABP1 has a greater tendency than BSA to be incorporated into lipoplexes, and the amount of protein incorporated into the lipoplexes is method dependent. Except method A, methods B, M, and N couple hl-FABP1 efficiently to liposomes, and the overall association efficiency follows the order of $B_f > M_f > N_f > A_f$. In general, extruding protein-lipid mixture (samples N_f and B_f) seems to be better than incubating proteins with pre-formed liposomes, and the processes would allow proteins not only to associate with the lipid membrane but also to be encapsulated in liposomes and thus have a higher total association efficiency. For processes A and M, the phospholipid bilayer in the pre-formed liposomes will deter the penetration of proteins into the inside cavity of the liposomes and result in a low overall protein association efficiency.

Thus, if the overall protein association efficiency is the major concern, such as for the cases where the assembled lipoplexes are intended to be used for drug delivery (Lee and Yuk, 2007), methods N and B will be the methods of choice. Meyer et al. (1994) and Anderson et al. (1994) used similar methods to encapsulate various proteins in liposome, and the protein-liposome association efficiency, as also shown in our results, was apparently highly dependent on the assembly process and the target protein to be encapsulated.

3.4 Study of externally accessible proteins in assembled lipoplexes

Concentrations of the target protein in assembled lipoplexes that are externally accessible were detected by a modified ELISA method. As noted earlier, the presence of Tween 20 (0.05%) will not disrupt the lipoplex particles during the assay to affect the validity of ELISA (Pappalardo et al., 2009). The absorbance signals and converted concentrations of externally accessible protein (per volume of sample) are shown in Fig. 5A and 5B, respectively. Fig. 5C and 5D show the conversion of light absorbance at OD 450nm to protein concentration with the standard curve used for hl-FABP1 and BSA, respectively. The fact that all hl-FABP1 samples have substantially higher signals than BSA samples in terms of externally accessible proteins can be contributed to the dramatically different nature of the two proteins. The fatty acid binding protein, hl-FABP1, has a β barrel rich domain that has a strong affinity to phospholipids (Hanhoff et al., 2002). Also, its small size enables the protein to more easily arrange itself inside the lipid bilayer at a high density with its hydrophobic domain inserting into the anhydrous zone of fatty acid chains of the lipids (Fig. 5B). In contrast, although BSA has some affinity to lipids (Yokouchi et al., 2001), its relatively large size introduces much spatial strains that limit a high density packing (Fig. 5B).

Externally accessible (exposed) protein per lipoplex was determined as the ratio of proteins detected by ELISA to the number of lipoplexes (data not shown) determined by FCM. The calculated concentrations of externally accessible protein on per particle base are shown in Table 2. Evidently, samples M_f and A_f have a higher externally accessible protein concentration than that of N_f and B_f. For a lipid binding protein such as hl-FABP1,

incubating the protein with pre-formed liposomes is more efficient to incorporate externally accessible proteins into lipoplexes than to add hl-FABP1 before extrusion. However, the trend is not readily observed for BSA formed lipoplexes likely due to its large size and relatively lower propensity to interact with lipids.

By combining with the protein association efficiency result, it can be found that although the total protein incorporated into liposomes by method N or B is quite high (Table 1), only low percentage of the protein was found to be externally accessible (Fig. 5E). This indicates methods N and B may be suitable for protein encapsulation rather than assembling lipoplexes with externally accessible proteins. Method M assembled the highest concentration of hl-FABP1 (1.48E-06 nmol/lipoplex, Table 2) in the lipoplexes that is externally accessible. This is understandable since the protein was incubated with preformed liposomes for an extended period of time at a temperature above the T_m of all three lipids used. Evidently, under such conditions, protein molecules can readily penetrate the lipid bilayer, which has a high permeability (Magin and Niesman, 1984).

Moreover, method A, in which the protein was incubated with preformed liposomes at room temperature, is also of interest because of the high concentration of externally accessible proteins in the lipoplexes (Table 2). Based on the results shown in Fig. 5E, although method A does not pack much protein in the lipoplexes, a large portion of the proteins (74%) are externally accessible. This indicates that under room temperature, it is difficult for proteins to penetrate through the lipid bilayer structure of the liposomes to be encapsulated. Thus, it may be advantageous to use this method for temperature sensitive proteins, because, unlike method M, it avoids a long period of incubation at high temperature.

Compared with samples prepared by method M, the high concentration of externally accessible proteins in lipoplexes assembled by method A is somewhat a surprise, since at room temperature it is considered difficult for the proteins to insert themselves into preformed lipid bilayers. One possible explanation is that proteins may simply bind to the outer surface of the liposomes with electrostatic interactions without being incorporated into the lipid bilayer structure. We thus postulated that the structure of the lipoplex particles may be different between samples prepared by method A and M. To test this hypothesis, M_f and A_f were treated with solutions with different salt concentration (0 M, 0.25 M, 0.5 M, 1.0 M NaCl) for 10 min at room temperature. After treatment, samples were run through sepharose CL-4B size exclusion column to remove possible disassociated proteins. Concentrations of hl-FABP1 remaining on the surface of particles were tested with the modified ELISA. As shown in Fig. 6A, the concentrations of externally accessible hl-FABP1 in both M_f and A_f decreased with increasing concentrations of salt. This indicates that some hl-FABP1 did dissociate from the lipoplexes, and those released proteins were likely bound to liposomes through electrostatic interactions. However, the ratios of hl-FABP1 remaining on lipoplex particles after salt treatment are significantly different as shown in Fig. 6B. It is obvious that hl-FABP1 molecules in sample M_f were less affected by the addition of salt. Even if treated with 1.0 M NaCl, about 85% hl-FABP1 remains in lipoplexes prepared by method M (sample M_f), in contrast to the 50% for A_f. This suggests that most exposed proteins in M_f were imbedded in the lipid bilayer, which would not be easily removed by increased salt concentration, and a large portion of the externally accessible proteins in A_f was not embedded into the lipid bilayer but instead was attached to the liposome surface through electrostatic interactions.

Comparing method M and A, it is apparent that the temperature under which the pre-formed liposomes and the target protein was incubated is the most significant factor affecting how the protein is incorporated into the lipid bilayer structure. At elevated temperature, particularly when the temperature is above the T_m of all lipids used (as in method M), liposomes begin to melt and become accessible for the integration of other molecules (Oja et al., 2000) and allow insertion and penetration of hl-FABP1 proteins. The extended incubation time likely amplified the effect of the high temperature. However, more experiments need to be conducted to study the exact influence of temperature and time during incubation on the protein incorporation and encapsulation for lipoplex assembly.

4. Conclusions

Lipopexes with externally accessible proteins could be assembled by incubating the lipid binding protein (hl-FABP1 in this case) with pre-formed liposomes. Large portion of incorporated hl-FABP1 was found to be externally accessible when the processing temperature was held at room temperature. Elevating incubation temperature to above the T_m of all containing lipids and extending the incubation time could increase the amount of surface exposed protein to as high as 2.75 μg/ml (or 1.48×10^{-6} nmol/particle). However, the structure of the lipoplexes is highly dependent on the processing conditions, particularly the temperature. Under room temperature, the protein is mainly attached to the liposomes via electrostatic interactions, and under elevated temperature, the externally accessible proteins are embedded in the lipid bilayer structure similar to common biological membranes. For lipoplexes assembled by extruding lipid protein mixture, most of incorporated proteins were encapsulated rather than being presented on the surface. This study shows that depending on the thermal stability of a target protein and how the protein is to be presented by the assembled lipoplexes (encapsulation vs. surface display), a processing method needs to be selected accordingly to assure successful production of the desired lipoplexes.

Acknowledgements

This work was supported primarily by the Institute for Critical Technology and Applied Science (ICTAS) at Virginia Tech. Authors gratefully acknowledge Dr. Richey M. Davis for his support in particle size experiments, Kathy Lowe for her technical assistance with TEM imaging, and Melissa Makris for the assistance with flow cytometry tests.

References

Anderson, P.M., Hanson, D.C., Hasz D.E., Halet, M.R., Blazar, B.R., Ochoa, A.C., 1994. Cytokines in liposomes; preliminary studies with IL-1, IL-2, IL-6, GM-CSF and Interferon-g. Cytokine 6, 92–101.

Baca-Estrada, M.E., Foldvari, M., Babiuk, S.L., Babiuk, L.A., 2000. Vaccine delivery: lipid-based delivery systems. J. Biotechnol. 83, 91–104.

Burakoff, S.J., Engelhard, V.H., Kaufman, J., Strominger, J.L., 1980. Induction of secondary cytotoxic T lymphocytes by liposomes containing HLA-DR antigens. Nature (London) 283, 495-497.

Chapman, D., 1984. Physicochemical properties of phospholipids and lipid-water systems, in: Gregoriadis, Gregory (Eds.), Liposome Technology. Vol. II, pp. 2-18.

Curman, B., Ostberg, L., Pettersson, P.A., 1978. Incorporation of murine MHC antigens into liposomes and their effect in the secondary mixed lymphocyte reaction. Nature (London) 272, 545-547.

Galdiero, F., Carratelli, CR., Nuzzo, I., Bentivoglio, C., De Martino, L., Folgore, A., Galdiero, M., 1995. Enhanced celluar response in mice treated with a Brucella antigen-liposome mixture. FEMS. Immunol Med. Microbiol. 10, 235-244.

Grgacic, E.V.L., Anderson, DA., 2006. Virus-like particles: Passport to immune recognition. Methods. 40, 60-65.

Grit, M., Zuidam, N.J., Underberg, W.J.M., Crommelin, D.J.A., 1993. Hydrolysis of partially saturated egg phosphatidylcholine in aqueous liposome dispersions and the effect of cholesterol incorporation on hydrolysis kinetics. J. Pharm. Pharmacol. 45, 490-495.

Gupta, P.N., Pattani, A., Malcolm, R.K., Curran, R.M., Andrews, G., 2010. Development of liposome-based freeze-dried rods for vaginal vaccine delivery against HIV-1. J. Control. Release 148, e105–e110.

Hale, A.H., Evans, D.L., McGee, M.P., 1981. H-2 antigens incorporated into phospholipid vesicles interact specifically with allogeneic cytotoxic T lymphocytes. Cell Immunol. 63, 42-56.

Hanhoff, T., Lucke, C., Spener, F., 2002. Insights into binding of fatty acids by fatty acid binding proteins. Mol. Cell Biochem. 239, 45-54.

Humphries, H.E., Williams, J.N., Blackstone, R., Jolley, K.A., Yuen, H.M., Christodoulides, M., Heckels, J.E., 2006. Multivalent liposome-based vaccines containing different serosubtypes of PorA protein induce cross-protective bactericidal immune responses against Neisseria meningitides. Vaccine 24, 36-44.

Idanpaan-Heikkila, I., Muttilainen, S., Wahlstrom, E., Saarinen, L., Leinonen, M., Sarvas, M., Makela, P.H., 1995. The antibody response to a prototype liposome vaccine containing Neisseria meningitides outer membrane protein P1 produced in Bacillus subtilis. Vaccine 13(16):1501-1508.

Ivanoff, N., Phillips, N., Schacht, A.-M., Heydari, C., Capron, A., Riveau, G., 1996. Mucosal vaccination against schistosomiasis using liposome-associated Sm 28 kDa glutathione S-transferase. Vaccine 14(12), 1123-1131.

Kaneda, Y., 2000. Virosomes: evolution of the liposome as a targeted drug delivery system. Adv. Drug Deliv. Rev. 43, 197-205.

Lee, K.Y., Yuk, S.H., 2007. Polymeric protein delivery systems. Prog. Polym. Sci. 32, 669–697.

Magin, R.L., Niesman, M.R., 1984. Temperature-dependent permeability of large unilamellar liposomes. Chem. Phys. Lipids 34(3), 245-256.

Manesis, E.K., Cameron, C.H., Gregoriadis, G., 1978. Incorporation of hepatitis B surface antigen into liposomes. Biochem. Soc. Trans. 6, 925-928.

Meyer, J., Whitcomb, L., Collins, D., 1994. Efficient encapsulation of proteins within liposomes for slow release in vivo. Biochem. Biophys. Res. Commun. 199, 433-438.

Mohammed, A.R., Bramwell, V.W., Kirby, D.J., McNeil, S.E., Perrie, Y., 2010. Increased potential of a cationic liposome-based delivery system: Enhancing stability and sustained immunological activity in pre-clinical development. Eur. J. Pharm. Biopharm. 76, 404–412.

Nagata, T., Toyota, T., Ishigaki, H., Ichihashi, T., Kajino, K., Kashima, Y., Itoh, Y., Mori, M., Oda, H., Yamamura, H., Taneichi, M., Uchida, T., Ogasawara, K., 2007. Peptides coupled to the surface of a kind of liposome protect infection of influenza viruses. Vaccine 25, 4914-4921.

Noad, R., Roy, P., 2003. Virus-like particles as immunogens. TRENDs Microbiol. 11(9), 438-444.

Oja, C., Tardi, P., Schutze-Redelmeier, M.-P., Cullis, P.R., 2000. Doxorubicin entrapped within liposome-associated antigens results in a selective inhibition of the antibody response to the linked antigen. Biochim. Biophys. Acta. 1468, 31-40.

Orellana, A., Mottershead, D., van der Linden, I., Keinanen, K., Oker-Blom, C., 1999. Mimicking rubella virus particles by using recombinant envelope glycoproteins and liposomes. J. Biotechnol. 75, 209-219.

Pappalardo, J.S., Quattrocchi, V., Langellotti, C., Giacomo, S.D., Gnazzo, V., Olivera, V., Calamante, G., Zamorano, P.I., Levchenko, T.S., Torchilin, V.P., 2009. Improved transfection of spleen-derived antigen-presenting cells in culture using TATp-liposomes. J. Control. Release 134, 41-46.

Park, J.W., Benz, C.C., Martin, F.J., 2004. Future directions of liposome- and immunoliposome-based cancer therapeutics. Semin. Oncol. 31(Suppl 13), 196-205.

Parmar, M.M., Blake, M.S., Madden, T.D., 1997. Biophysical and antigenic characterization of gonococcal protein I incorporated into liposomes. Vaccine 15(15), 1641-1651.

Pellequer, Y., Ollivon, M., Barratt, G., 2004. Formulation of liposomes associated with recombinant interleukin-2: effect on interleukin-2 activity. Biomed. Pharmacothe. 58, 162-167.

Steers, N.J., Peachman, K.K., McClain, S., Alving, C.R., Rao, M., 2009. Liposome-encapsulated HIV-1 Gag p24 containing lipid A induces effector CD4+T-cells, memory CD8+ T-cells, and pro-inflammatory cytokines. Vaccine 27, 6939–6949.

Strejan, G.H., Smith, P.M., Grant, C.W., Sarlan, D., 1979. Naturally occurring antibodies to liposomes. Rabbit antibodies to sphingomyelin containing liposomes before

and after immunization with unrelated antigens. J. Immunol. 123, 370-378.

Sunamoto, J., Noguchi, T., Sato, T., Akiyoshi, K., Shibata, R., Nakayama, E.-I., Shiku, H., 1992. Direct transfer of tumor surface antigenic protein (TSAP) from tumor cell to liposome for making liposomal vaccine. J. Control. Release 20, 143-154.

Szoka, F.C. Jr., 1992. The macrophage as the principal antigen-presenting cell for liposome-encapsulated antigen. Res. Immunol. 143, 186-188.

Torchilin, V.P., Omel'yanenko, V.G., Klibanov, A.L., Mikhailov, A.I., Gol'Danskii, V.I., Smirnov, V.N., 1980. Incorporation of hydrophilic protein modified with hydrophobic agent into liposome membrane. Biochim. Biophys. Acta. 602, 511-521.

Wright, S., Huang, L., 1989. Antibody-directed liposomes as drug-delivery vehicles. Adv. Drug Deliv. Rev. 3(3), 343-389.

Yokouchi, Y., Tsunoda, T., Imura, T., Yamauchi, H., Yokoyama, S., Sakai, H., Abe, M., 2001. Effect of adsorption of bovine serum albumin on liposomal membrane characteristics. Colloids Surf. B: Biointerfaces 20, 95-103.

Table 1. Calculated associated protein concentration.

Free protein concentrations were determined by SDS-PAGE. Associated protein concentration = (total added protein - the amount of free protein) / the corresponding sample volume. M, N, A, and B represent the method for lipid-protein assembly; subscription “f” or “b” represents FABP1 and BSA, respectively.

Sample	Associated protein concentration (μg/ml)
M_f	8.531
N_f	7.390
A_f	2.561
B_f	8.898
M_b	1.053
N_b	1.543
A_b	0.243
B_b	0.711

Table 2. Dependence of externally accessible protein concentration on protein and processing method.

Externally accessible protein concentration and particle quantity were determined by ELISA and FCM, respectively. Free unassociated proteins were eliminated by a Sepharose CL 4B size exclusion column prior to ELISA.

Sample	Exposed protein/lipoplex (nmol/EA)
M_f	1.48E-06
N_f	8.04E-07
A_f	1.03E-06
B_f	4.84E-07
M_b	5.13E-08
N_b	1.78E-07
A_b	3.21E-08
B_b	2.65E-08

Figure Captions

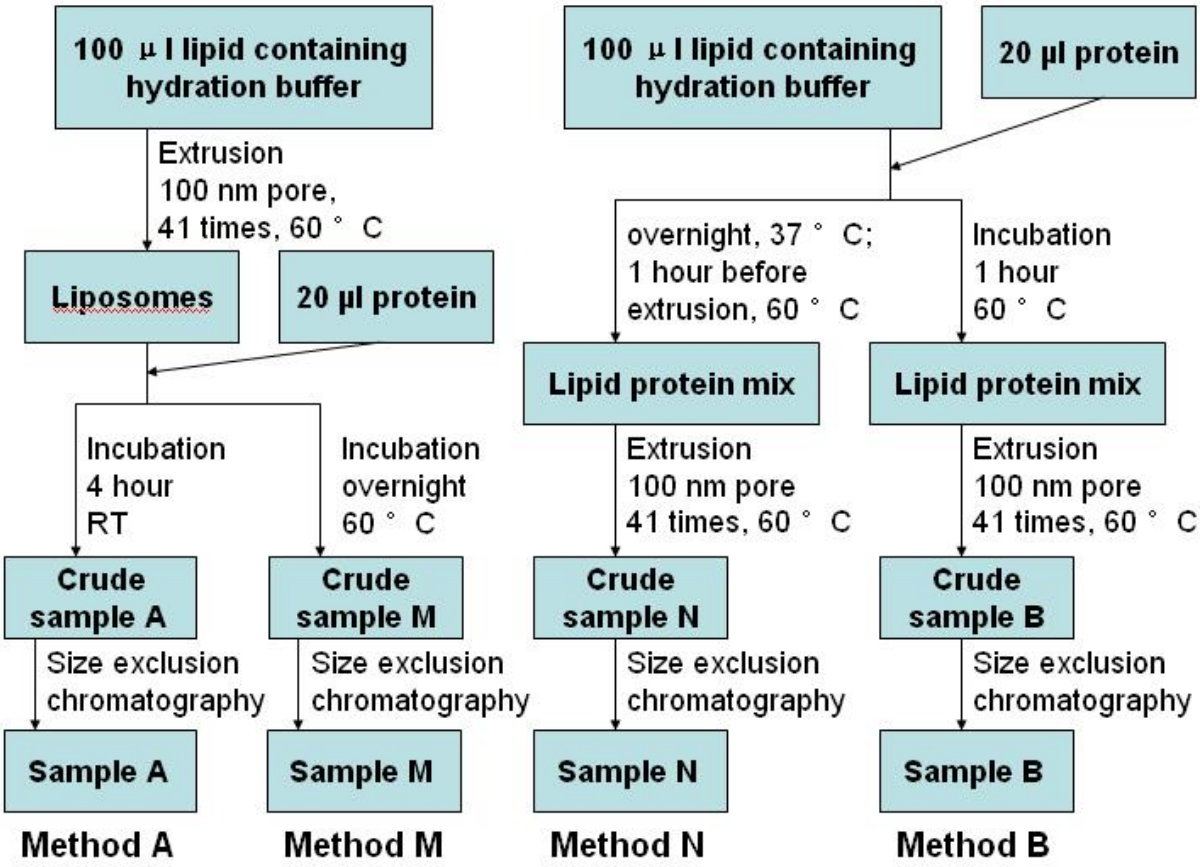

Figure 1. Flow chart of sample processing.

Protein used was either 50 µg/ml of hl-FABP1 or BSA. 0.25 µg lipid mixture consisting of DSPC, DOPE, DOPS at a mass ratio of 2:5:3 was dissolved in 100 µl hydration buffer of Tris-HCl (0.05 M, pH 7.8), 0.9% Sodium Chloride, 5% dextrose and 10% sucrose. 250 µl gas-tight glass syringes and 100 nm pore size membranes were used in all experiments.

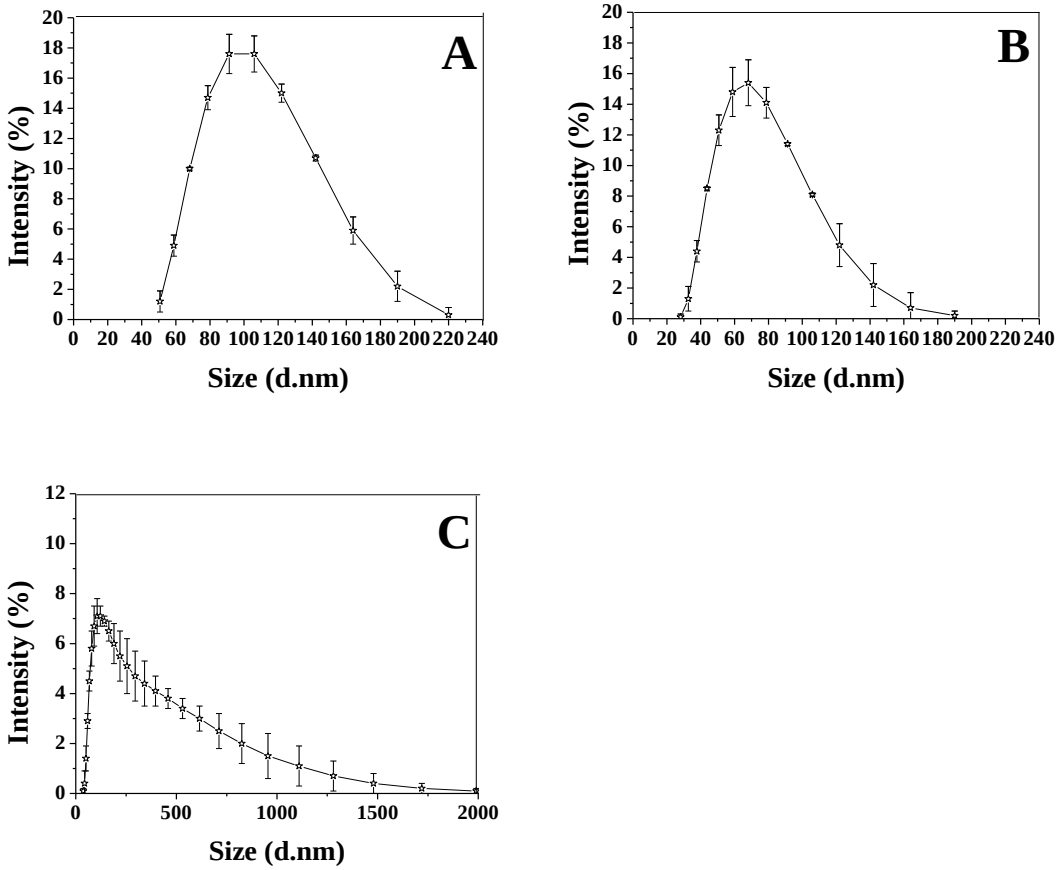

Figure 2. Size distribution of lipoplexes.

(A) M_f; (B) M_f after 30 days of storage under room temperature; (C) crude M_f before SEC purification. Data were obtained by DLS and analyzed by Dispersion Technology Software (Malvern Instruments, Southborough, MA). Sizes of spherical lipoplexes are given in diameters (Mean ± S.D., n=45).

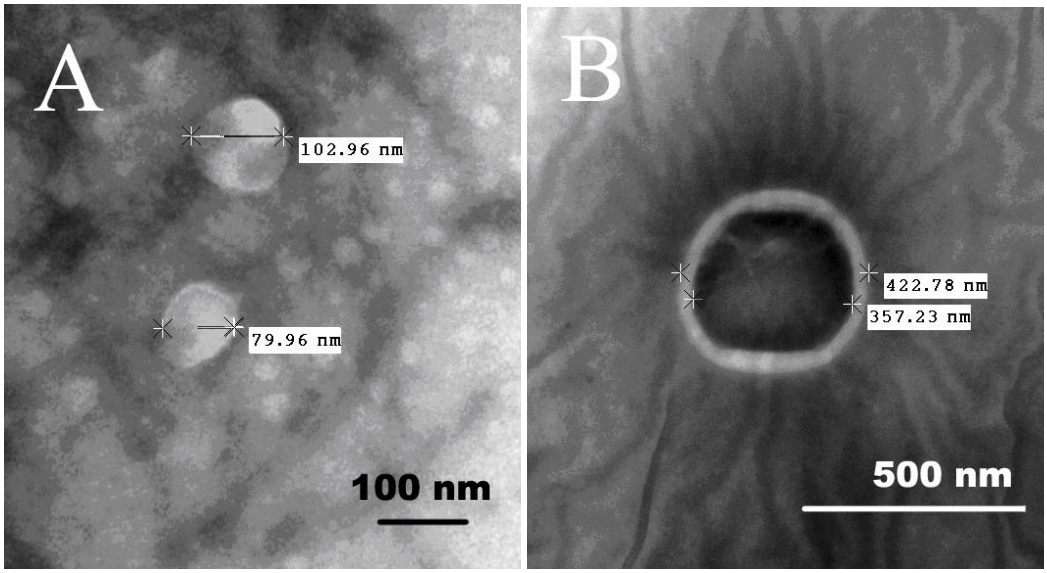

Figure 3. Negative staining TEM images of ultra thin sectioned lipoplexes.

(A) M_f, Direct magnification: 100,000x. Scale bar indicates 100 nm; (B) cross-section view of a single lipoplex of M_f. Direct magnification: 50,000x. Scale bar indicates 500 nm.

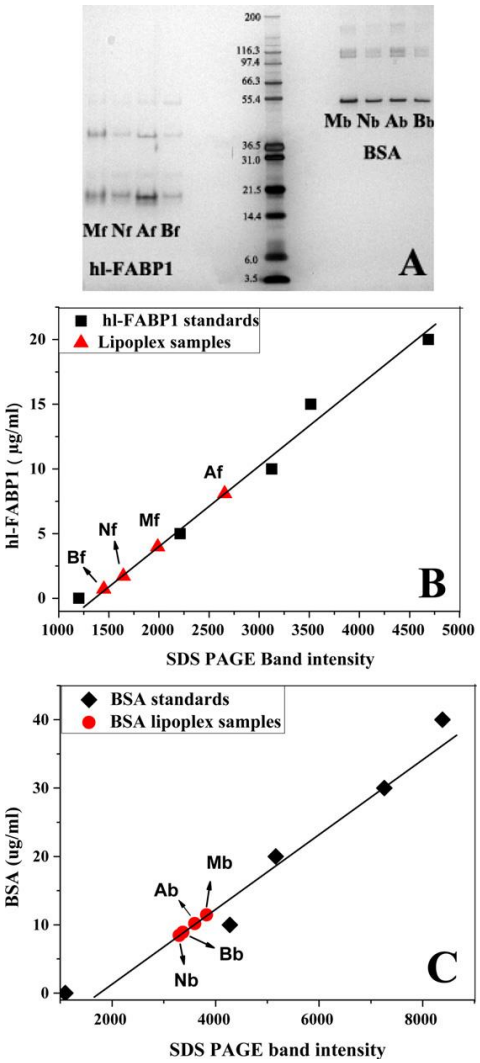

Figure 4. Silver stained SDS-PAGE of crude lipoplexes samples for free unassociated protein measurement.

(A) Silver stained SDS-PAGE of all crude samples; (B) concentrations of free hl-FABP1 in samples (triangles) made from four methods versus standards (squares); (C) concentration of free BSA in each sample (circles) versus standards (diamonds). Loading volume was 10 µl. Electrophoresis was run under a denatured condition. 4-12% Bis-Tris gel was used with SDS sample buffer and MES SDS running buffer. No SEC purification was applied to any sample.

For more accurate quantification, in (B) and (C), samples and the corresponding standards were run and stained on the same gel.

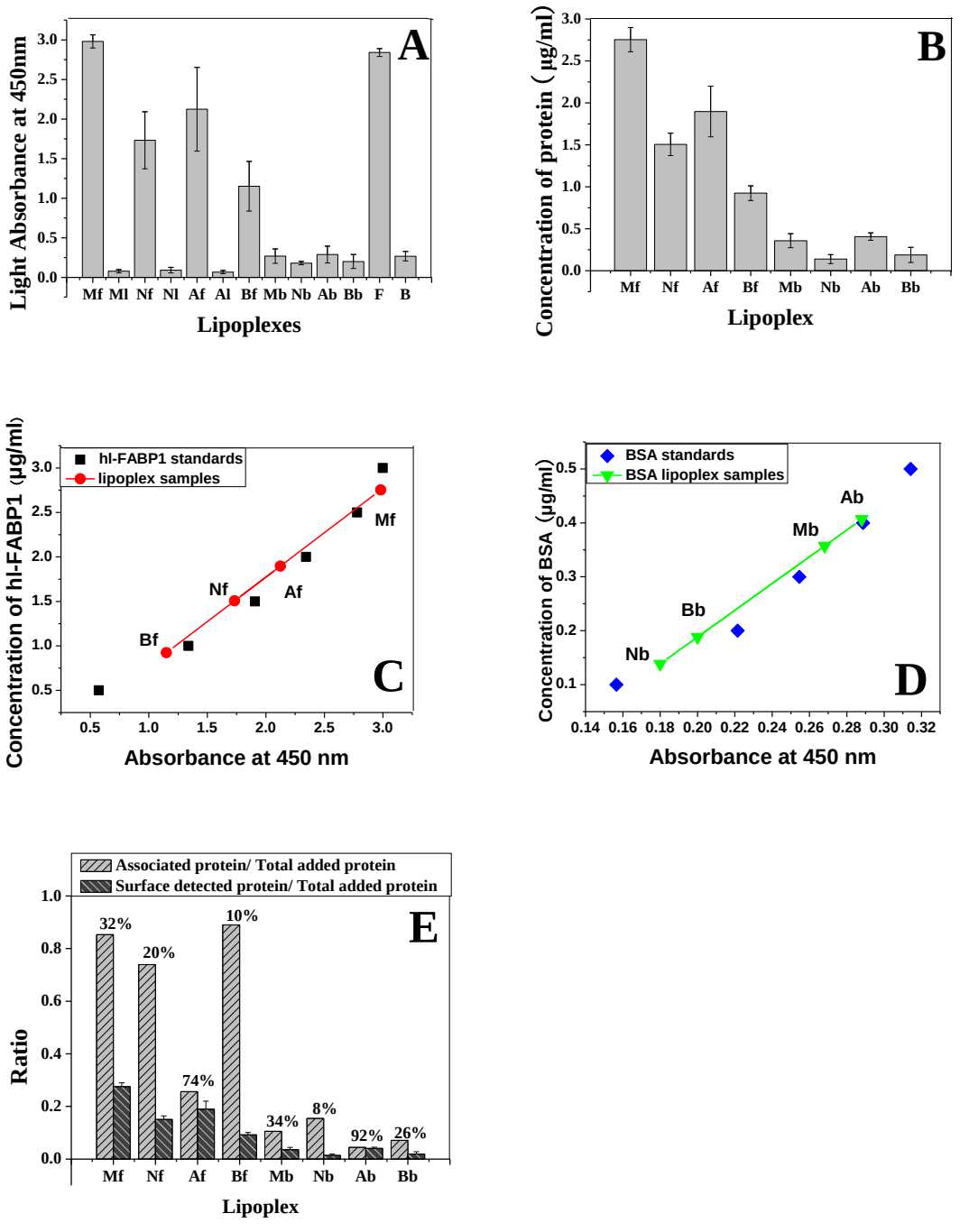

Figure 5. ELISA test of externally accessible protein on lipoplexes.

(A), light absorbance of hl-FABP1 and BSA samples (OD 450 nm); M_l, N_l, A_l were liposome samples made by method M, N and A, respectively. F and B are positive controls. F indicates

hl-FABP 1 protein (2.5μg/ml), and B indicates BSA protein (0.4μg/ml). (B), converted concentrations of protein molecules on surface of lipoplexes (μg/ml); (C) and (D), conversion of absorbance signals to protein concentrations using a standard curve for hl-FABP1 and BSA, respectively. (E) ratios of associated protein / total added protein and surface detected protein / total added protein; ratios of surface detected protein / associated protein are given as the percentages shown above each column. Results are given as mean ± S.D., n=6.

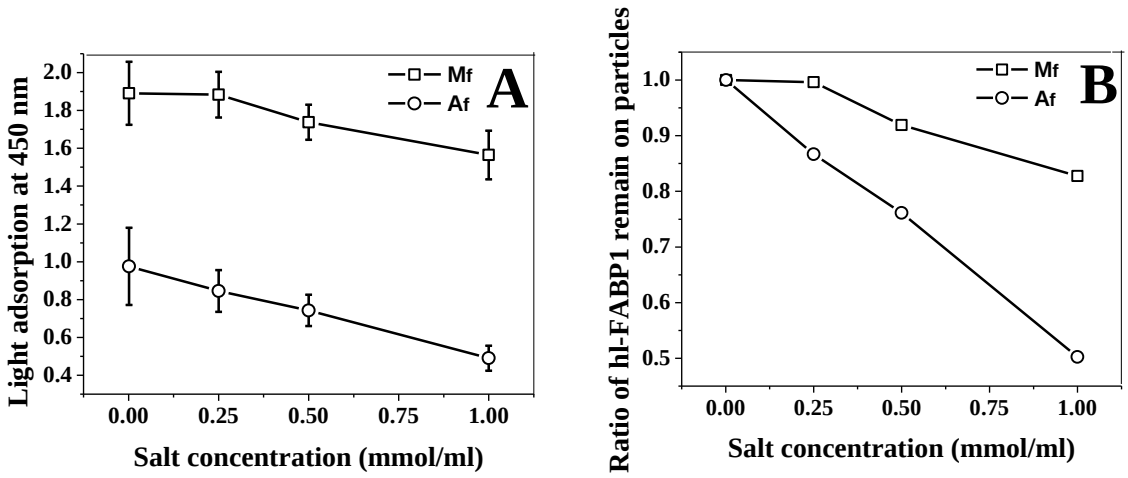

Figure 6. Effect of salt concentration on surface protein in lipoplexes.

(A) Absorbance at 450 nm of sample M_f and A_f treated with different concentrations of sodium chloride. (B) Percent of hl-FABP1 remaining on the surface of particles after salt treatment.

Chapter IV: Assembly of Single Wall Carbon Nanohorn Supported Liposome Particles

Wei Huang,[1] Jianfei Zhang,[2] Harry C. Dorn,[2] David Geohegan,[3] Chenming Zhang[1]*

1. Department of Biological Systems Engineering

2. Department of Chemistry

Virginia Tech

Blacksburg, VA 24061

3. Center for Nanophase Materials Sciences and SHaRE Facilities,

Oak Ridge National Laboratories, Oak Ridge, TN, 37831

Bioconjugate Chemistry, 2011, 22, 1012-1016

Abstract

Nanoparticle supported liposomes can be a promising platform for drug delivery, vaccine development, and biomedical imaging. Single wall carbon nanohorns are a relatively new carbon nanomaterial, and they could be used as carriers of drug and imaging reagents. Assembling lipids around carbon nanohorns would confer this nanomaterial much broader applications such as vaccine development and target drug delivery by embedding a target protein or immunogenic protein in the lipid bilayer structure. Here, we show the assembly of functionalized single wall carbon nanohorns ($-CH_2-CH_2-COOH_x$, ~100 nm) with positively charged lipids through a freeze and thaw cycle. The assembled complex particles can be readily separated from individual nanohorns or liposomes under specific centrifugation conditions. The results from transmission electronic microscopy, flow cytometry through nitrobenzoxadiazole labeled lipids, and zeta potential analysis clearly show that the nanohorns are encapsulated by liposomes with a median size of ca. 120 nm.

Liposomes and many types of nanoparticles have been studied as potential drug delivery vehicles. Despite the similarities that they both can have a desirable loading capacity and release the content at a controlled rate at a specific location when attached with targeting ligands, liposomes and nanoparticles are complementary delivery systems because: (1) nanoparticles tend to have a longer half-life during the circulation in blood and the extravasations from plasma to the tumor cells;[1,2] (2) liposomes provide a better chance to deliver drugs across cell membrane at the targeting site; and (3) they have different drug preferences, loading, and releasing chemistry.[1,2] However, the combination of the two types of particles could possess unique advantages over any of the particles alone. Nanoparticle supported liposomes (NsLs) have recently been assembled and described.[3] Nanoparticles usually stabilize the liposomes through electrostatic interactions and may also increase the concentrations of polyethylene glycol (PEG) that can be attached to the surface of liposomes, resulting in NsLs, when intravenously injected, with improved ability to evade clearance by the reticuloendothelial system (RES).[3] NsLs could have a large loading capacity and a desirable controlled release rate depending on the large adsorption area and special pore surface chemistry of the encapsulated nanoparticle.[4] Moreover, a targeting ligand attached liposome could transport

nanoparticles into cells through receptor mediated endocytosis. This is critical when large molecule drugs or therapeutic gene is to be released in the cytoplasm.[5]

In this report, functionalized (carboxylated) carbon single wall nanohorns, SWNH $(-CH_2-CH_2-COOH)_x$, were prepared to provide SWNHs with hydrophilic surface for encapsulation into the liposomes. The SWNH$(-CH_2-CH_2-COOH)_x$ are nontoxic[6,7] nanoparticle aggregates of single graphene tubules and are spherical dahlia-like shaped with a narrow diameter range reported as 80-100 nm.[8] The surface area of SWNHs range from 300 to 1000 m^2/g.[9] The functionalization process introduces mesoporous structures on the SWNHs, and consequently drug molecules could not only bind to the surface but also to the inner graphene wall. Researches also showed that molecules that have stacking aromatic rings once diffused into SWNHs will release in a slow and stable manner.[10]

Single wall nanohorns were synthesized by Nd: YAG laser vaporization of graphite rods in an argon atmosphere at 1100 °C as described in detail elsewhere.[11,12] Functionalized SWNH$(-CH_2-CH_2-COOH)_x$ with carboxyl groups were obtained by high speed vibration milling method as previously described.[13] Briefly, a mixture of nanohorns and succinic acid acyl peroxide (1:100 in mass) was vigorously shaken in a stainless steel capsule for 1.5 h. The grinded ultrafine powder was washed three times with acetone and centrifuged to collect the sediment. 20 min sonication was performed to dissolve the sediment in ultrapure water yielding solutions of the SWNH$(-CH_2-CH_2-COOH)_x$. On the other hand, cationic liposomes were made by extruding 0.4 mg hydrated 1,2-dioleoyl-3-trimethylammonium-propane (DOTAP) lipid film through polycarbonate membranes with pore sizes of 100 nm. The hydration buffer contains 0.9 NaCl, 5% dextrose and 10% sucrose in Tris-HCl buffer with a pH at 7.4. SWNH$(-CH_2-CH_2-COOH)_x$ were briefly sonicated to break up aggregates and incubated with freshly made cationic liposomes. Particles of these functionalized SWNHs and liposome were quantified by flow cytometer (FCM) and the concentrations were both optimized to ~100 particles/μl. After gently homogenizing the optimized samples at a volume ratio of 1:10 SWNH$(-CH_2-CH_2-COOH)_x$: liposomes, a ratio chosen to ensure there are excessive liposomes for functionalized SWNHs. Three freeze and thaw cycles were applied using liquid nitrogen and warm water bath. Samples were then centrifuged under 10,000 rcf for 10 min, and SWNH$(-CH_2-CH_2-COOH)_x$ supported liposomes were collected within the top layer. It was also found that, in the presence of 10% sucrose, DOTAP liposomes could be collected in the top layer after 30 min of centrifugation under 16,000 rcf; and SWNH$(-CH_2-CH_2-COOH)_x$ could be collected in the top liquid layer after 30 min of centrifugation under 10,000 rcf. Therefore, washing the SWNH$(-CH_2-CH_2-COOH)_x$ supported liposomes with the hydration buffer and repeating the centrifugation (10,000 rcf, 10 min) can significantly increase the purity.

Transmission electronic microscopy (TEM) images for SWNH$(-CH_2-CH_2-COOH)_x$, hollow liposomes, and SWNH$(-CH_2-CH_2-COOH)_x$ supported liposomes are shown in **Figure 1**. As it can be seen, all particles are of spherical shape and have a narrow diameter distribution centered at around 120 nm, which was confirmed by the dynamic light scattering test result shown in **Figure 2**. As shown in **Figure 1C**, a SWNH$(-CH_2-CH_2-COOH)_x$ supported liposome is a combination of the particles shown in (**A**) and (**B**). A negatively charged SWNH$(-CH_2-CH_2-COOH)_x$ is encapsulated in a cationic liposome and could stabilize and support the liposome from inside. The zoom out look of the particles shown in **Figure 1D** illustrates that a high purity of the assembled complex particles can be achieved by the centrifugation step described above. Centrifugation in the presence of 10% sucrose was performed only once in this case, but no hollow liposome or un-encapsulated SWNH$(-CH_2-CH_2-COOH)_x$ was observed in **Fig. 1D**.

To further confirm the structure of the particles, nitrobenzoxadiazole (NBD) labeled 1,2-dioleoyl-sn-glycero-3-phosphoethanolamine was added to the lipid mixture (up to 15% mass ratio) to produce NBD-DOTAP liposomes and SWNH$(-CH_2-CH_2-COOH)_x$ supported NBD-DOTAP liposome assembly. Results of the fluorescence of different particles detected by FCM are shown in **Figure 3**. The overlay histogram shows a similar fluorescence intensity shared by NBD-DOTAP liposomes and SWNH$(-CH_2-CH_2-COOH)_x$ supported NBD-DOTAP liposomes, and SWNH$(-CH_2-CH_2-COOH)_x$ particles without liposomes assembled around show no fluorescence signal. These results indicate that the surface structure of SWNH$(-CH_2-CH_2-COOH)_x$ supported liposome samples is most likely the same as that of hollow NBD-DOTAP liposomes, since the granularity and fluorescence intensity are almost identical (see FCM scatter plots in **Figure 3**). Zeta potential and electrophoresis mobility of the three particles shown in **Table 1** further confirm the similar surface characteristics of DOTAP liposomes and SWNH$(-CH_2-CH_2-COOH)_x$ supported DOTAP liposomes (N^-sL^+, negatively charged nanohorn supported positively charged liposomes) since their zeta potentials significantly differ from that of SWNH$(-CH_2-CH_2-COOH)_x$. As expected, those N^-

sL^+ particles and SWNH(-CH_2-CH_2-COOH)$_x$ particles travel in opposite directions in an applied electric field. These results confirm the encapsulation of SWNH(-CH_2-CH_2-COOH)$_x$ in liposomes and that the gray circle surrounding SWNH(-CH_2-CH_2-COOH)$_x$ in **Figure 1C and D** represents DOTAP lipid bilayers. The FCM results shown in **Figure 3** also serve as a strong indication that a high purity of the N^-sL^+ particles can be achieved using the purification method described above.

Conceivably, functionalized nanohorn supported liposomes will not be limited just to N^-sL^+ type of particles. Positively charged nanohorns can be synthesized by the aryl diazonium functionalization as reported,[14] and therefore it is possible to assemble the complex particles using negatively charged lipids (N^+sL^-), which are more commonly found in various biological membranes, for biomimetic purposes. The combination of positively or negatively charged nanohorns with anionic or cationic liposomes will significantly broaden the types of drugs that can be loaded, depending specifically on their charge or hydrophobicity. So far, many successful cases have shown that SWNH(-CH_2-CH_2-COOH)$_x$ could be a very promising drug delivery vehicle in terms of the loading capacity and the controlled release. A good example is the anticancer drug cisplatin which has recently become a commonly used molecule to test the two properties of certain functionalized nanohorns mentioned above.[15,16] However, the effects were mainly evaluated by directly providing cancer cell cultures with treatment of the drug carrying nanohorns. The targeting effect of nanohorns *in vivo* has not been well addressed. How many of the particles injected would nonspecifically bind to normal living cells and lead to their apoptosis is still unknown. On the other hand, liposomes conjugated with targeting ligands such as antibodies can navigate themselves to the cells that have corresponding receptors presenting on the cell surface.[17] The particles assembled by the combination of ligands attached liposomes and nanohorns could present a new and much improved drug delivery platform. For example, cisplatin could be loaded into SWNH(-CH_2-CH_2-COOH)$_x$ particles,[15,16] which could subsequently be assembled with liposomes that contain lipids sensitive to the change of pH (such as dioleoyl-phosphatidyl-ethanolamine, DOPE). Targeting antibodies, such as anti-human epidermal growth factor receptor-2 (HER2) antibody (Herceptin),[18] could be attached to the assembled particles via polyethylene glycol (PEG) on PEGylated phospholipids.[3] The presence of the lipid bilayer will deter the escape of cisplatin from the particles through diffusion during circulation in blood. However, once the particles enter the targeted cells (such as breast cancer cells via Herceptin-HER interaction[18]), defects will appear on the lipid bilayer structure due to the presence of pH sensitive lipids[19] and cisplatin will be released from the particles via the lipid bilayer defects. Research on this novel drug delivery system is currently under investigation in our labs.

Functionalized single wall nanohorn supported liposomes can have more novel applications beyond drug deliver systems. Magnetic resonance imaging (MRI) contrast agent containing Gd^{+3} ions have been loaded into SWNH(-CH_2-CH_2-COOH)$_x$ in the form of $Gd_3N@C_{80}$, trimetallic nitride template endohedral metallofullerenes (TNT-EMFs)[10] to lower the toxicity to the host because of (1) less amount required due to the high ^{1}H Magnetic resonance (MR) relaxivities of these TNT-EMF contrast agents;[20] and (2) the encapsulation of $(Gd_3N)^{+6}$ clusters into fullerene cages limits the exposure to free Gd^{+3} ions.[12] Gadolinium containing SWNH(-CH_2-CH_2-COOH)$_x$ supported liposomes open an opportunity to make the drug carrier itself an MRI biosensor. This allows the in situ monitoring of the in vivo bio-distributions of drugs in a macro or real-time manner.[21] For example, the clearance of liposomes from blood stream by the RES, which has much limited the development and applications of liposomal models, can be further studied and understood in details. Locating the pathogenic cells also becomes a possibility when using $Gd_3N@C_{80}$ TNT-EMFs encapsulated targeting nanohorn supported liposomes. The SWNH(-CH_2-CH_2-COOH)$_x$ along with the contrast agent will most likely be found inside the cytoplasm and remain there allowing a slow release of the therapeutic drugs, as the $(Gd_3N)^{+6}$ clusters remain detectable for several days post infusion.[12]

Liposomal vaccines are a new type of vaccines that are assembled by associating antigens with liposomes, and they have attract much attention because of the high immunogenicity[22] and gene free nature.[23] Size, exposure of epitopes, and stability of the liposomal vaccine particles are parameters most critical for their immunogenicity.[24,25] A commonly accepted measure to increase the stability is to incorporate PEGylated phospholipids into the liposome, especially when the vaccines are to be injected intravenously. However, the grafting density and polymer length of PEG strongly influence the exposure of the epitopes that need to be presented.[26] SWNH(-CH_2-CH_2-COOH)$_x$ stabilizes liposomes from inside and enables the entire liposome surface to be solely used for epitope presenting, and the size of the assembled particle (80-220 nm, see **Figure 2**) falls within the range that can be efficiently taken up by dendritic cells.[24]

In summary, we have shown the assembly and structure of SWNH(-CH_2-CH_2-COOH)$_x$ supported DOTAP liposomes. The combination of functionalized single wall nanohorns with liposomes opens a variety of opportunities for the complex particle not only as drug delivery vehicles in terms of high loading capacity, broad drug selectivity, cell targeting and controlled release, but also as many more potential promising applications such as drug bio-distribution real-time MRI, MRI contrast agent targeting, and liposomal vaccine assembly. It can be a useful platform to be loaded with different types of molecules or a promotion of developing other similar nanoparticle complexes for various applications.

Acknowledgment. This work was supported primarily by the Institute for Critical Technology and Applied Science (ICTAS) at Virginia Tech, and partially funded by a grant from Jeffress Memorial Trust, Grant no. J-994. Authors gratefully acknowledge Dr. Richey M. Davis for his support in particle size experiments, Kathy Lowe for her technical assistance with TEM imaging, and Melissa Makris for the assistance with FCM.

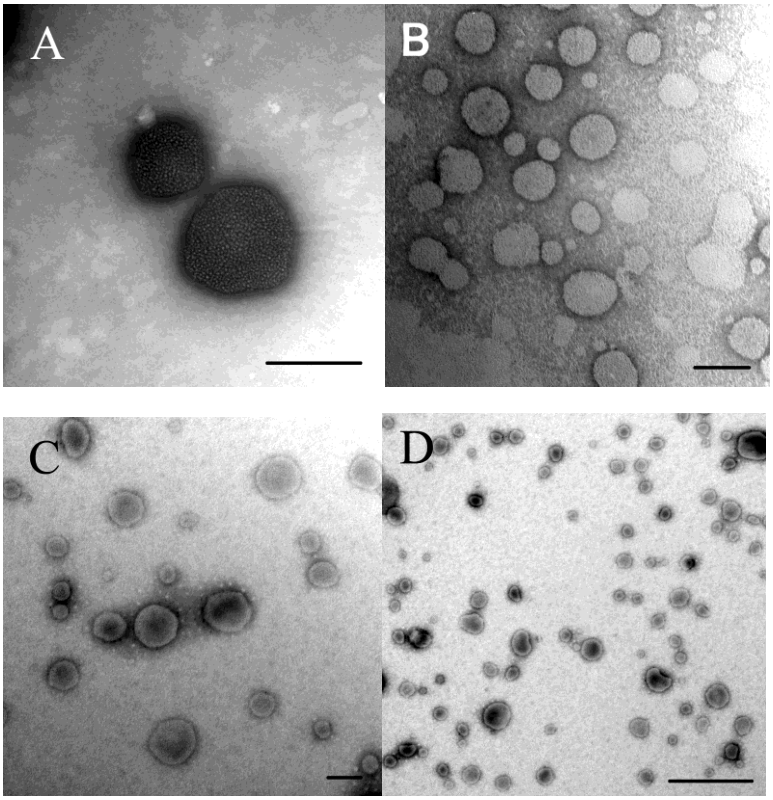

Fig. 1. Representative TEM images

of (A) SWNH(-CH_2-CH_2-COOH)$_x$, (B) Hollow DOTAP liposomes, (C) and (D) SWNH(-CH_2-CH_2-COOH)$_x$ supported liposomes. Scale bar in (A), (B) and (C) = 100 nm. Scale bar in (D) = 500 nm. Samples were deposited onto carbon coated copper grids. Negative staining was performed using 2% phosphotungstic acid.

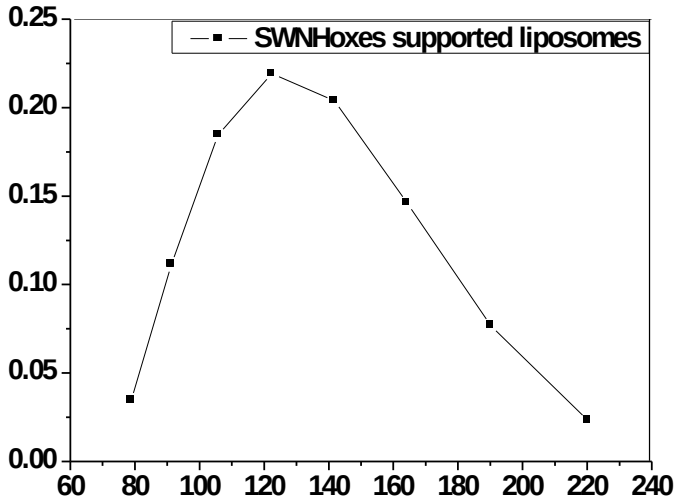

Fig. 2**.** Size distribution of SWNH(-CH_2-CH_2-COOH)$_x$ supported liposomes.

Refraction index = 1.33. Viscosity = 0.8872 cp. Samples were measured at 25 °C.

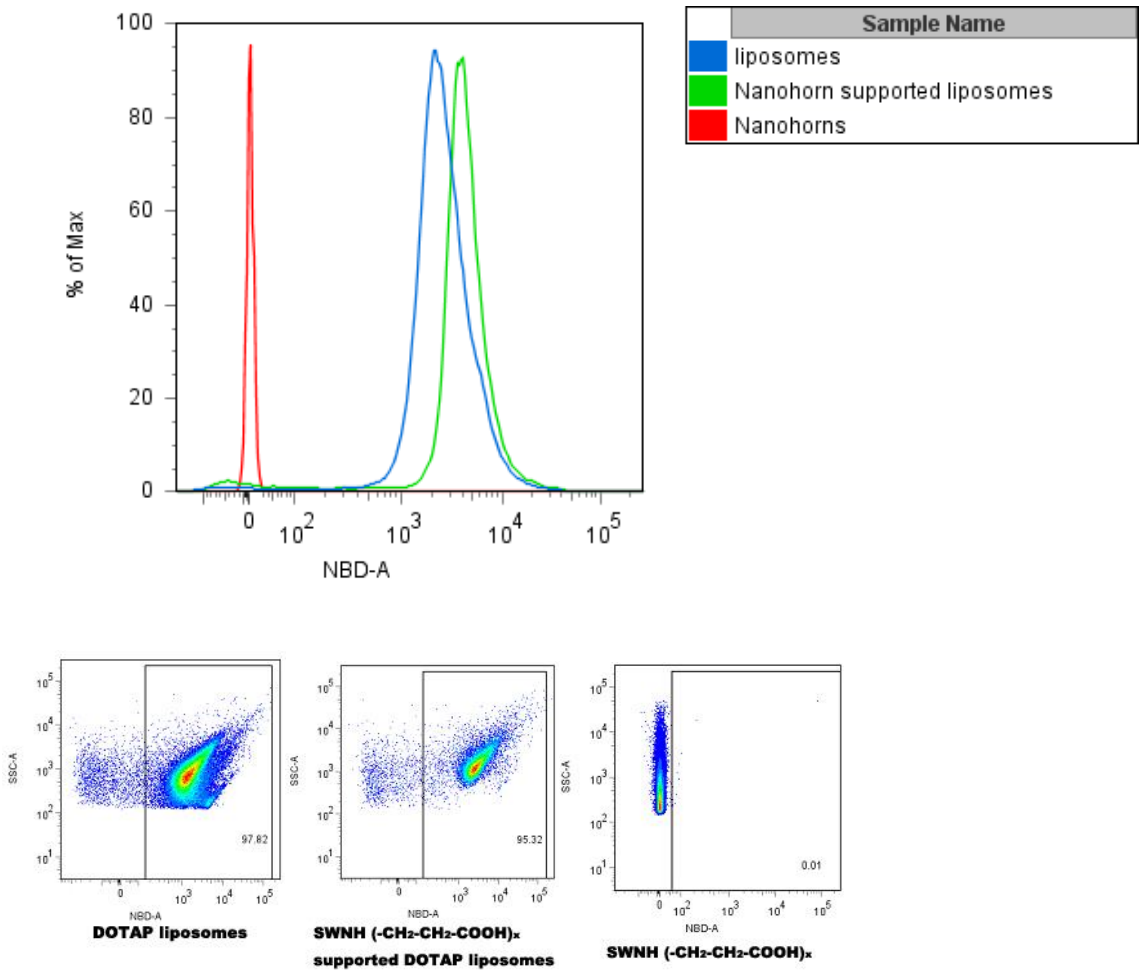

Fig. 3**.** Fluorescent intensity of different particles.

The histogram shows the fluorescent intensity distribution of NBD-DOTAP liposomes (blue), SWNH(-CH_2-CH_2-COOH)$_x$ (red) and SWNH(-CH_2-CH_2-COOH)$_x$ supported liposomes (green). The three corresponding FCM scatter plots show distribution of fluorescent intensity (horizontal axis, NBD-A) versus granularity (vertical axis, SSC-A).

Tab. 1**.** Zeta potential and electrophoresis mobility of particles.

All samples are in the hydration buffer (pH = 7.4), 25°C.

Sample	Zeta potential (mv)	Electrophoretic Mobility (μm·cm/V·s)
Hollow DOTAP liposome	24.6	1.928
Nanohorn	34.4	-2.694
SWNH(-CH_2-CH_2-COOH)$_x$ supported liposome	22.1	1.732

References

(1) Sapra, P., and Allen, T. M. (2003) Ligand-targeted liposomal anticancer drugs. *Prog. Lipid Res. 42*, 439-462.

(2) Singh, R., and Lillard Jr., J. W. (2009) Nanoparticle-based targeted drug delivery. *Exp. Mol. Pathol. 86*, 215-223.

(3) Li, S. D., and Huang, L. (2009) Nanoparticles evading the reticuloendothelial system: Role of the supported bilayer. *BBA. Biomembranes, 1788*, 2259-2266.

(4) Liu, J., Stace-Naughton, A., Jiang, X., and Brinker, C. J. (2009) Porous nanoparticle supported lipid bilayers (Protocells) as delivery vehicles. *J. Am. Chem. Soc. 131*, 1354-1355.

(5) Kunisawa, J., Masuda, T., Katayama, K., Yoshikawa, T., Tsutsumi, Y., Akashi, M., Mayumi, T., and Nakagawa, S. (2005) Fusogenic liposome delivers encapsulated nanoparticles for cytosolic controlled gene release. *J. Control. Release 105*, 344-353.

(6) Miyawaki, J., Yudasaka, M., Azami, T., Kubo, Y., and Iijima, S. (2008) Toxicity of single-walled carbon nanohorns. *ACS Nano 2*, 213-226.

(7) Lynch, R. M., Voy, B. H., Glass, D. F., Mahurin, S. M., Zhao, B., Hu, H., Saxton, A. M., Donnell, R. L., and Cheng, M.-D. (2007) Assessing the pulmonary toxicity of single-walled carbon nanohorns. *Nanotoxicology 1*, 157-166.

(8) Iijima, S., Yudasaka, M., Yamada, R., Bandow, S., Suenaga, K., Kokai, F., and Takahashi, K. (1999) Nano-aggregates of single-walled graphitic carbon nano-horns. *Chem. Phys. Lett. 309*, 165-170.

(9) Iijima, S. (2002) Carbon nanotubes: past, present, and future. *Physica B 323*, 1-5.

(10) Xu, J., Yudasaka, M., Kouraba, S., Sekido, M., Yamamoto, Y., and Iijima, S. (2008) Single wall carbon nanohorn as a drug carrier for controlled release. *Chem. Phys. Lett. 461*, 189-192.

(11) Kasuya, D., Yudasaka, M., Takahashi, K., Kokai, F., and Iijima, S. (2002) Selective production of single-wall carbon nanohorn aggregates and their formation mechanism. *J. Phys. Chem. B 106*, 4947-4951.

(12) Zhang, J., Ge, J., Shultz, M. D., Chung, E., Singh, G., Shu, C., Fatouros, P. P., Henderson, S. C., Corwin, F. D., Geohegan, D. B., Puretzky, A. A., Rouleau, C. M., More, K., Rylander, C., Rylander, M. N., Gibson, H. W., and Dorn, H. C. (2010) In vitro and in vivo studies of single-walled carbon nanohorns with encapsulated metallofullerenes and exohedrally functionalized quantum dots. *Nano Lett. 10*, 2843-2848.

(13) Shu, C., Zhang, J., Ge, J., Sim, J. H., Burke, B. G., Williams, K. A., Rylander, N. M., Campbell, T., Puretzky, A., Rouleau, C., Geohean, D. B., More, K., Esker, A. R., Gibson, H. W., and Dorn, H. C. (2010) A facile high-speed vibration milling method to water-disperse single-walled carbon nanohorns. *Chem. Mater. 22*, 347- 351.

(14) Pagona, G., Karousis, N., and Tagmatarchis, N. (2008) Aryl diazonium functionalization of carbon nanohorns. *Carbon 46*, 604-610.

(15) Ajima, K., Yudasaka, M., Murakami, T., Maigne, A., Shiba, K., and Iijima, S. (2005) Carbon nanohorns as anticancer drug carriers. *Mol. Pharm. 2*, 475-480.

(16) Matsumura, S., Ajima, K., Yudasaka, M., Iijima, S., and Shiba, K. (2007) Dispersion of cisplatin-loaded carbon nanohorns with a conjugate comprised of an artificial peptide aptamer and polyethylene glycol. *Mol. Pharm. 4*, 723-729.

(17) Wright, S., and Huang, L. (1989) Antibody-directed liposomes as drug-delivery vehicles. *Adv. Drug Deliv. Rev. 3*, 343-389.

(18) Arehalli, S. M., Kiran, R.C., Makam, P.V., Prudhviraju, D., Biswarup, N., Chennakesavulu, S., Krutika, K.S., Rayasa, S.R.M. (2010) Antibody derivatization and conjugation strategies: Application in preparation of stealth immunoliposome to target chemotherapeutics to tumor. J. Control. Release. 10, 1016.

(19) Sudimack, J.J., Guo, W., Tjarks, W., Lee, R.J. (2002) A novel pH-sensitive liposome formulation containing oleyl alcohol. Biochim. Biophys. Acta. 1564, 31-37.

(20) Shu, C., Corwin, F. D., Zhang, J., Chen, Z., Reid, J. E., Sun, M., Xu, W., Sim, J. H., Wang, C., Fatouros, P. P., Esker, A. R., Gibson, H. W., and Dorn, H.C. Facile preparation of a new gadofullerene-based magnetic resonance imaging contrast agent with high ^{1}H relaxivity. (2009) *Bioconjug. Chem. 20*, 1186-1193.

(21) Sato, K. T., Larson, A. C., Rhee, T. K., Salem, R. A., Nemcek, A. A., Mounajjed, T., Paunesku, T., Woloschak, G., Nikolaides, P., and Omary, R. A. (2005) Real-time MRI monitoring of transcatheter hepatic artery contrast agent delivery in rabbits. *Acad. Radiol. 12*, 1342-1350.

(22) Galdero, F., Carratelli, C. R., Nuzzo, I., Bentivoglio, C., De Martino, L., Folgore, A., and Galdiero, M. (1995) Enhanced cellular response in mice treated with a Brucella antigen-liposome mixture. *FEMS Immunol. Med. Microbiol. 10*, 235-243.

(23) Noad, R., and Roy, P. (2003) Virus-like particles as immunogens. *Trends Microbiol. 11,* 438-444.
(24) Xiang, S. D., Scholzen, A., Minigo, G., David, C., Apostolopoulos, V., Mottram, P. L., and Plebanski, M. (2006) Pathogen recognition and development of particulate vaccines: does size matter? *Methods 40,* 1-9.
(25) Pellequer, Y., Ollivon, M., and Barratt, G. (2004) Formulation of liposomes associated with recombinant interleukin-2: effect on interleukin-2 activity. *Biomed. Pharmacother. 58,* 162-167.
(26) Kaasgaard, T., Mouritsen, O. G., and Jorgensen, K. (2001) Screening effect of PEG on avidin binding to liposome surface receptors. *Int. J. Pharm. 214,* 63-65.

Chapter V: Assembly of biomemetic nanoparticles for double controlled drug release

Wei Huang,[1] Jianfei Zhang,[2] Harry C. Dorn,[2] Chenming Zhang[1]*

1. Department of Biological Systems Engineering

2. Department of Chemistry

Virginia Tech

Blacksburg, VA 24061

(Manuscript submitted to Journal of Controlled Release)

ABSTRACT

A critical limiting factor of chemotherapy is the unacceptably high toxicity. The use of nanoparticle based drug carriers has significantly reduced the side effects and facilitated the delivery of drugs. Source of the remaining side effect includes (1) the broad final in vivo distribution of the administrated nanoparticles, and (2) strong basal drug release from nanoparticles before they could reach the tumor. Despite the advances in pH-triggered release, undesirable basal drug release has been a constant challenge under in vivo conditions. In this study, functionalized single walled carbon nanohorn supported immunoliposomes were assembled for paclitaxel delivery. The immunoliposomes were formulated with polyethylene glycol, thermal stable and pH sensitive phospholipids. Results showed a highly pH dependent release of paclitaxel in the presence of serum at body temperature with minimal basal release under physiological conditions. Upon acidification,

paclitaxel was released at a steady rate over 30 days with a cumulative release of 90% of the loaded drug. The drug release results proved our hypothesized double controlled release mechanism of the nanoparticles. Other results showed the nanoparticles have doubled loading capacity compared to that of traditional liposomes and higher affinity to breast cancer cells overexpressing her2 receptors. Internalized nanoparticles were found in lysosomes.

Key words: breast cancer, single walled carbon nanohorn, immunoliposome, controlled release

1. Introduction

Nanoparticle (NP) based drug carriers have been studied as a potential model for tumor diagnostic and treatment [1,2]. The advantages include their ability of transporting high dose of toxic drugs or contrast agent specifically to the tumor, and gradually releasing the drug thereafter [3], and the ability of co-delivering a therapeutic cocktail (i.e. combinations of chemotherapy and immunotherapy [4], chemotherapy and anti-drug resistance agent [5]), which is critical for an effective cancer treatment. So far, the major efforts to improve nano-drug carriers fall into three categories, (1) using better particles (i.e. replace non-biocompatible particles with biodegradable ones [6]); (2) shifting the in vivo distribution towards the tumor (i.e. use polyethylene glycol (PEG) coated, or targeting ligand grafted particles [7]); and (3) eliminating basal drug release in the circulation (i.e. use advanced particles with pH [8], temperature triggered release [9]).

For intravenously administrated chemotherapies, the basal drug leakage from the drug carrier is a critical problem since the hindrances of in blood movement and lack of attraction to the target site have largely delayed the arrival of NPs to the tumor. Studies have shown that, 24 to 72 hours post administration, the particles were still mostly trapped in the liver, spleen and kidney, few were found in the lung, skin and at the tumor site [7,10,11]. NP size, shape, rigidity, surface chemistry and the tendency of adsorption onto other surfaces are the known factors that can slow the in vivo transportation [10]. The accumulation of NPs at the tumor site is still mainly based on the enhanced permeability and retention (EPR) effect. Therefore, drug carriers with minimum basal drug leakage, preferably with accurately controlled triggered release, are strongly needed.

A typical drug release from NPs is usually initiated with a burst phase (up to 50% of total loading) within the first a few hours post exposure, and followed with a slow release phase [4,12,13]. The burst phase corresponds to the release of drug molecules that are loosely

associated with the particle, mostly located in the surface of the NPs. The slow release phase is resulted from the drug release from the inner core via diffusion and erosion (for biodegradable particles) [12]. When injected, the initial burst release occurs before most of the NPs can reach the tumor. This would result in an undesirable drug leakage into the circulation and the organs, causing toxic side effect to the body and loss of drug potency at the tumor. On the other hand, pH-sensitive NPs can theoretically eliminate those unwanted leakage [8]. After administration, the NPs encounter a series of decreasing pH gradient during their journey to tumor cells. Firstly, the NPs travel with the blood flow (pH 7.2) [14] and extravasate at the tumor site through EPR. The NPs that successfully get into the tumor (pH 6.5) [15] could then have close contact with the receptors located at the surface of tumor cells. The receptors recognize the grafted targeting ligand on the NPs and initiate a receptor-mediated endocytosis into tumor cells [4]. Internalized NPs are transported within endosomes to the lysosomes (pH of endosomes keep dropping from 6.5, as they approaching lysosomes, to 4.6 when they merge into a lysosome [15].). pH-sensitive NPs are engineered to only release the content into low pH environment so as to eliminate any premature drug leakage prior to the lysosome stage.

In this work, we present the elimination of in serum paclitaxel release by functionalized single walled carbon nanohorns (SWNHs) supported pH-sensitive immunoliposomes (NsiL). NsiL is a combination of two types of traditional NPs, namely SWNHs [16] and liposomes. Combined NPs have been described most recently and shown to inherit combined advantages of both NPs [17-19]. Here, functionalized SWNHs function as a hydrophobic drug carrier and the backbone of the NP. While immunoliposomes serve as a tunable boundary confining the drug before the NP enters the tumor cells and mimic the surface of bacterial that facilitate cell recognition and endocytosis. Properties of loading capacity, size distribution,

morphology, in buffer and in serum drug release profile, cell binding and internalization rate of NsiL were studied in comparison with liposomes and SWNHs.

2. Methods

2.1. Materials

Lipid materials and mini extruder were purchased from Avanti Polar Lipid (Alabaster, AL). Monoclonal anti-ErbB2 mouse IgG2bk (clone 4B8) was purchased from Sigma-Aldrich (St. Louis, MO). Herceptin was a generous gift from Genentech (San Francisco, CA). Paclitaxel was purchased from LKT Laboratories (St. Paul, MN). Cell lines, culture related products were purchased from ATCC (Manassas, VA). Molecular probes were purchased from Invitrogen (Carlsbad, CA). Luna 5u C18 (2) reverse phase high performance liquid chromatography column was purchased from Phenomenex (Torrance, CA).

2.2. Synthesis of functionalized SWNH(-CH2-CH2-COOH)x

SWNHs were synthesized by Nd:YAG laser vaporization of graphite rods in an argon atmosphere at 1100 °C as described elsewhere [20]. SWNHs are then functionalized with carboxyl groups by high-speed vibration milling. Briefly, a mixture of SWNHs and succinic acid acyl peroxide (1:100 in mass) was vigorously shaken in a stainless steel capsule for 1.5 h. The ground ultrafine power was collected and washed three times with acetone and centrifuged to collect the sediment. Twenty minutes sonication was performed to dissolve the sediment in ultrapure water yielding solutions of SWNH(-CH2-CH2-COOH)x.

2.3. Liposome formula and formation

PEGylated liposomes were made by extruding hydrated lipid mixture of 1,2-dioleoyltrimethylammoniumpropane (DOTAP), 1,2-dioleoyl-sn-glycero-3-phosphoethanolamine (DOPE), cholesterol (CHOL), 1,2-dioleoyl-sn-glycero-3-

phosphoethanolamine-N-[methoxy(polyethylene glycol)-2000] (ammonium salt) (DSPE-mPEG2000). For 'DOTAP' liposomes or 1,2-distearoyl-sn-glycero-3-phosphocoline (DSPC), DOPE, CHOL, DSPE-mPEG2000 for 'DSPC' liposomes through polycarbonate membranes with pore sizes of 100 nm. Prior to extrusion, lipid cake was hydrated in Tris-HCl buffer (pH 7.4) that contains 0.9% NaCl, 5% dextrose and 10% sucrose, at 55 °C with perturbation for at least 1 h. Extrusion was conducted at the same temperature and repeated 7 times. Detailed properties of the liposomes used are shown in Table 1. Wherein 1,2-distearoyl-sn-glycero-3-phosphethanolamine-N-[maleimide(polyethylene glycol)-2000] (ammonium salt) (DSPE-PEG2000-mal) will be added post formation of the liposomes in conjugation with the targeting ligand to ensure a certain orientation, which will be discussed in the 'NsiL formation' section. Rhodamin B (rhB) labeled NsiLs were made by adding DOPE-N-(lissamine rhodamine B sulfonyl) (ammonium salt) (up to 15%, w/w) to the lipid mixture.

2.4. NsiL formation and purification

Excessive high concentration of paclitaxel (1-5mg/ml) in methanol were well mixed with SWNH(-CH2-CH2-COOH)x powder with brief sonication. Methanol was then eliminated in a fume hood overnight. Paclitaxel loaded SWNH(-CH2-CH2-COOH)x was washed in ultra-pure water 3 times and suspended in the hydration buffer. Aliquot of drug loaded SWNH(-CH2-CH2-COOH)x was dispersed in methanol with agitation. Samples were taken from the dispersion after 6 h of extraction for paclitaxel concentration measurement by high performance liquid chromatography (HPLC) equipped with Luna C18(2) reverse phase column (RPC) at UV 227 nm [21].

Paclitaxel loaded SWNH(-CH2-CH2-COOH)x were encapsulated into liposomes as described previously [17]. Briefly, excessive liposomes were incubated with SWNH(-CH2-CH2-COOH)x. Three freeze and thaw cycles were applied using liquid nitrogen and a warm

water bath. Nanohorn supported liposome (NsL) with high purity was collected at the bottom layer after 10 min centrifugation at 10,000 g in the presence of 10% sucrose.

Targeting ligand was conjugated to NsL particles through PEG. Briefly, anti-ErBb2 (HER2) monoclonal antibody (mAb) mouse IgG1 (Novus biologicals, Litteton, CO) was thiolated by Traut's reagent in HBS buffer (25 mM HEPES, 140 mM NaCl, pH 7.4). Unreacted Traut's reagent was removed by Sephadex G25 column on a fast flow liquid chromatography (FPLC) system. Immediately after concentration by an ultra-filtration centrifuge unit, corresponding (1:1 molar) amount of DSPE-PEG-mal was added and the mixture was incubated overnight at room temperature. The product was added to the NsL suspension described in the previous section to a final ratio of 2% (Table 1) and incubated at 55 ºC overnight. The DSPE-PEG-mal mAb conjugates were added to pre-formed NsL particles to maximize the orientation with (1) the DSPE fatty acid tails inserted in the liposome bilayers and (2) the hydrophilic mAb end projecting away from the NsiL [22]. This orientation optimizes the exposure of mAb active binding sites resulting in improved efficiency of the receptor recognition, and a reduced chance of non-specific binding.

2.5. Particle characterization

Size distribution and zeta potential of NPs were analyzed on a Zetasizer Nano ZS (Malvern Instruments, Southborough, MA). Samples were freshly prepared before use by adding aliquots of NPs to 0.01 M sodium chloride buffer to make a solution with a lipid concentration of 0.01 mg/ml. During the test, samples were injected into a disposable capillary cell DTS1060 (Malvern Instruments, MA) and loaded onto the analyzer. Measurements were taken at 25 ºC with a material refraction index of 1.33 and viscosity of 0.8872 cp.

TEM images were taken for morphology study. Briefly, samples were deposited onto carbon coated copper grids for 5 min. 2% phosphotungstic acid was used for negative staining for 30 s. TEM images were taken by a JEOL JEM 1400 (JEOL Ltd, Tokyo, Japan).

2.6. Drug release profile and loading capacity

Loaded drug (SWNH(-CH2-CH2-COOH)x and NsiL) was extracted by dialysis and analyzed by high performance liquid chromatography (HPLC) [23,27]. Release profile of NPs in aqueous solution and in serum at pH 7.2, 6.5 and 4.6 are measured by dialyzing equal amount of particles (0.1 mg SWHN or 0.4 mg lipid) against 20 ml corresponding buffer (citric acid at pH 4.6, sodium diphosphate at pH 6.5 and 7.2, each with 0.2% Tween 80) with agitation. Samples were collected at predetermined time point for a total of 30 days. After each collection, sample in the dialysis tubes were transferred to another 20 ml of fresh extraction buffer. Drug release in serum was conducted at 37 ºC.

For total loading capacity, 20 ml methanol was used for dialysis. Samples were thoroughly rinsed with ultrapure water and dialyzed at room temperature for 6 h. The extracted paclitaxel concentration was analyzed on an HPLC system equipped with Luna C18 (2) reverse phased chromatography column (at UV 227 nm).

2.7. Cytotoxicity assay

Cell toxicity of empty NPs was evaluated by cell proliferation assay. SK-BR-3 and BT-20 breast cancer cells were seeded onto 96 well plates at a concentration of 6k/200 µl and incubated overnight (37 ºC, 5% CO2). Up to 0.64 µg lipid particles (or 0.1 mg SWNH) of aliquots NsL, SWNH(-CH2-CH2-COOH)x and liposomes were added and incubated for 24 h. Cells were allowed to incubate with 1 mg/ml 3-(4,5-dimethylthiazol-2-yl)-2,5-diphenyltetrazolium bromide (MTT) in 0.1 M phosphate buffered saline (PBS) for 4 h. 200 µl dimethyl sulfoxide was used to dissolve the formazan crystals. Absorbance was measured on

a Synergy HT Multi-Mode Microplate Reader (Bio Tek, Winooski, VT). Cell viability was calculated with an in test calibration curve using the optical density of 560 nm subtracted by that of 670 nm.

2.8. Cell binding assay

Affinity of NsiL particles to cells was measured by cell binding assay. Briefly, SK-BR-3 and BT-20 breast cancer cells were seeded onto 96 well plates at a concentration of 10k/ well and incubated overnight (37 ºC, 5% CO2). Up to 40 µg (lipid mass) of aliquots rhB labeled NsiL particles were added to incubate for 1 h. Each well was carefully rinsed and filled with a final volume of 200 µl with 0.1M PBS. Fluorescent intensities were measured immediately on the Synergy HT Multi-Mode Microplate Reader (excitation: 530, emission: 645, sensitivity: 40, optic position: bottom). Non-targeting ligand attached NsL and Herceptin NsiL were used for comparison.

2.9. Cell uptake assay

The cell uptake efficiency was evaluated by confocal laser microscopy. Briefly, 3 ml SK-BR-3 cells were seeded onto glass bottom microwell dishes (35 mm petri dish, 14 mm microwell, 0.16-0.19 mm coverglass, MatTeck, Ashland, MA) at a concentration of 100k / ml, incubated over night at 37 ºC, 5% CO2. 20 µl rhB labeled NsiL was added to the cell culture and incubated for 4-6 h. Culture medium was discarded and cells were rinsed 3 times with 0.1 M PBS. 30 µg calcein AM was added 15-30 min prior to the microscopy. Images were taken by a Zeiss LSM510 Meta (LSM TECH, PA).

3. RESULTS AND DISCUSSION

3.1. Size distribution and zeta potential of PEGylated DSPC liposome, SWNH(-CH2-CH2-COOH)x and NsiL

Size distributions of the NPs were analyzed by dynamic light scattering (DLS). Results are shown in Fig. 1. Mean diameters of 121 nm, 142 nm and 164 nm were observed for PEGylated DSPC liposome (Fig. 2a), SWNH(-CH2-CH2-COOH)x (Fig. 2b), and NsiL (Fig. 2c, 2d), respectively. It is well recognized that sizes have significant influence on the in vivo distribution and loading capacity of NPs. Large NPs (d > 200 nm) are known to be more vulnerable to the clearance by spleen and liver [24], not readily permeate to the tumorous capillaries [25,26], nor, in some cases, good carriers of drugs due to the relatively smaller surface to volume ratio. On the other hand, small NPs (d < 5 nm) leak out of the circulation at the kidney. It has been reported that administrated NPs with diameters around 150 nm tend to facilitate receptor-mediated endocytosis and had maximum accumulation in the tumor [27]. Noticing that the PEGylated liposomes and SWNH(-CH2-CH2-COOH)x particles had relatively broad size distributions even though the mean diameter appeared within the desirable range. The purification process that has been applied to the NsiL NPs seemed to result in a narrow distribution for purified NsiL NPs as shown in Fig. 1.

Nevertheless, the mechanism of how SWNH(-CH2-CH2-COOH)x gets encapsulated into liposomes is still unclear. One SWNH(-CH2-CH2-COOH)x entering one liposome during the freeze and thawing process is unlikely the case, since the supported liposomes are much larger than the parental ones (Fig. 1). Li and Huang hypothesized that a supported double bilayer could form when two cationic liposomes approached one negatively charged core via membrane fusion [28]. Indications of such process were observed (Fig. 2e) in our tests as multiple DOTAP or DSPC liposomes (cationic liposomes) were observed to attach to the

surface of a SWNH(-CH2-CH2-COOH)x (anionic core). The supported liposome was most likely formed through membrane fusion during the freeze and thaw process.

The zeta potential values for DSPC PEGylated liposomes, SWNH(-CH2-CH2-COOH)x and DSPC NsiLs are determined as 24.3, 34.6 and 22.5 respectively. We tested the size distribution of the same samples after 2 months of storage at room temperature (lipid concentration, 1.6 mg/ml). No aggregation was detected (data not shown). This is most likely resulted from the use of PEGylated lipids in the assembly of the NPs.

3.2. Morphology study of NPs by TEM

Structures of nanohorn supported liposome (NsL, particles without targeting ligand) and NsiL were confirmed by transmission electronic microscopy (TEM). Spherical shaped PEGylated DSPC liposomes and SWNH(-CH2-CH2-COOH)x were observed and shown in Fig 2a and b, respectively. Structures of NsL NPs were shown in Fig. 2c and d. SWNH(-CH2-CH2-COOH)x were seen encapsulated in the liposomes. The inter-space between SWNH(-CH2-CH2-COOH)x and liposome could vary. DSPC NsiL showed identical morphology as NsL particles (not shown).

3.3. Paclitaxel Loading Capacity

Total paclitaxel was extracted from PEGylated DSPC liposomes, SWNH(-CH2-CH2-COOH)x and DSPC NsiL. Loading capacities were calculated from the corresponding HPLC peak area using a calibration curve. Drug loading efficiency (DLE, %, w/w) was calculated as the ratio of mass of drug loaded to mass of NPs. Drug encapsulation efficiency (DEE, %, w/w) was calculated as the ratio of mass of drug loaded to mass of drug added. DLE and DEE for DSPC NsiL were determined as 251.8% and 75.5%, respectively. In comparison, PEGylated DSPC liposomes showed a DLE of 118.4% and a DEE of 33.8%. The use of

SWNH(-CH2-CH2-COOH)x particles has doubled the total loading of liposome particles. DLE and DEE of SWNH(-CH2-CH2-COOH)x NPs were identical to DSPC NsiL indicating a rapid internalization of SWNH(-CH2-CH2-COOH)x into liposomes, such that the drug loss during NsL assembly is negligible.

SWNHs have been reported as potential carriers for hydrophobic drug molecules. Besides the high loading capacity, loaded drug would have a long-term controlled release resulting from the slow diffusion rate of hydrophobic drug between graphene sheets [13]. Liposome, on the other hand, has seen more usages in delivering protein and gene based therapeutic agents and other water-soluble small molecules [2]. The loading of hydrophobic molecules in liposome is largely limited by their aqueous solubility.

3.4. In Serum Drug Release From NsiL

Drug releases from PEGylated DOTAP NsiL in saline buffer and in serum were tested. As shown in Fig. 3a, at pH 7.2 and room temperature in saline buffer, PEGylated DOTAP liposome (light blue) and SWNH(-CH2-CH2-COOH)x (black) showed a 24 h cumulative release of 30%, in comparison to 2% of that from PEGylated DOTAP NsiL (red). A stronger release for NsiL NPs only started to show as the pH decreased to 6.5 and 4.6 (green and blue). The hypothesized mechanism is illustrated in Fig. 4. When the surrounding pH is neutral (i.e. 7.2 in the blood), the PEGylated liposome is intact and has a closed structure (Fig. 4a). The paclitaxel molecules (green dots) can slowly diffuse out of SWNH(-CH2-CH2-COOH)x into the inter-space between SWNH and the liposome driven by concentration gradient. The paclitaxel accumulated in the inter-space could either diffuse back to the SWNH(-CH2-CH2-COOH)x or continue diffuse to the outside of the NsiL. The latter is, however, largely limited by the presence of the lipid bilayer. Liposomes with varying resistance could be theoretically formulated by changing the lipid composition. We hypothesize that, using carefully formulated liposomes, the closed structure of the NsL NPs

could be maintained for a given environment. The liposome used in this study consists 33% (mol/mol) DOPE, a pH sensitive phospholipid, which will have conformational changes and form defects on the liposomes under acidic pHs such as 4.6 (i.e. in lysosomes) [29]. Fig. 4b shows the release of drug under control of the diffusion out of SWNH(-CH2-CH2-COOH)x and porous PEGylated liposome upon acidification mimicking the pH environment of that inside lysosomes of a tumor cell.

According to the hypothesized mechanism described above, the double controlled release (pH and diffusion) could eliminate basal drug leakage. To test this hypothesis, drug release from NsiL, SWNH(-CH2-CH2-COOH)x and PEGylated DOTAP liposome were tested in serum at 37 °C. Unexpectedly, NsiL and SWNH(-CH2-CH2-COOH)x showed almost identical release profile (red and green respectively, Fig. 3b). This indicates, for the NsiL sample, the supported liposome failed to provide any containment to the paclitaxel molecules in serum at pH 7.2. On the other hand, leakage of the drug from PEGylated DOTAP liposome evidently is much more severe (black, Fig. 3b), indicating that, under physical condition, liposome alone provides almost no control on the release and the hydrophobic interaction between the drug molecules and SWNH plays an important role in controlling the release of the drug molecules. It is worth to note that the in serum release was conducted in the absent of macrophages or other RES components. To our best knowledge, opsonisation alone does not break the lipid bilayer [30]. We thus suspect it is the 37 °C temperature that has induced the formation of defects in lipid bilayer and rendered the liposome permeable. DOTAP has a transition temperature (Tm) of 0 °C. Under 37 °C, DOTAP liposomes are in a melting state. Therefore, to minimize the undesired drug release, some temperature tolerable phospholipids (i.e. DSPC, Tm = 55 °C) would be good substitutions of DOTAP.

PEGylated DSPC liposomes and DSPC NsiL were thus prepared. In serum release results showed a linear release of drug up to 90% in 7 days at pH 4.6 with a burst release of 60%

within the first 10 hours for both NPs (Fig. 3c). Minimum release from both NPs at pH 6.5 and 7.2 were observed and shown in Fig. 3d. Although the PEGylated DSPC liposomes showed almost identical drug release profile as that of DSPC NsiL under acidic pH, it is worth noting that at pH 7.2, NsiL NPs have half of the basal release of that from the liposome particles. In addition, NsiL NPs have the following advantages in drug delivery over liposome NPs: (1) NsiL has more than twice of the loading capacity as PEGylated liposomes; (2) PEGylated liposomes are nonetheless susceptible to electrostatic, hydrophobic and van der Waals forces [31]; (3) NsiL particles are self-stabilized through the electrostatic attractions between the negatively charged SWNH(-CH2-CH2-COOH)x (at pH 7.2) and the positively charged DSPC head group (N+), which renders the NsiL more resistant to physical ruptures such as shear force and turbulence of blood flow and collisions with other components of blood (i.e. red blood cells, lipoproteins). Although it is out of the scope of this study, we suspect that under dynamic conditions as that in in vivo blood flow, NsiL NPs will perform much better than PEGylated DSPC liposomes in terms of basal drug release.

3.5. Cytotoxicity Study

Cytotoxicity of NPs without paclitaxel and antibodies was evaluated by MTT assay. As shown in Fig. 5, both SK-BR-3 and BT-20 cells were incubated with up to 640 μg/ml NPs (in lipid concentration) for 24 h, and no significant cytotoxicity was observed for all tested NPs. Both PEGylated liposomes and SWNH(-CH2-CH2-COOH)x have been previously reported as nontoxic [4,32,33]. As expected, the combined NPs appeared to be compatible with the breast cells. However, a noteworthy fact is that the in vivo fate of SWNH(-CH2-CH2-COOH)x is still unclear. A possible degradation product, singlet or small cluster of nanohorn, will have a similar structure as a single-walled carbon nanotube, which has been reported to

cause DNA damage, cell dividing interruption and inflammation [34]. Further study of in vivo long-term toxicity of SWNH(-CH2-CH2-COOH)x is needed.

3.6. Affinity of NPs to Her2-possitive and negative cells

Binding affinity of NPs to SK-BR-3 (a Her2-possitive cell line) and BT-20 (a Her2-negative cell line) was evaluated. As shown in Fig. 6, NsiL attached with the anti-ErBb2 (HER2) monoclonal antibody (mAb) mouse IgG1 showed the strongest affinity to SK-BR-3 cells (group A), whereas the affinity of NsL particles without the targeting ligand (group B) and NsiL attached with herceptin (a humanized monoclonal antibody of Her2 receptors [35-37]) (group C) to SK-BR-3 cells were relatively weaker. Evidently, NsL NPs also had certain degree of interaction with the cells, although the signal is only half as strong as NsiL at all tested concentrations. It is currently believed the targeting ligands provide no guidance for the NPs towards the tumor. They only facilitate the binding and internalization when NPs and cells get close to nanometer range [38,39]. The difference between group A and group B seems to support this belief. Moreover, NsiL with anti-ErBb2 mouse mAb showed slightly higher affinity to the SK-BR-3 cells than the ones with Herceptin (Herceptin NsiL), and this can likely be attributed to the primary structural difference between the two antibodies.

Furthermore, the affinity of different NPs to a Her2 negative cell line, BT-20, was also evaluated, as shown in Fig. 6 group D-F. Theoretically, since the cells do not overexpress Her2 receptors on their surface, all three NPs should show affinity to the cells similar to that between NsL and SK-BR-3 cells. It is not a surprise to see the almost identical signal intensities between group B and E for NsL NPs. Surprisingly, however, group D and F showed stronger signals than NsL particles (group E) at all concentrations, albeit the signals at corresponding concentrations are not as strong compared with that between these NPs and

SK-BR-3 cells (group A and C). We hypothesize that the presence of proteins on NsiL and Herceptin-NsiL allows those NPs to engage in non-specific interactions with some proteins on the cells surface. Based on this hypothesis, attaching protein based targeting ligands on NPs really is a double edged sword, i.e. the ligands will enhance not only the interaction of the NPs with the targeted cells but also those cells the ligands are not intended to target [40].

Based on the over-expressed receptors, breast cancer cells have four main types, namely luminal, normal-like, Her2 and basal-like [41]. 20-30% of human breast cancer cells are Her2 (human epidermal growth factor receptor-2, Her2 or ErbB2) positive. Her2 is the most aggressive type of the four because of its high cell proliferation rate and propensity to early metastatization [42]. Dire prognosis and a less than 24-30 months median survival period are usually seen with her2 positive patients [43-46]. The NsiL NPs were designed to target her2 positive breast cancer cells since the cells over-express her2 receptor at the surface. Although the cell binding test results (Fig. 6) did not show a significantly preferential affinity of NsiL to her2 positive cells, the targeting ligand tethered NPs still showed improved selectivity towards the targeted cells compared to NPs without any targeting ligands. It is worth noting that the cell binding test performed in this study is an in vitro test, in which different cell lines were cultured and evaluated separately. Thus, the test results were affinities without consideration of competition and a 3D cell network. Some works need to be done to better evaluate the NP distribution on different cells, such as testing on a matrix assisted in vitro tumor model composed of both her2 positive and negative cells. On the other hand, the mAb and herceptin used in this study were more than just targeting ligands. They are also a critical part of the potential treatment. Single-agent chemotherapy is usually not efficient for most of the cases [47]. Herceptin and other antibodies could attenuate the aberrant her2 kinase-associated signal transduction, resulting in interrupted cell proliferation and metastatization

[48,49]. Co-delivery of paclitaxel (chemotherapy) and herceptin (immunotherapy) has been shown effective by many [50].

3.7. In Cell Distribution of NPs

The internalized NsiL NPs were observed by confocal laser microscopy after a 6 h incubation of NsiL NPs with SK-BR-3 cells. As negative controls, either unstained NsiL or cells were used to prepare the sample and images were taken under stacks of FITC and rhodamine channel, as shown in Fig. 7a and b, respectively. Cellular distribution of NsiL NPs was shown in Fig. 7c and d. A lysosomal distribution was observed as particles scattered in the cytoplasm with slight higher density around the nucleus (Fig. 7d). This indicates the NsiL NPs were most likely internalized via receptor mediated endocytosis and delivered intracellularly into lysosomes for digestion.

3.8. Other considerations

It has to be pointed out that, in vivo drug availability always deviates from in vivo NPs distribution depending on the degree of undesirable premature leakage. The NsiL NPs could largely reduce the deviation, but will unlikely affect the NP distribution. Hence, to increase the proportion of NPs that reach the tumor has become a key for improved pharmacokinetics. Further studies are needed to improve the targeting specificity, stealth effect, and decrease the enhanced clearance upon repeatedly administration of PEGylated NPs (accelerated blood clearance phenomenon) [51].

NsiL could be used for many other applications. A magnetic resonance imaging (MRI) contrast agent Gd3+ containing (Gd3N@C80) trimetallic nitride template endohedral metallofullerenes (TNT-EMFs) has been loaded into SWNH(-CH2-CH2-COOH)x with high

MRI sensitivity and low toxicity [52]. PEGylated immunoliposomes could deliver the contrast agent containing SWNH(-CH2-CH2-COOH)x to the targeting site allowing real-time monitoring of the in vivo distribution [53] or imaging or the pathogenic area within several days post infusion [48].

4. Conclusion

A major advantage of NP based drug delivery is the precise targeting ability. However, over half of the loaded drugs were usually seen lost before the NPs can reach the tumor. The basal release in the circulation will cause reduced efficacy of the treatment and toxic side effect to the other parts of the body. In this study, NsiL NPs were assembled to eliminate the basal release of paclitaxel in the blood. SWNH(-CH2-CH2-COOH)x are dahlia-like-shaped nanoparticle aggregates of single graphene tubules [16]. Functionalized SWHN has defects on the extensive surface and the surface is negatively charged at neutral pH. Paclitaxel was loaded to SWNH(-CH2-CH2-COOH)x and cationic PEGylated pH sensitive, temperature insensitive liposomes was used to encapsulate the SWNH(-CH2-CH2-COOH)x NPs. The NsL particle was self-stabilized through electrostatic interactions making it less susceptible to chemical and physical disruptions. Anti-her2 mAb was grafted onto the NPs. Results showed the particles were formed with the described structure. The NsiL NPs had a narrow size distribution and high loading capacity. They could eliminate in blood release of paclitaxel based on a 2-level release control mechanism. Release of the drug was initiated upon acidification (around pH 4.3) and controlled by diffusion out of SWNH(-CH2-CH2-COOH)x and the defects formed on liposomes. A composite release profile will contain 3 drug release stages, a minimum leakage in the blood, a burst release on entering lysosomes of tumor cells,

and a slow linear release thereafter. In vitro tests showed NsL particles were low in cytotoxicity and active in cell binding and receptor mediated endocytosis.

Acknowledgment. This work was supported primarily by the Institute for Critical Technology and Applied Science (ICTAS) at Virginia Tech, and partially funded by a grant from Jeffress Memorial Trust, Grant no. J-994. Authors gratefully acknowledge Kathy Lowe for her technical assistance with TEM imaging.

Reference:

[1] Brigger, C. Dubernet, P. Couvreur, Nanoparticles in cancer therapy and diagnosis, *Adv. Drug Deliv. Rev.* 54 (2002) 631-651.

[2] S. Parveen, R. Mistra, S.K. Sahoo, Nanoparticles: a boon to drug delivery, therapeutics, diagnostics and imaging, *Nanomedicine* 8 (2012) 147-166.

[3] L.H. Reddy, Drug delivery to tumors: recent strategies, J. Pharm. Pharmacol. 37 (2005) 1231-1242.

[4] T. Yang, M. Choi, F. Cui, J.S. Kim, S. Chung, C. Shim, D. Kim, Preparation and evaluation of paclitaxel-loaded PEGylated immunoliposome, *J. Control. Release* 120 (2007) 169-177.

[5] Y. Ptail, T. Sadhukha, L. Ma, J. Panyam, Nanoparticle-mediated simultaneous and targeted delivery of paclitaxel and tarquidar overcomes tumor drug resistance, *J. Control. Release* 136 (2009) 21-29.

[6] L.B. Peppas, Recent advances on the use of biodegradable microparticles and nanoparticles in controlled drug delivery, *Int. J. Pharm.* 116 (1995) 1-9.

[7] S. Dufort, L. Sancey, J.L. Coll, Physico-chemical parameters that govern nanoparticles fate also dictate rules for their molecular evolution, *Adv. Drug Deliv. Rev.* 64 (2012) 179-189.

[8] S. Simoes, V. Slepushkin, N. Duzgunes, M.C.P. de Lima, On the mechanisms of internalization and intracellular delivery mediated by pH-sensitive liposomes, *Biochim. Biophys. Acta* 1515 (2001) 23-37.

[9] S.I. Kang, K. Na, Y.H. Bae, Physicochemical characteristics and doxorubicin-release behaviors of pH/temperature-sensitive polymeric nanoparticles, *Colloids Surf. A Physicochem. Eng. Asp.* 231 (2003) 103-112.

[10] K. Xiao, Y. Li, J.S. Li, W. Xiao, A.M. Gonik, R.G. Agarwal, K.S. Lam, The effect of surface charge on in vivo biodistribution of PEG-oligocholic aid based micellar nanoparticles, *Biomaterials* 32 (2011) 3435-3446.

[11] S.J. Kennel, J.D. Woodward, A.J. Rondinone, J. Wall, Y. Huang, S. Mirzadeh, The fate of MAb-targeted $Cd^{125m}Te$/ZnS nanoparticles in vivo, *Nucl. Med. Biol.* 35 (2008) 501-514.

[12] S. Fredenberg, M. Wahlgren, M. Reslow, A. Axelsson, The mechanisms of drug release in poly (lactic-co-glycolic acid)-based drug delivery systems-A review, *Int. J. Pharm.* 415 (2011) 34-52.

[13] J. Xu, M. Yudasaka, S. Kourada, M. Sekido, Y. Yamamoto, S. Iijima, Single wall carbon nanohorn as a drug carrier for conrolled release, *Chem. Phys. Lett.* 461 (2008) 189-192.

[14] L.E. Gerweck, Tumor PH: Implications for treatment and novel drug design, *Semin. Radiat. Oncol.* 8 (1998) 176-182.

[15] U. Repnik, V. Stoka, V. Turk, B. Turk, Lysosomes and lysosomal cathepsins in cell death, *Biochim. Biophys. Acta* 1824 (2012) 22-33.

[16] S. Iijima, M. Yudasaka, R. Yamada, S. Bandow, K. Suenaga, F. Kokai, K. Takahashi, Nano-aggregates of single-walled graphitic carbon nano-horns, *Chem. Phys. Lett.* 309 (1999) 165-170.

[17] W. Huang, J. Zhang, H. Dorn, D. Geohegan, C. Zhang, Assembly of single-walled carbon nanohorn supported liposome particles, *Bioconjugate Chem*. 22 (2011) 1012-1016.

[18] J. Liu, A. Stace-Naughton, X. Jiang, C.J. Brinker, Porous nanoparticle supported lipid bilayers (protocells) as delivery vehicles, *J. Am. Chem. Soc.* 131 (2009) 1354-1355.

[19] C.E. Ashley, E.C. Carnes, G.K. Phillipos, D. Padilla, P.N. Durfee, P.A. Brown, T.N. Hanna, J. Liu, B. Phillips, M.B. Carter, N.J. Carroll, X. Jiang, D.R. Dunphy, C.L. Willman, D.N. Petsev, D.G. Evans, A.N. Parikh, B. Chackerian, W. Wharton, D.S. Peabody, C.J.

Brinker, The targeted delivery of multicomponent cargos to cancer cells by nanoporous particle-supported lipid bilayers, *Nat. Mater.* 10 *(*2011) 389-397.

[20] D. Kasuya, M. Yudasaka, K. Takahashi, F. Kokai, S. Iijima, Selective production of single-wall carbon nanohorn aggregates and their formation mechanism, *J. Phys. Chem. B* 106 (2002) 4947-4951.

[21] W. Guo, J.L. Johnson, S. Khan, A. Ahmad, I. Ahmad, Paclitaxel quantification in mouse plasma and tissues containing liposome-entrapped paclitaxel by liquid chromatography-tandem mass spectrometry: application to a pharmacokinetics study, *Anal. Biochem.* 336 (2005) 213-220.

[22] A.S. Manjappa, K.R. Chaudhari, M.P. Venkataraju, P. Dantuluri, B. Nanda, C. Sidda, K.K. Sawant, R.S.R. Murthy, Antibody derivatization and conjugation strategies: Application in preparation stealth immunoliposome to target chemotherapeutics to tumor, *J. Control. Release* 150 (2011) 2-22.

[23] P. Jie, S.S. Venkatraman, F. Min, B.Y. Chiang Freddy, G.L. Huat, Micelle-like nanoparticles of starbranched PEO-PLA copolymers as chemotherapeutic carrier, *J. Control. Release* 110 (2005) 20-33.

[24] M. Cho, W.S. Cho, M. Choi, S.J. Kim, B.S. Han, S.H. Kim, H.O. Kim, Y.Y. Sheen, J. Jeong, The impact of size on tissue distribution and elimination by single intravenous injection of silica nanoparticles, *Toxicol. Lett.* 189 (2009) 177-183.

[25] D.F. Baban, L.W. Seymour. Control of tumor vascular permeability, *Adv. Deliv. Rev.* 34 (1998)109-119.

[26] G.A. Hughes, Nanostructure-mediated drug delivery, *Nanomedicine* 1 (2005) 22-30.

[27] C. He, Y. Hu, L. Yin, C. Tang, C. Yin, Effects of particle size and surface charge on cellular uptake and biodistribution of polymeric nanoparticles, *Biomaterials* 31 (2010) 3657-3666.

[28] S.D. Li, L. Huang, Nanoparticles evading the reticuloendothelial system: Role of the supported bilayer, *Biochim. Biophys. Acta* 1788 (2009) 2259-2266.

[29] S. Simoses, V. Slepushkin, N. Duzgunes, M.C.P. Lima, On the mechanisms of internalization and intracellular delivery mediated by pH-sensitive liposomes, *Biochim. Biophys. Acta* 1515 (2001) 23-37.

[30] M.N. Jones, A.R. Nicholas, The effect of blood serum on the size and stability of phospholipid liposomes, *Biochim. Biophys. Acta* 1065 (1991) 145-152.

[31] D.D. Lasic, Doxorubicin in sterically stabilized liposomes, *Nature* 380 (1996) 561-562.

[32] J. Miyawake, M. Yudasaka, T. Azami, Y. Kubo, S. Iijima, Toxicity of single-walled carbon nanohorns, *ACS Nano* 2 (2008) 213-226.

[33] R.M. Lynch, B.H. Boy, D.F. Glass, S.M. Mahurin, B. Zhao, H. Hu, A.M. Saxton, R.L. Donnell, M.D. Cheng, Assessing the pulmonary toxicity of single-walled carbon nanohorns, *Nanotoxicology* 1(2007) 157-166.

[34] P. Constantine, M.S. Firme III, R.B. Prabhakar, Toxicity issues in the application of carbon nanotubes to biological systems, *Nanomedicine* 6 (2010) 245-256.

[35] J.M. Extra, F. Cognetti, S. Chan, D. Maraninchi, R. Snyder, L. Mauriac, First-line trastuzumab (Herceptin ®) plus docetaxel versus docetaxel alone in women with HER2-possitive metastatic breast cancer (MBC): results from a randomized phase II trail (M77001), *Breast Cancer Res. Treat.* 82 (2003) A 217.

[36] D.J. Slamon, B. Leyland-Jones, S. Shak, H. Fuchs, V. Paton, A. Bajamonde, et al. Use of chemotherapy plus a monoclonal antibody against HER2 for metastatic breast cancer that overexpresses HER2, *N. Engl. J. Med.* 344 (2001) 783-792.

[37] M. Marty, F. Cognetti, D. Maraninichi, et al. Randomized phase II trail of the efficacy and safety of trastuzumab combined with docetaxel in patients with human epidermal growth

factor receptor 2-positive metastatic breast cancer administrated as first-line treatment: the M77001 study group, *J. Clin. Oncol.* 23 (2005) 4265-4274.

[38] T. Lammers, F. Kiessling, W.E. Hennink, G. Storm, Drug targeting to tumors: Principles, pitfalls and (pre-) clinical progress, *J. Control. Release* 161 (2012) 175-187.

[39] S.R. Grobmyer, G. Zhou, L.G. Gutwein, N. Iwakuma, P. Sharma, S.N. Hochwald, Nanoparticle delivery for metastatic breast cancer, *Maturitas* 73 (2012) 19-26.

[40] M.S. Ehrenberg, A.E. Friedman, J.N. Finkelstein, G. Oberdorster, J.L. McGrath, The influence of protein adsorption on nanoparticle association with cultured endothelial cells, *Biomaterials* 30 (2009) 603-610.

[41] C.M. Perou, T. Sorlie, M.B. Eisen, M. van de Rijn, S.S. Jeffrey, C.A. Rees, et al. Molecular portraits of human breast tumours, *Nature* 406 (2000) 747-752.

[42] Ww Dean-Colomb, F.J. Esteva, Her2-positive breast cancer: herceptin and beyond, *Eur. J. Cancer* 44 (2008) 2806-2812.

[43] D.J. Slamon, G.M. Clark, S.G. Wong, W.J. Levin, A. Ullrich, W.L. McGuire, Human breast cancer: correlation of relapse and survival with amplification of the HER-2/neu oncogene, *Science* 235 (1987) 177-182.

[44] N.E. Hynes, D.F. Stern, The biology of erbB-2/neu/HER-2 and its role in cancer, *Biochim. Biophys. Acta* 1198 (1994) 165-184.

[45] N. Wilcken, R. Dear, Chemotherapy in metastatic breast cancer: a summary of all randomized trials reported 2000-2007, *Eur. J. Cancer* 44 (2008) 2218-2225.

[46] F. Puglisi, F. Cardoso, F. Lerun, M. Piccart, First-line treatment of metastatic breast cancer: available evidence and current recommendations, *Am. J. Cancer* 5 (2006) 99-110.

[47] C. Andreetta, A.M. Minisini, M. Miscoria, F. Puglisi, First-line chemotherapy with or without biologic agents for metastatic breast cancer, *Crit. Rev. Oncol. Hematol.* 76 (2010) 99-111.

[48] M.A. Olayioye, R.M. Neve, H.A. Lane, N.E. Hynes, The ErbB signaling network: receptor heterodimerization in development and cancer, *EMBO J.* 19 (2000) 3159-3167.

[49] H.S. Cho, K. Mason, K.X. Ramyar, A.M. Stanley, S.B. Gabelli, Jr D.W. Denney, D.J. Leahy, Structure of the extracellular region of HER2 alone and in complex with the Herceptin Fab, *Nature* 421 (2003) 756-760.

[50] A. Cirstoiu-Hapca, F. Buchegger, N. Lange, L. Bossy, R. Gurny, F. Delie, Benefit of anti-HER2-coated paclitaxel-loaded immuno-nanoparticles in the treatment of disseminated ovarian cancer: Therapeutic efficacy and biodistribution in mice, *J. Control. Release* 144 (2010) 324-331.

[51] E.T. Dams, P. Laverman, W.J. Oyen, G. Storm, G.L. Scherphof, J.W. van Der Meer, F.H. Corstens, O.C. Boerman, Accelerated blood clearance and altered biodistribution of repeated injections of sterically stablilized liposomes, *J. Pharmacol. Exp. Ther.* 292 (2000) 1071-1079.

[52] J. Zhang, J. Ge, M.D. Shultz, E. Chung, G. Singh, C. Shu, P.P. Fatouros, S.C. Henderson, F.D. Corwin, D.B. Geohegan, A.A. Puretzky, C.M. Rouleau, K. More, C. Rylander, M.N. Rylander, H.W. Gibson, C. Dorn, In vitro and in vivo studies of single-walled carbon nanohorns with Encapsulated metallofullerenes and exohedrally functionalized quantum dots, *Nano Lett.* 10 (2010) 2843-2848.

[53] K.T. Sato, A.C. Larson, T.K. Rhee, R.A. Salem, A.A. Nemcek, T. Mounajjed, T. Paunesku, G. Woloschak, P. Nikolaides, R.A. Omary, Real-time MRI monitoring of transcatheter hepatic artery contrast agent delivery in rabbits, *Acad. Radiol.* 12 (2005) 1342-1350.

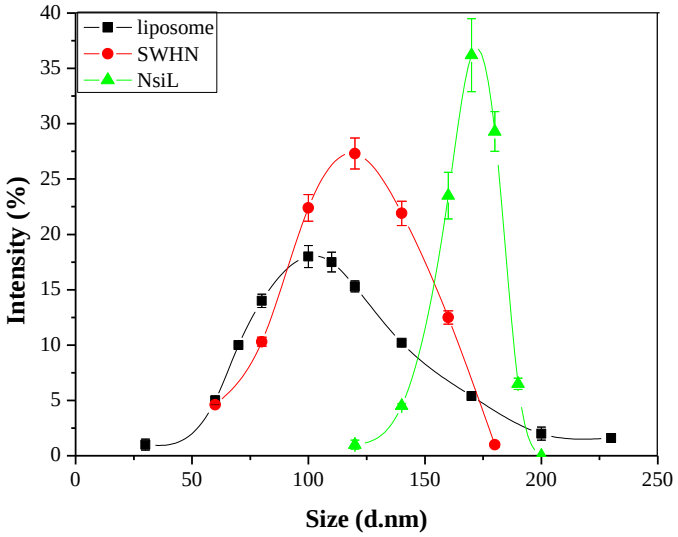

Figure 1. Size distribution of different nanoparticles.

PEGylated DSPC lipsome (black), SWNH(-CH2-CH2-COOH)x (red) and DSPC NsiL (green). Sizes are shown in diameters (mean ± S.D., n = 45).

a

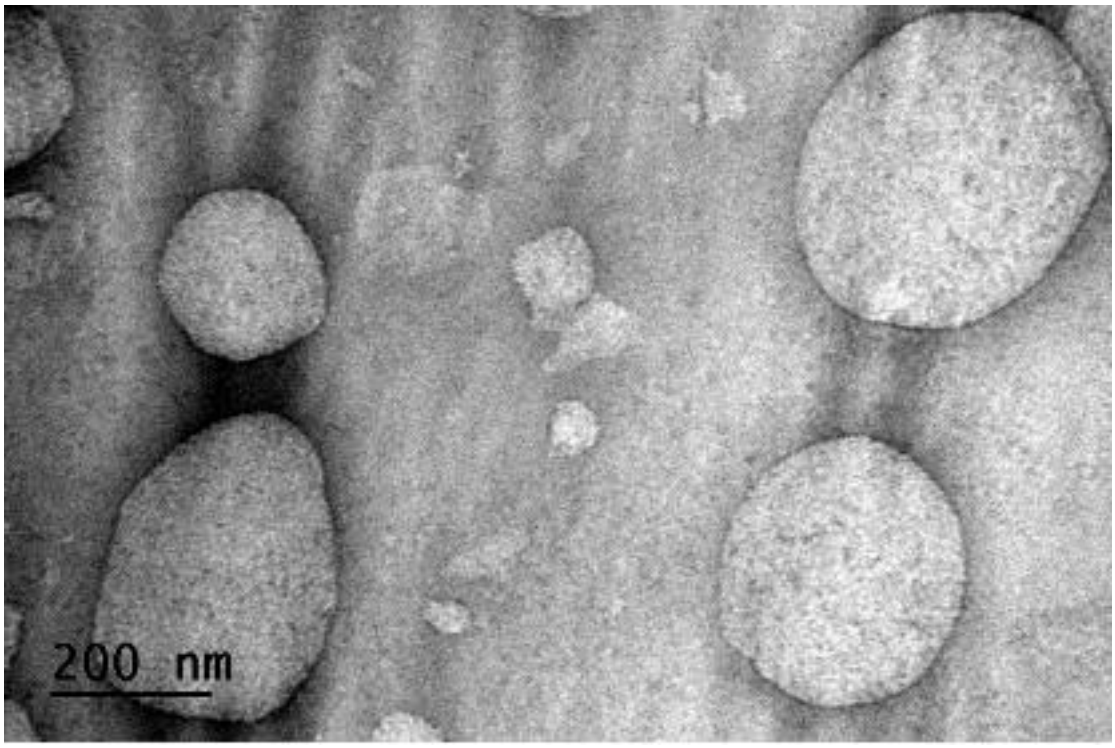

b

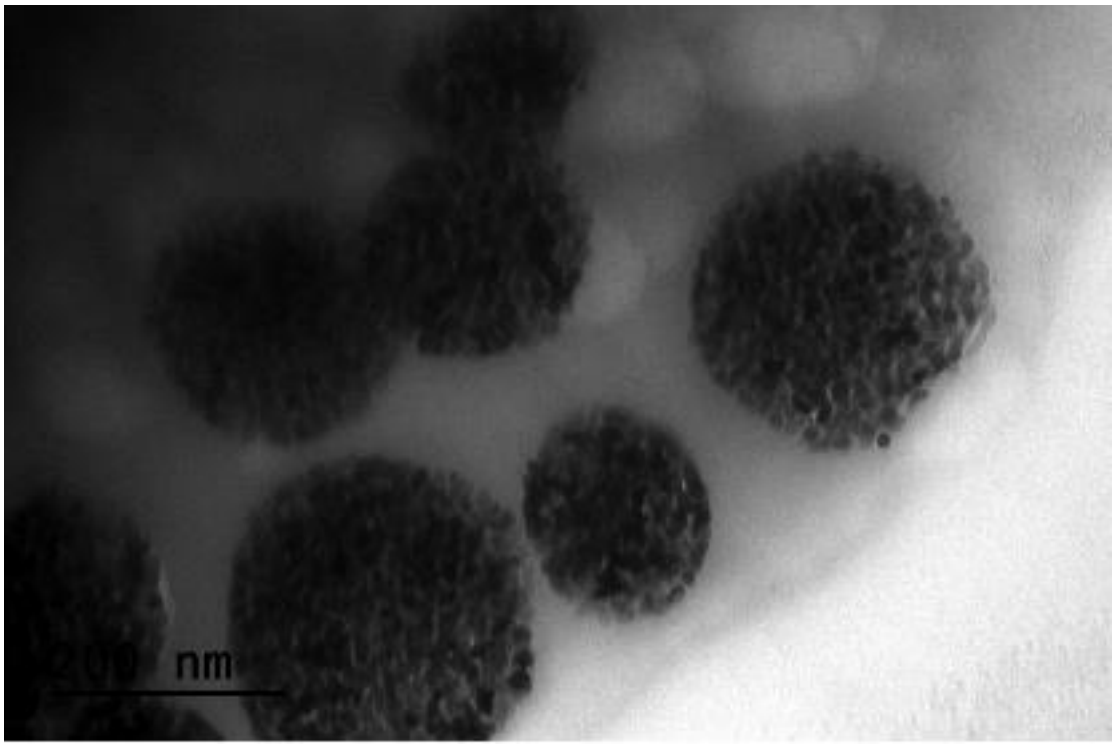

c

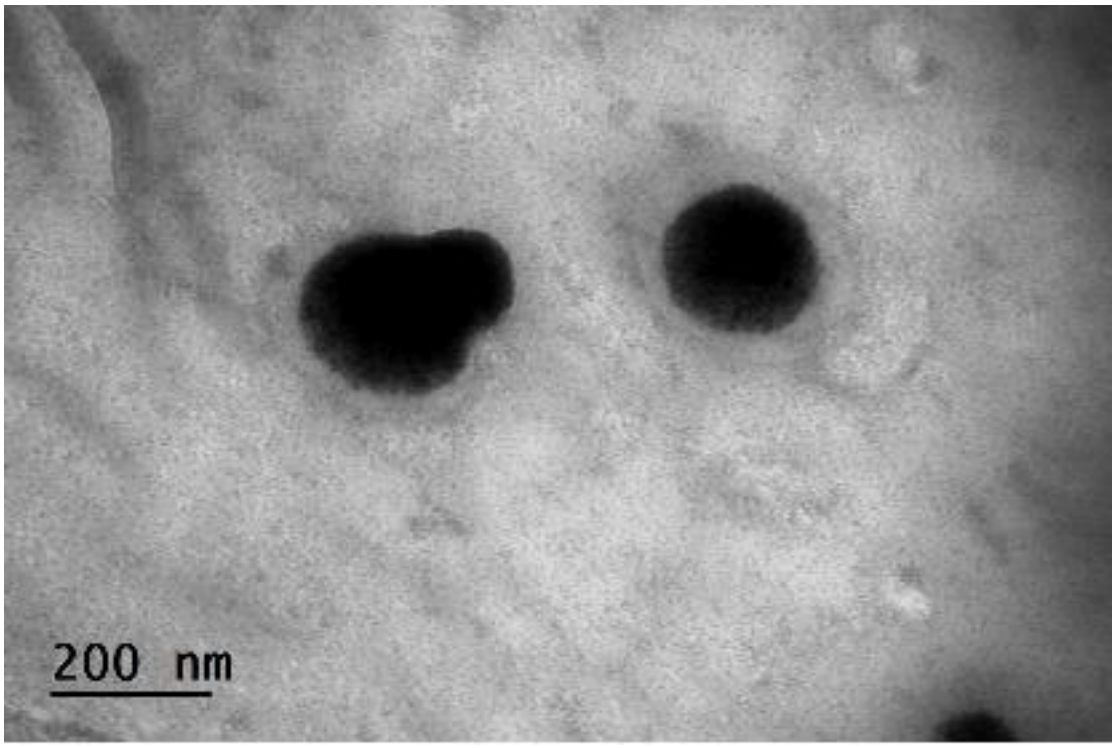

d

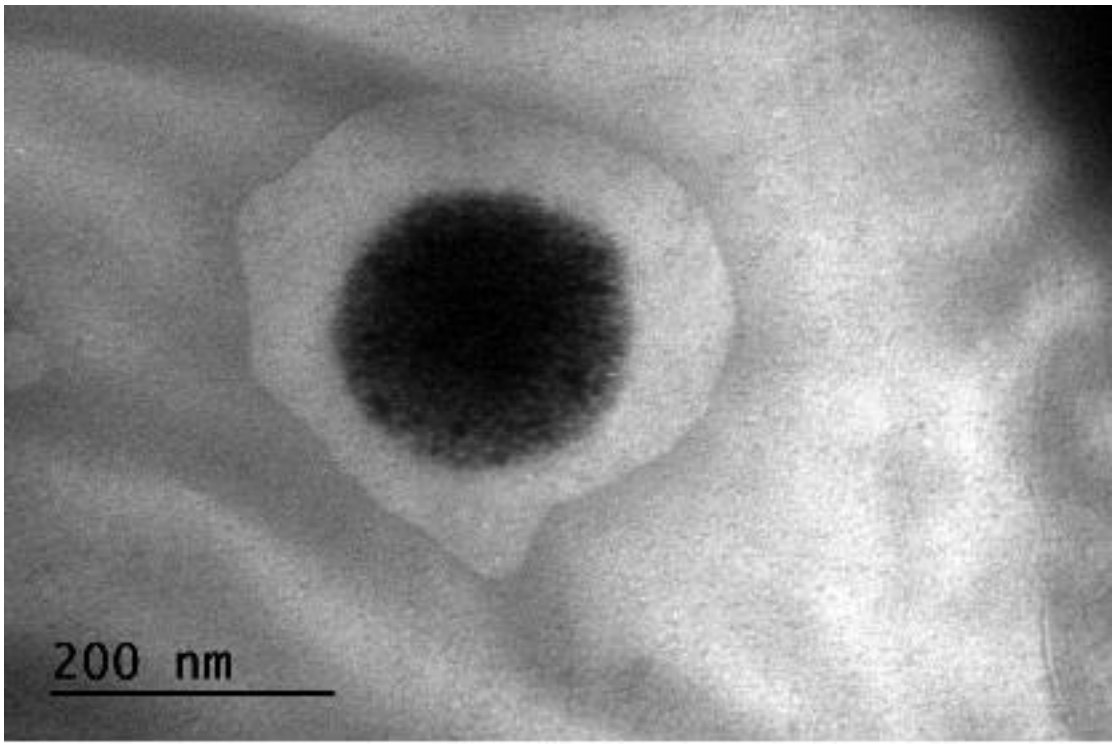

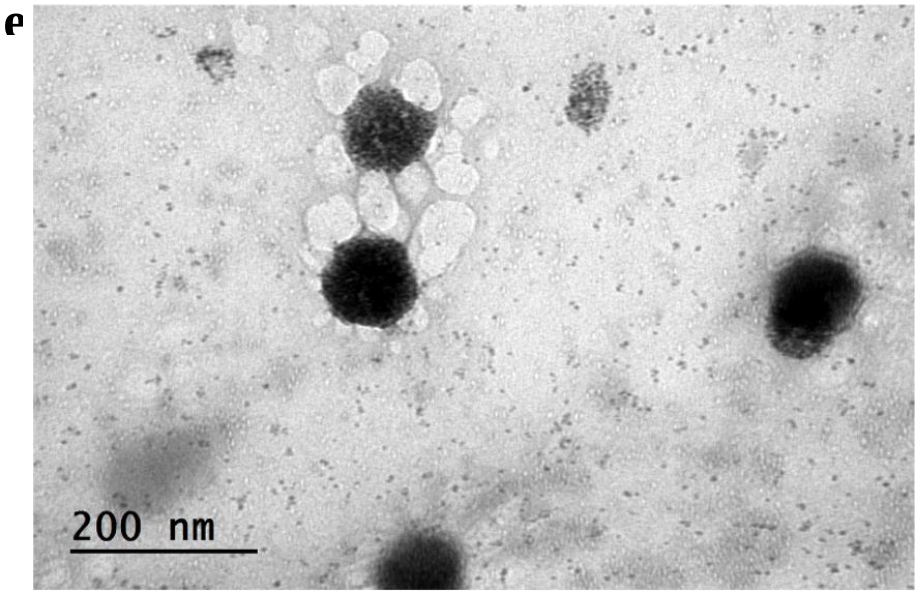

Figure 2. Morphology study of different nanoparticles by TEM.

a, PEGylated DSPC liposomes. b, SWNH(-CH2-CH2-COOH)x. c,d, DSPC NsL. e, SWNH(-CH2-CH2-COOH)x surrounded by liposomes. Immediately before TEM tests, samples were deposited onto carbon coated cupper grids and negatively stained with 2% phosphotungstic acid.

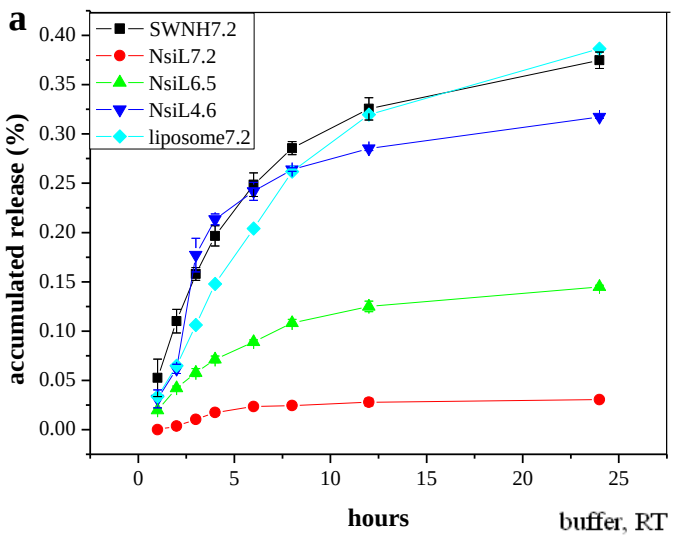
a
SWNH7.2
NsiL7.2
NsiL6.5
NsiL4.6
liposome7.2
accumulated release (%)
0.40
0.35
0.30
0.25
0.20
0.15
0.10
0.05
0.00
0
5
10
15
20
25
hours
buffer, RT

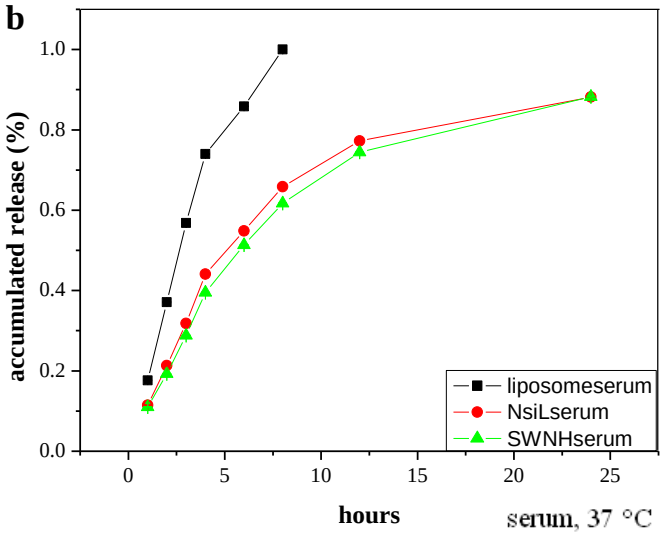
b
liposomeserum
NsiLserum
SWNHserum
accumulated release (%)
1.0
0.8
0.6
0.4
0.2
0.0
0
5
10
15
20
25
hours
serum, 37 °C

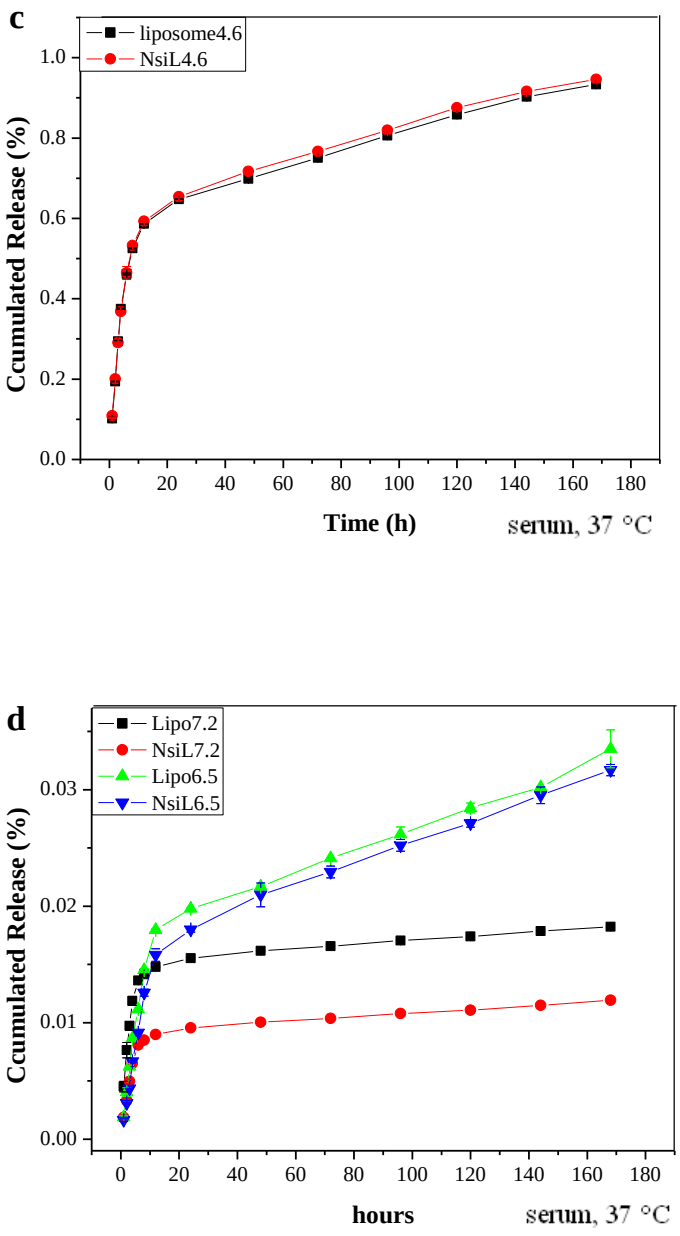

Figure 3. Paclitaxel release profile of different carriers.

a, in buffer paclitaxel release from PEGylated DOTAP liposome, SWNH(-CH2-CH2-COOH)x and DOTAP NsiL. b, in serum paclitaxel release from PEGylated DOTAP liposome, SWNH(-CH2-CH2-COOH)x and DOTAP NsiL. c, in serum paclitaxel release from PEGylated DSPC

liposome at pH 4.6. d, in serum paclitaxel release from PEGylated DSPC liposome at pH 7.2 and 6.5. All liposomes were PEGylated. All SWNHs were functionalized. Numbers indicate the pH.

a

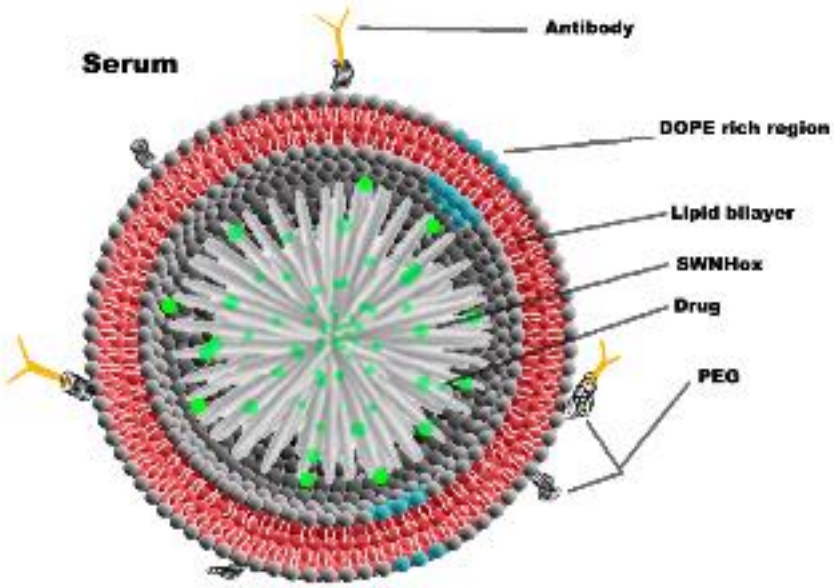

b

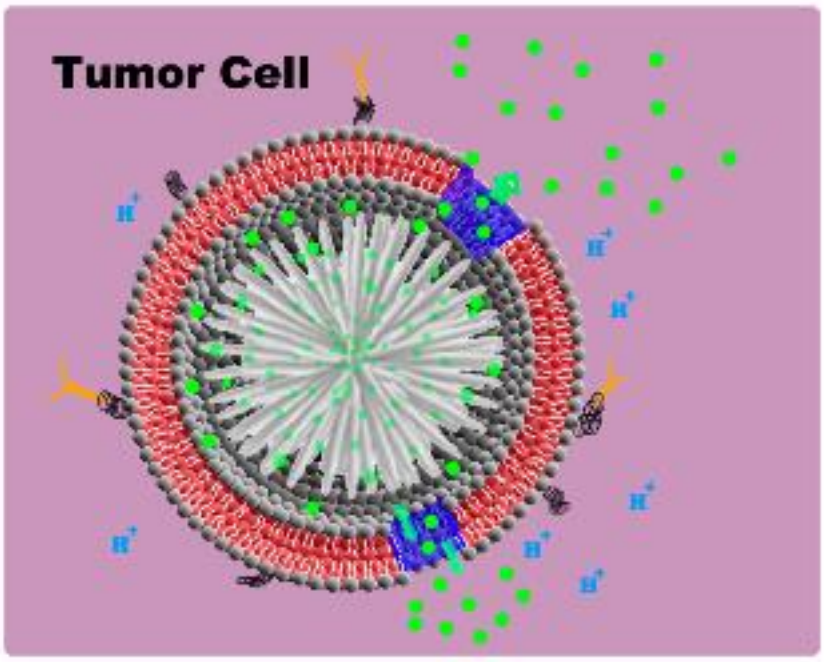

Figure 4. Structure and releasing mechanism of NsiL. a, in serum. b, in tumor cells.

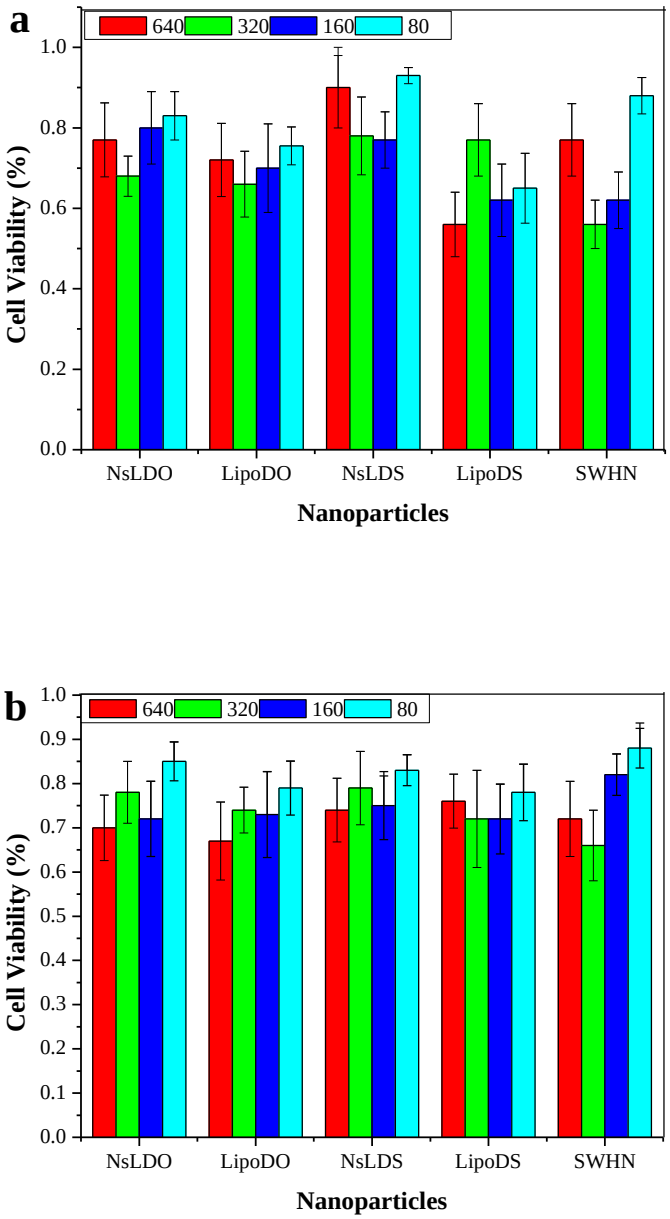

Figure 5. Study of NPs cytotoxicity by cell viability test.

a, SK-BR-3 cells. b, BT-20 cells. Cells were treated with 640, 320, 160 and 80 µg/ml NPs (in lipid concentration). NsLDO and LipoDO are DOTAP NsL and PEGylated DOTAP liposomes, respectively. NsLDS and LipoDS are DSPC NsL and PEGylated DSPC liposomes, respectively. SWHN indicates SWNH(-CH2-CH2-COOH)x.

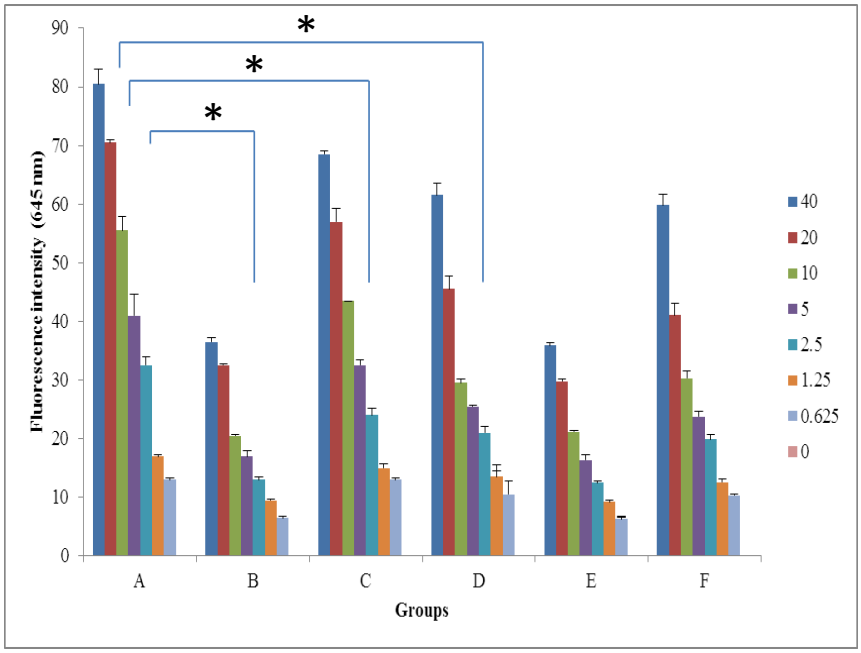

Figure 6. Cell binding affinity of different NPs.

Different concentrations of particles were incubated with cell cultures, 40 µg/ml, 20 µg/ml, 10 µg/ml, 5 µg/ml, 2.5 µg/ml, 1.25 µg/ml, 0.625 µg/ml and blank control. A: NsiL with SK-BR-3; B: NsL with SK-BR-3; C: herceptin NsiL with SK-BR-3; D: NsiL with BT-20; E: NsiL with BT-

20; F: herceptin NsiL with BT-20. NPs were labeled with rhB. Fluorescence emissions at 645 nm were measured. (*, $p < 0.05$)

a

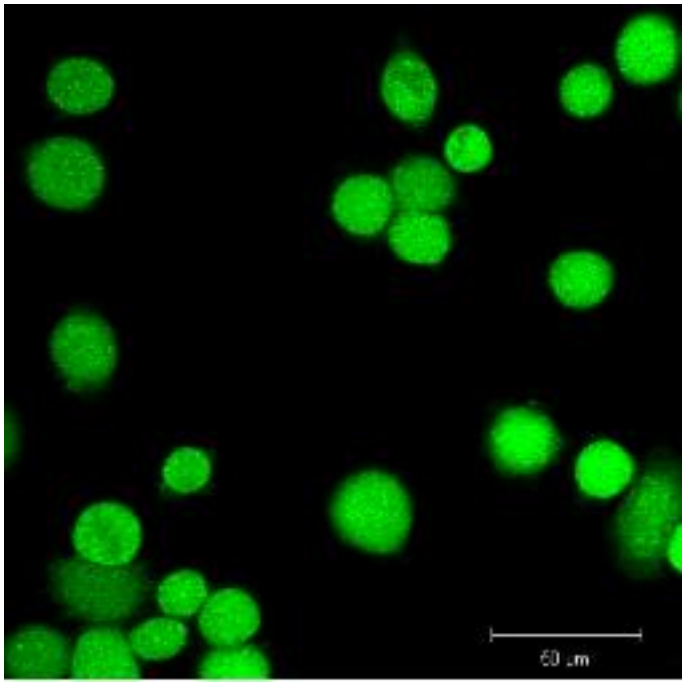

b

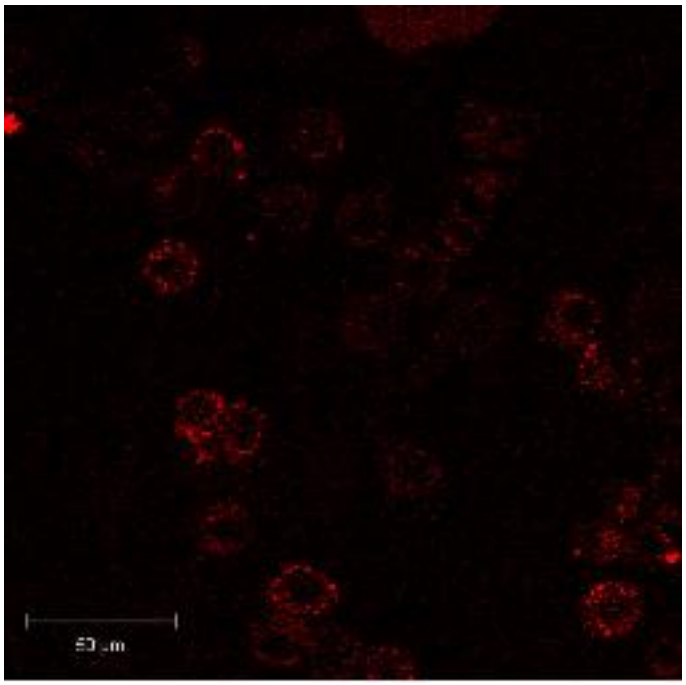

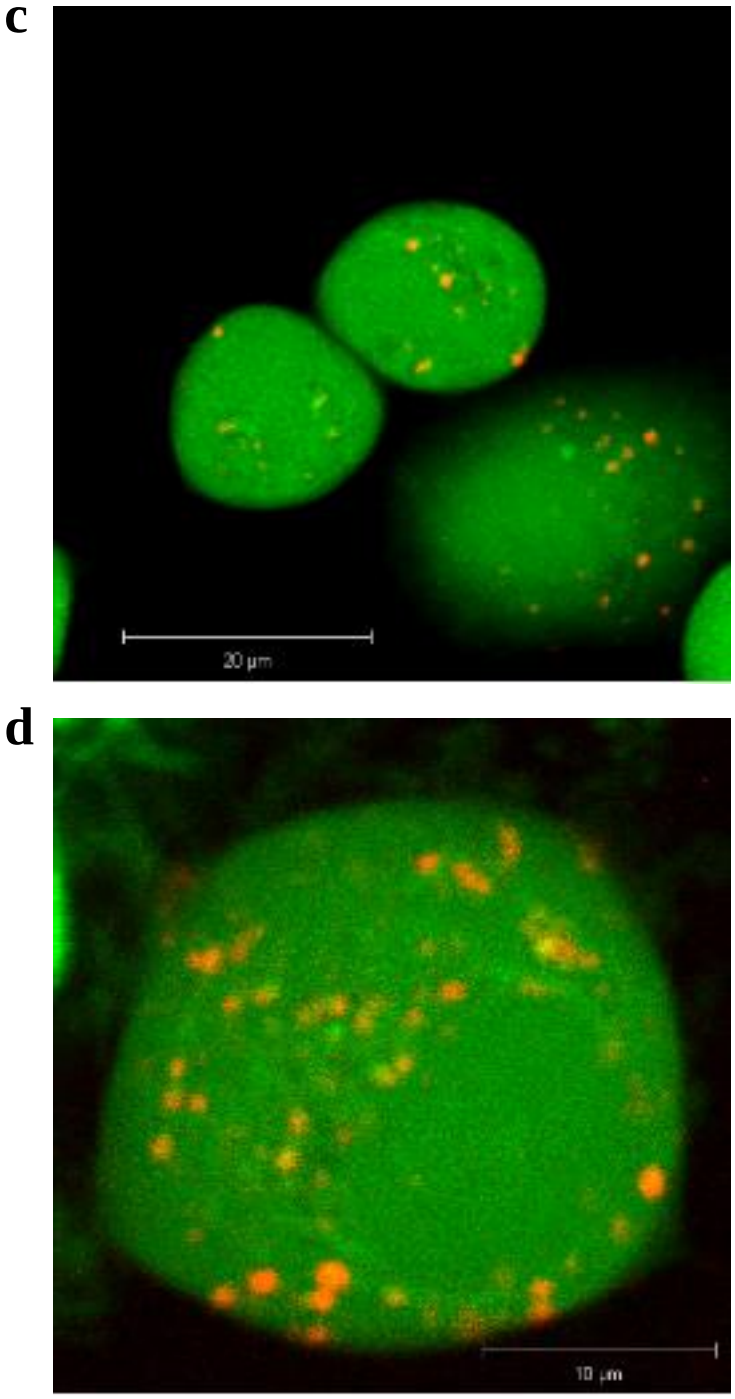

Figure 7. Cell internalization observed by confocal laser microscopy.

a, stained SK-BR-3 cells with unstained NsiL. b, unstained SK-BR-3 cells with stained NsiL. c,d, co-stained NsiL in SK-BR-3 cells.

Table (1) Properties of lipid used in NsiL immunoliposome formulation.

Lipid	Head group net charge	Fatty acid tail	Molar ratio	Function
DOTAP/ DSPC	+1/ 0	18:1, 9 cis/ 18:0	40%	Form cationic liposome; interact with negatively charged nanohorn
DOPE	0	18:1, 9 cis	33%	Form pH sensitive area in the lipid bilayer structure on NsiL
CHOL	NA	NA	20%	Increase fluidity to lipid bilayer
DSPE-mPEG2000	0	18:0	5%	Coat NsiL with proper amount of PEG; increase half life of NsiL in circulation
DSPE-PEG2000-mal	0	18:0	2%	Covalently couple with anti ErBb2 monoclonal mouse IgG

Chapter VI: Accurate control of polymeric nanoparticle size by nanoprecipitation

Wei Huang, Chenming Zhang

(Manuscript in preparation to be submitted to Acta Biomaterialia)

Abstract

Polymeric nanoparticles (PNP) have received much attention as drug carriers, because they could have high loading of the toxic drugs, accumulate at the target site and release the drug at a controlled rate thereafter. Size of the particle has large impact on drug loading, *in vivo* distribution, extravasation, intratumor diffusion and cell uptake, thus is critical for a successful delivery. Particles with 100-200 nm range are generally preferred. Such particles are usually prepared by the nano-precipitation technique. However, the control of the size is still based on the concentration of the polymer in the organic phase, which is largely limited by the solubility. In this study, we systematically investigated the effect of polymer concentration, organic solvent, temperature, ionic strength, organic injection rate, aqueous phase agitation rate, gauge of the needles and final polymer concentration on the size distribution. Poly(lactic-*co*-glycolic acid) nanoparticles with accurate controlled size distribution, such as 50 nm, 100 nm, 150 nm and 200 nm were fabricated.

Key words: polymeric nanoparticles, nano-precipitation, size, diffusion, tumor targeting

1. Introduction

Polymeric nanoparticles (PNP) are used to deliver high dose of toxic drugs to target the pathologic tissue and release the drug at a controlled rate [1]. PNPs can be fabricated with biocompatible or biodegradable materials, so they bring no dire effect to the body. Many researches have been focused on PNP tumor targeting. Briefly, intravenously administrated PNPs would extravasate and accumulate at the tumor site by the enhanced permeability and retention effect (EPR) [2]. At this stage, if the therapeutics are anti-receptor antibodies, they can already begin functioning as inhibitors of the receptors located on the surface of the tumor cells to interrupt the cell growth or invasion [3]. If the drugs are to be delivered into the cytoplasm or nucleus (i.e. chemotherapy or gene-therapy agents), cell internalization or nucleus targeting will be involved. The PNPs will need to go through processes such as endocytosis [4] and lysosome escaping [5], wherein PNPs are transported across the membrane and intracellularly. Similarly, therapeutics loaded PNPs have also been sent across the blood-brain barrier (BBB) in attempts to treat brain diseases (i.e. Alzheimer's disease, Parkinson's disease), where the PNPs are required to locate and penetrate the brain capillary endothelial cells, one of the major component of the BBB [6]. Other efforts have been made to treat organ [7,8] and infectious diseases [9.10]. Transportation of the PNPs in blood to tissues and into the pathological cells occurs in both cases.

The side effects (i.e. immunosuppression, cardio toxicity, neurotoxicity, nausea) of the drugs could be conceivably eliminated if all injected particles reached the target site. However, *in vivo*

studies usually showed a rather broad distribution of the PNPs inside the body. Instead of accumulating at the tumor, in the case of cancer, large portions of the PNPs are rapidly cleared from the blood circulation by the mononuclear phagocyte system (MPS) upon opsonisation, or filtered out in other particular organs [11]. The process is strongly affected by the particle size. Generally, PNPs larger than 200 nm are frequently sieved by sinusoid of spleen, 100 to 150 nm ones are captured by the Kupffer cells of liver, and the ones smaller than 5.5 nm are found leak out from the kidney [11]. Jong et al. investigated the size dependent organ distributions of intravenously injected nanoparticles. A distinguishable presence of 10 nm particles was found in blood, liver, spleen, kidney, testis, thymus, heart, lung and brain while the other larger particles (50 nm, 100 nm and 250 nm) were only dominantly found in blood, liver and spleen [12]. Mirahmadi et al. [13] and Liu et al. [14] compared tissue distribution of particles around 200 nm with the ones over 1000 nm and they both showed a higher tendency of MPS clearance for the larger particles.

Variations of PNP sizes can also result in different cell uptake rates. Cells internalize particles via different pathways depending on the size, generally, receptor-mediated endocytosis for 100-200 nm ones and phagocytosis for the larger ones [15]. Win et al. observed a highest uptake rate for 100 nm particles when 50 nm, 100 nm, 200 nm, 500 nm and 1000 nm PNPs were incubated with Caco-2 cells [16]. The rate decreases exponentially as the size exceeded 100 nm [16]. They also found that 150 nm PNPs had the optimal uptake rate by murine non-phagocytes [17]. A large range (40-15000 nm) of PNPs were tested on dendritic cells by Foged et al. and the result favored the particles smaller than 500 nm [18]. Zauner et al. reported a cell type dependent uptake as human umbilical vain endothelial cells, ECV 304 and HNX 14C can take up

microspheres up to 1010 nm, whereas Hepa 1-6 and HepG2 only uptake PNPs smaller than 93 nm [19].

Florence pointed out that the diffusion rate of PNPs through the extracellular matrix (ECM) has to be considered when studying the in tumor drug distribution [20], and based on a finding by Goodman et al. that only 20-40 nm particles were found penetrated into an enzyme treated tumor spheroid (i.e. enzyme treatment degrade ECM inside the tumor) [21]. The Stokes-Einstein equation applies to the diffusion rate and explains the difficulty of in tumor drug spreading and the influence of the particle size [20]. It is also noteworthy to mention the impact of size on drug loading, and colloid stability. Larger particles commonly have a higher drug loading capacity, but the colloid stability was found to drop with the increase of the particle size above a threshold [22].

One efficient way of controlling PNP size is by carefully selecting the fabrication technique and pertinent synthesis parameters [23]. Among the fabrication methods (i.e. the bottom-up and top-down methods), the most widely used ones in producing nano-drug carriers include double emulsion [24], nano-precipitation [25], and spray drying [26]. The double emulsion and spray drying methods usually lead to production of large PNPs (over 300 nm) [27,28]. Smaller PNPs (i.e. 100-200 nm) have been reported to result from nano-precipitation. However, the concentration of the polymer is believed to be the only control of the particle size [23]. Therefore, the producible particle size is largely limited by the solubility of the polymer. In this work, nano-precipitation method was systematically investigated in order to establish an accurate way of fabricating intravenous injection PNPs for tumor targeting with suitable size. Poly (D,L-lactide-co-glycolide) (PLGA) was used as a model material.

2. Materials and methods

2.1 Materials

PLGA (50:50, mw: 30,000-60,000) and polyvinyl alcohol (PVA) were purchased from Sigma-Aldrich (St. Louis, MO). Solvent and other chemicals were purchased from Fisher Scientific (Pittsburg, PA) unless otherwise specified. Deuterium oxide was purchased from Cambridge Isotope Laboratories (Andover, MA).

2.2 PLGA PNP fabrication by nano-precipitation

Predetermined amount of PLGA was dissolved in the organic phase and injected at predetermined rate into the aqueous phase by a vertically mounted syringe pump with magnetic stir agitation. The resulted suspension was placed under vacuum with agitation in a safety fume hood overnight to eliminate the organic solvent. Powder PNPs were produced from the liquid suspensions by freeze drying.

2.3 Size and zeta potential measurement

Size distribution and zeta potential of PLGA PNPs were analyzed on a Zetasizer Nano ZS (Malvern Instruments, Southborough, MA). Samples were freshly prepared before use by adding aliquots of PNPs to 0.01 M sodium chloride buffer to make a solution with a PLGA concentration of 0.1 mg/ml. During the test, samples were injected into a disposable capillary cell DTS1060 (Malvern Instruments, MA) and loaded onto the analyzer. Measurements were taken at 25 ºC with a material refraction index of 1.33, and viscosity of 0.8872 cp.

2.4 Morphology study of PLGA PNPs

Transmission electronic microscopy (TEM) images were taken for morphology study. Briefly, liquid samples were deposited onto carbon coated copper grids for 5 min. 2% phosphotungstic acid was used for negative staining for 30 s. TEM images were taken by a JEOL JEM 1400 (JEOL Ltd, Tokyo, Japan).

2.5 Size distribution versus altered relative diffusion rate

Impacts of polymer concentration, organic solvent, ionic strength of aqueous phase and temperature of aqueous phase on particle size were studied. To make the PNPs, 2 ml of the organic phase (10 mg/ml PLGA acetonitrile solution) was injected into 100 ml filtered 0.1% PVA aqueous solution at a rate of 2 ml/ min at 25 ºC for each case unless otherwise specified.

For the polymer concentration test, final concentrations of 1 mg/ml, 5 mg/ml, 10 mg/ml, 20 mg/ml and 40 mg/ml PLGA in acetonitrile were made with brief sonication. For the solvent test, the organic phase was made by dissolving PLGA in three types of solvent, acetonitrile, acetone and tetrahydrofuran (THF), with a final concentration of 10 mg/ml. For the ionic strength test, the organic phase was injected into aqueous phase containing increasing amount of sodium chloride (0 mM, 0.1 mM, 1 mM, 10 mM, 100 mM and 1000 mM). For the temperature test, the aqueous phase was adjusted to the predetermined temperature (0 ºC, 10 ºC, 20 ºC, 30 ºC, 40 ºC, 50 ºC, 60 ºC, 70 ºC and 80 ºC) before the injection.

2.6 Size distribution versus constant relative diffusion rate

Impacts of organic phase injection rate, aqueous phase flow rate, gauge of the needle and final concentration of polymer in the suspension on particle size were studied. Again, to make the PNPs, 2 ml of the organic phase (10 mg/ml PLGA acetonitrile solution) was injected into 100 ml

filtered 0.1% PVA aqueous solution at a rate of 2 ml/ min at 25 ºC for each case unless otherwise specified.

For the injection rate test, four flow rate of the organic phase were compared, 2 µl/min, 20 µl/min, 200 µl/min and 2000 µl/min. For the aqueous phase flow rate test, decreasing magnetic stir agitation speed was applied to the aqueous phase (1200 rpm, 1100 rpm, 700 rpm, 350 rpm, 125 rpm and 0 rpm). For the needle gauge test, five commonly accessible syringe needles were used for the injection (14G, 16G, 20G, 23G, 27G). For the final polymer concentration test, predetermined volume of organic phase was constantly added to 2 ml of aqueous phase to make the final PLGA concentration in water from 0.1 mg/ml to 10 mg/ml. Increase of particle numbers resulted from higher concentrations were monitored by flow cytometer (FCM).

2.7 Diffusion coefficient measurement

All NMR diffusion experiments were performed with a Bruker Avance III NB 600 MHz (14.1 T) NMR spectrometer, using a TBI single-axis gradient probe and a 5 mm inner coil. The diffusion measurements were acquired with ^{1}H signal with pulsed-gradient stimulated-echo pulse sequence.

3. Results and discussion

3.1 Influence of the polymer concentration in organic phase on size

The concentration of the polymer is a known factor that controls the PNP size. As expected, the PLGA particles showed a stepwise increase in size with the concentration in the range of 0-20 mg/ml (Fig. 1A). Each concentration tested led to a narrow distribution of PNP size. The increase of the concentration to 40 mg/ml raised the mean PNP diameter to 291.35 ± 7.21 nm. However, the mode size of the population remained the same as that of 20 mg/ml. The increase

of overall size distribution is due to the formation of large particles (over 500 nm) (Fig. 1A). A calibrated curve for the dependency of size on polymer concentration is shown in Fig. 1B. Notice that within the 0-20 mg/ml region, the PNP size in fact increases quite linearly with polymer concentration. This is reasonable in a sense that the PNPs are formed *via* precipitation from the oil in water (o/w) droplets as the organic solvent diffuses into the aqueous phase [29]. Therefore, more concentrated PLGA in a droplet would lead to larger particles given that the o/w droplets formed from each batch are comparable and homogenous in volume. The size broadening of the 40 mg/ml batch is most likely resulted from the formation of polydispersed droplets due to the increased viscosity at high polymer concentration. The polydispersity of the droplets and thus the PNPs are also observed in the other following experiments when the viscosity of the aqueous phase becomes high (i.e. when using organic solvent with higher viscosity, high salt concentration aqueous phase, low temperature, high total polymer concentration in the suspension).

3.2 Influence of the organic solvent on size

Two important properties of the organic solvent used for nano-precipitation are the polymer solubility and water miscibility [25]. The most commonly used solvents include acetonitrile, acetone, ethanol, methanol, dichloromethane (DCM). A solvent is usually selected empirically. However, there is still no clear understanding of the effect of the solvent nature on the resulting PNP size [23]. Representative size distribution and mean diameter results are shown in Fig. 2A and B respectively (data for ethanol and methanol are not shown due to the lower solubility in the two solvents). As it can be seen that, dissolved with the same concentration of PLGA, the three solvents (acetonitrile, acetone and THF) produced increasing size of PNPs. Noticing the molecule size of the three solvents shared the same trend; we measured the diffusion coefficient

(D_{pw}) of the solvent with/without the presence of PLGA in water. The results showed a trend of acetonitrile > acetone > THF in both cases (see table 1). We hypothesize that the in water D_{pw} of the solvent with the presence of the polymer can be a good indication of the corresponding PNP size distribution. Solvents with higher D_{pw} assist the formation of smaller PNPs with narrow distribution and *vise versa*. The other solvents (data not shown) we tested also support the hypothesis. Methanol and ethanol have high D_{pw} and resulted in sharp size distribution within the 50–100 nm range. However, the solubility of PLGA in those solvents is relatively low compared to that in acetonitrile. On the other hand, no instant formation of PNP was observed using dimethyl sulfoxide or DCM. Instead, the solvent polymer mixture formed an oily layer at the bottom of the reactor. With agitation, PNPs with an extremely broad size distribution (i.e. microspheres) were formed after the organic solvent removal.

3.3 Influence of the temperature on size

The viscosity of water slightly alters with temperature. Changes of the temperature should shift the D_{pw} of the solvent and provide a fine adjustment of the PNP size. The temperature dependence of size distribution and average are shown in Fig. 3A and B respectively. On average, there is a 10 nm increase of particle size with every 10 degree temperature drop (Fig. 3A), and overall the mean diameter of the particle decreased for about 100 nm with the increase of 80 degree in termperature (Fig. 3B). Including PLGA, some polymeric materials undergo fast hydrolytic degradation especially at high temperature [30]. Meanwhile, degradation or denaturing of the loaded bio-materials (i.e. protein, nucleic acids) may also occur. However, it is noteworthy to mention that the precipitation duration is relatively transient to the degradation of the polymer and potential contents the particles may carry. The combination of polymer

concentration and aqueous temperature could serve as an accurate way of controlling the PNP size.

3.4 Influence of the salt concentration on size

The inclusion of salt in macroionic suspensions is known to cause a formation of a highly ordered crystal-like network of the charged colloid particles with the counter ions and thus increase the viscosity of the system [31]. Based on our hypothesis, the salt concentration should have an impact on the PNP size. As shown in Fig. 4A, 10 mM seems to be a critical concentration, below which the PNPs grew very slowly in size and showed narrow distributions, and above which from 10 to 100 mM the PNP size increased significantly but a moderate size-increase rate from 100 to 1000 mM was observed. All PNPs made at above 10 mM NaCl showed broadened size distributions due to the low. Trend of zeta potential and diffusion coefficient of the PNPs with the increase of NaCl concentration are shown in Fig. 4B and C respectively. The 10 mM data point showed significantly larger error than that under other salt concentrations, which is most like due to the high viscosity and D_{pw} variation in corresponding to small concentration change around 10 mM. The high sensitivity of viscosity and D_{pw} indicates the 10 mM region is a very robust range for the transformation from PNP free dispersion to the ordered crystal-like network to occur, as also evidenced by many other works using poly (2-vinyl pyridine), sodium polystyrene sulfonate and poly-L-lysine [31]. A calibration curve is shown in Fig. 4D. The mean size of 100 mM and 1000 mM batch exceeded 1000 nm (microspheres), which are out of the range of the preferred PNPs for intravenously tumor drug delivery.

3.5 Some none influential factors

Influences of organic injection rate, aqueous phase agitation rate and gauge of the needles on the size of PNPs were also investigated. As shown in Fig. 5, 6 and 7, the three parameters have no

apparent effect on the PNP size. Small variations in size were likely due to random measurement error. No distinguishable mean size differences were shown within the tested levels (data not shown). Zeta potential values of the PNPs were determined as between -30 mV to -40 mV for all tested batches. The particles gained the high charge upon formation and started to repel each other. The colloidal stability was thus maintained regardless of mixing rate of the two phases in a given space. Since the three parameters only affect the rate of mass transport but not D_{pw}, as expected, the size of the PNPs were found unchanged even when extreme values such as 2 ml/min (for organic injection rate), 0 rpm (for aqueous agitation speed) were used.

Although the three parameters are proved to have no noticeable effect on PNP size, they are meaningful from the manufacture point of view. The production of PNP with controlled size can be scaled up. For example, a multiple injection points, temperature controlled, continuously stirred reactor will be suitable for high output, size controlled production of PNPs.

3.6 Influence of the final concentration on size

It is of interest to determine the endpoint of the producing process. Although the mechanism how the concentration of macroion affects the viscosity is still unclear, a few theories that can help explain the data: (1) within the low concentration range, the viscosity of the suspension will increase with the concentration but reach its maximum value and then remain stable thereafter; (2) above a certain threshold, the high concentration will lead to less charged particles due to the compressed electric double layer and raise the viscosity [32]. In agreement with the theory, from 0.1 to 10 mg/ml, the resulted size distribution showed a slow increase to steady then to fast increase trend (Fig. 8A), indicating 0.3 to 1 mg/ml is the viscosity steady region. PNP concentrations were monitored by FCM. Particle numbers were found linearly increasing with the final PLGA concentration within this region. Further increase in concentration could result in

increased viscosity and D_{pw} and therefore lead to the precipitation of larger particles. Noticing a mode size (20%) of 170 nm was observed for the PLGA concentration as high as 10 mg/ml, indicating the wide coverage of concentration by nano-precipitation to get PNPs within the desirable range. To further testify whether the increase of size above 1 mg/ml was due to the reduced charge density at PNP surface and the related viscosity increase, trends of zeta potential and diffusion coefficient of the PNPs were monitored. Results are shown in Fig. 8B and C. The increase in zeta potential within the 1-10 mg/ml region indicates the neutralizing process of PNPs when space becomes limited and the delocalization of carboxyl protons are restricted. The decrease of charge density of PNPs resulted in an increase of the viscosity of the system, as indicated by the diffusion coefficient data (Fig. 8C).

3.7 Morphology study

Morphology of the PNPs of different size was studied by TEM. Results are shown in Fig. 9. For each size range, spherical PNPs were observed with slight variations in size.

4. Summary

Versatile as nanoparticle based drug carrier is, the right size is found crucial for the proper functioning. In the case of a tumor targeting and drug delivery, currently a commonly recognized size range for the PNPs is 100-200 nm. Variations in sizes have negative impact on the *in vivo* distribution, in tumor spreading and the cell uptake rate, and therefore cause the loss of drug potency and side effects. Synthesis method and parameters of operation have been shown to be important for PNP size controlling. Some researches showed the loading of drug and surface modifications can cause swelling of the particles. The increases in size are, however, minor and

predictable [23]. Therefore, accurate control of the size by method selecting and parameter optimizing are critical.

Nano-precipitation was selected as the model synthesis method in this work because of its ability of producing 100-200 nm PNPs. Impacts of a few relevant parameters on the produced size were tested within practical levels, namely the concentration of polymer in the organic phase (1-40 mg/ml), organic solvent (acetonitrile, acetone, THF), temperature (0-80 °C), ionic strength (0.1-1000 mM NaCl), flow rate of injection (2-2000 μl/min), agitation rate (0-1200 rpm), gauge of the needle (14-27G) and final concentration of polymer (0.1-10 mg/ml). The first four were shown to have impact on the PNP size. Among them, ionic strength, polymer concentration in the organic phase, temperature and solvent could be used in combination for accurate size control. We hypothesize that the resulting size can be predicted by the diffusion coefficient of solvent in water with the presence of the polymer, D_{pw}. D_{pw} is determined by the solvent, polymer nature and the system viscosity. Large D_{pw} results in narrowly distributed small PNPs, while small D_{pw} can cause increase of overall size and distribution broadening. The last four parameters showed no significant impact on the PNP size. However they are of great importance for maximizing the efficiency of the potential preparative processes.

Acknowledgement

This work is mainly supported by a grant from USDA-NIFA administered through the Biodesign and Bioprocessing Center at Virginia Tech and partially by a grant from NIH (R21DA030083).

Reference

[1] Reddy, L.H. Drug delivery to tumors: recent strategies. J. Pharm. Pharmacol. 37 (2005) 1231-1242.

[2] Meada, H., Wu, J., Sawa, T., Matsumura, Y., Hori, K., Tumor vascular permeability and the EPR effect in macromolecular therapeutics: a review. J. Control. Release 65 (2000) 271-284.

[3] Lee, A.L.Z., Wang, Y., Cheng, H., Pervaiz, S., Yang, Y., The co-delivery of paclitaxel and Herceptin using cationic micellar nanoparticles. Biomaterials 30 (2009) 919-927.

[4] Yang, T., Choi, M., Cui, F., Kim, J. S., Chung, S., Shim, C., Kim, D. Preparation and evaluation of paclitaxel-loaded PEGylated immunoliposome. Journal of Controlled Release 120, 169-177 (2007).

[5] Ashley, C.E., Carnes, E.C., Phillipos, G.K., Padilla, D., Durfee, P.N., Brown, P.A., Hanna, T.N., Liu, J., Phillips, B., Carter, M.B., Carroll, N.J., Jiang, X., Dunphy, D.R., Willman, C.L., Petsev, D.N., Evans, D.G., Parikh, A.N., Chackerian, B., Wharton, W., Peabody, D.S., Brinker, C.J. The targeted delivery of multicomponent cargos to cancer cells by nanoporous particle-supported lipid bilayers. Nature Materials 10, 389-397 (2011).

[6] Wohlfart, S., Gelperina, S., Kreuter, J., Transport of durgs across the blood-brain barrier by nanoparticles. J. Control. Release 161 (2012) 264-273.

[7] Wolfrum, C., Shi, S., Jayaprakash, K.N., Jayaraman, M., Wang, G., Pandey, R.K., Rajeev, K.G., Nakayama, T., Charrise, K., Ndungo, E.M., Zimmermann, T., Koteliansky, V., Manoharan, M., Stoffel, M. Mechanisms and optimization of in vivo delivery of lipophilic siRNA. Nat. Biotechnol. 25 (2007) 1149-1157.

[8] Moritz, B.B., Olivia, M.M., Thomas, K., Controlled pulmonary rug an gene delivery using polymeric nano-carriers. Journal of Controlled Release 161 (2012) 214-224.

[9] Bell, I.R., Schwartz, G.E., Boyer, N.N., Koithan, M., Brooks, A.J., Advances in integrative nanomedicine for improving infectious disease treatment in public health. Eur J Integr Med (2012), http://dx.doi.org/10.1016/j.eujim.2012.11.002.

[10] Gaspar, R., Preat, V., Opperdoes, F.R., Roland, M. Macrophage activation by polymeric nanoparticles of polyalkylcyanoacrylates: activity against intracellular Leishmania donovani associated with hydrogen peroxide production. Pharm. Res. 9 (1992) 782-787.

[11] Bertrand, N., leroux, J. C. The journey of a drug-carrier in the body: An anatomo-physiological perspective. J. Control. Release 161, 152-163 (2012).

[12] Jong, W.H.D., Hagens, W.I., Krystek, P., Burger, M.C., Sips, A.J.A.M., Geertsma, R.E. Particle size-dependent organ distribution of gold nanoparticles after intravenous administration. Biomaterials 29 (2008) 1912-1919.

[13] Mirahmadi, N., Babaei, M.H., Vali, A.M., Dadashzadeh, S., Effect of liposome size on peritoneal retention and organ distribution after intraperitoneal injection in mice. International Journal of Pharmaceutics 383 (2010) 7-13.

[14] Liu, G., Zhang, D., Jiao, Y., Guo, H., Zheng, D., Jia, L., Duan, C., Liu, Y., Tian, X., Shen, J., Li, C., Zhang, Q., Lou, H., In vitro and in vivo evaluation of riccardin D nanosuspensions with different particle size. Colloids and Surfaces B: Biointerfaces 102 (2013) 620-626.

[15] Rabinovitch, M., Professional and non-professional phagocytes: an introduction, Trens Cell Biol. 5 (1995) 85-87.

[16] Win, K.Y., Feng, S. Effects of particle size and surface coating on cellular uptake of polymeric nanoparticles for oral delivery of anticancer drugs. Biomaterials 26 (2005) 2713-2722.

[17] He, C., Hu, Y., Yin, L., Tang, C., Yin, C., Effects of particle size and surface charge on cellular uptake and biodistribution of polymeric nanoparticles. Biomaterials 31 (2010) 3657-3666.

[18] Foged, C., Brodin, B., Frokjaer, S., Sundblad, A., Particle size and surface charge affect particle uptake by human dendritic cells in an in vitro model. International Journal of Pharmaceutics 298 (2005) 315-322.

[19] Zauner, W., Farrow, N.A., Haines, A.M.R., In vitro uptake of polystyrene microspheres: effect of particle size, cell line and cell density. J. Control. Release 71 (2001) 39-51.

[20] Florence, A.T., "Targeting" nanoparticles: The constraints of physical laws and physical barriers. J. Control. Release 164 (2012) 115-124.

[21] Goodman, T.T., Chen, J., Matveev, K., Pun, S.H., Spatio-temporal modeling of nanoparticle delivery to multicellular tumor spheroids. Biotechnol. Bioeng. 101 (2008) 388-396.

[22] Wiese, G.R., Healy, T.W., Effect of particle size on colloid stability. Trans. Faraday Soc. 66 (1970) 490-499.

[23] Astete, C., Sabliov, C.M. Synthesis and characterization of PLGA nanoparticles. J. Biomater. Sci. Polymer Edn. 17 (2006) 247-289.

[24] Kuluge, J., Fusaro, F., Casas, N., Mazzotti, M., Muhrer, G., Production of PLGA micro- and nanocomposites by supercritical fluid extraction of emulsions: I. Encapsulation of lysozyme. J. of Supercritical Fluids 50 (2009) 237-335.

[25] Fessi, H., Puisieux, F., Devissaguet, J.P., Ammoury, N., Betina, S., Nanocapsule formation by interfacial deposition follwing solvent displacement. Int. J. Pharm. 55 (1989) R1-R4.

[26] Liu, J., Meisner, D., Kwong, E., Wu, X., Johnston, M.R., A novel trans-lymphatic drug delivery system: Implantable gelatin sponge impregnated with PLGA-paclitaxel microspheres. Biomaterials 28 (2007) 3236-3244.

[27] Ficheux, M.F., Bonakdar, L., Leal-Calderon, F., Bibette, J., Some stability criteria for double emulsions. Langmuir 14 (1998) 2702-2706.

[28] Mu, L., Feng, S.S., Fabrication, characterization and in vitro release of paclitaxel (Taxol) loaded poly (lactic-co-glycolic acid) microspheres prepared by spray drying technique with lipid/cholesterol emulsifers. J. Control. Release 76 (2001) 239-254.

[29] Katou, H., Wandrey, A.J., Gander, B. Kinetics of solvent extraction/evaporation process for PLGA microparticle fabrication. International Journal of Pharmaceutics 364 (2008) 45-53.

[30] Park, T.G., Degradation of poly (lactic-co-glycolic acid) microspheres: effect of copolymer composition. Biomaterials 16 (1995) 1123-1130.

[31] Ise, N., Sogami, I.S. Structure formation in solution, Ionic polymers and colloidal particles, Chapter 3.2 Scattering study of dilute solutions of ionic polymers. (2005) 82-89.

[32] Ise, N., Sogami, I.S. Structure formation in solution, Ionic polymers and colloidal particles, Chapter 7 Scattering study of dilute solutions of ionic polymers. (2005) 279-293.

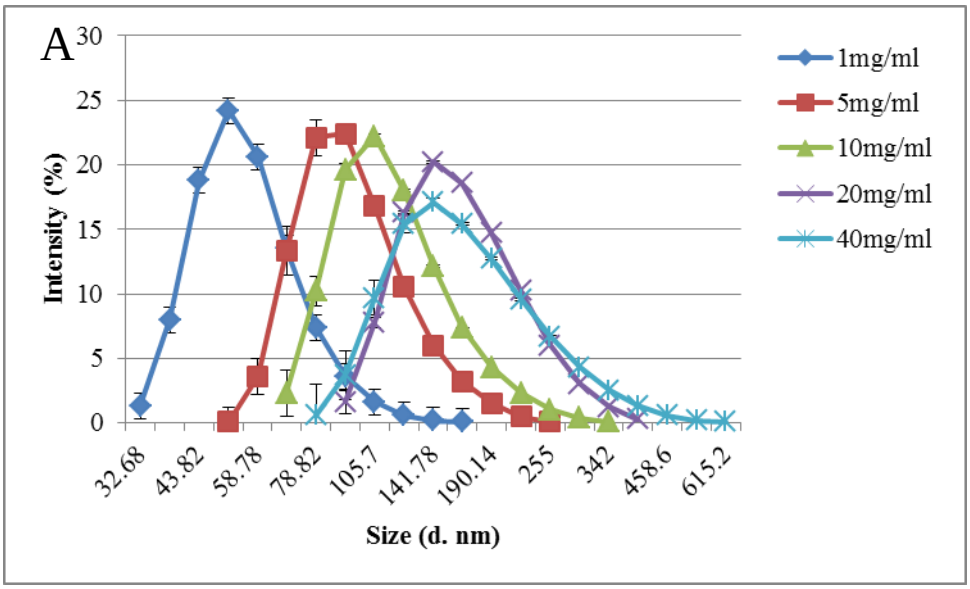

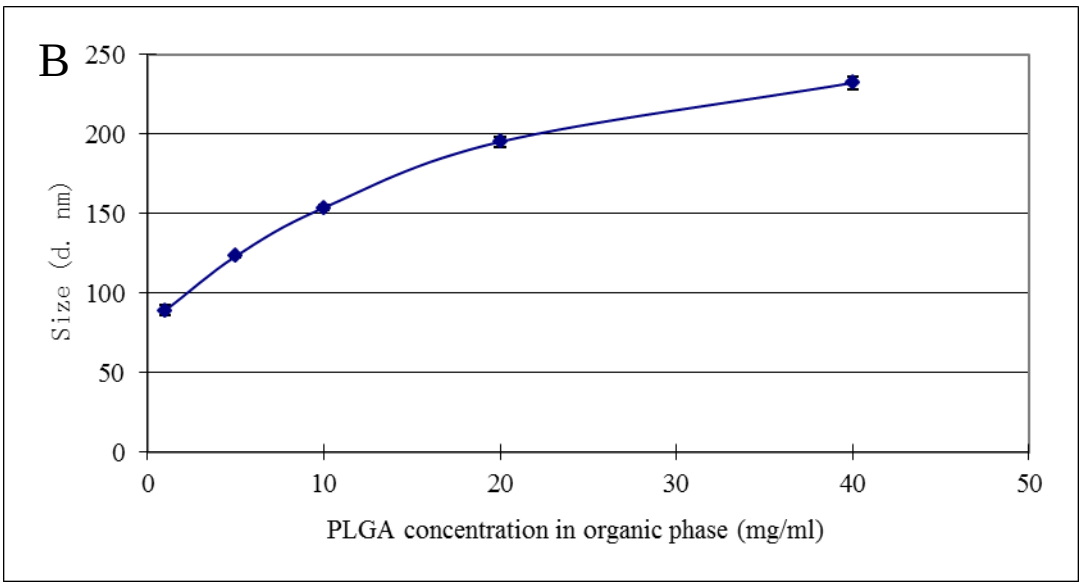

Figure (1) Size distribution vs. PLGA concentration in organic phase.

(A) Size distribution vs. concentration, (B) mean size vs. concentration.

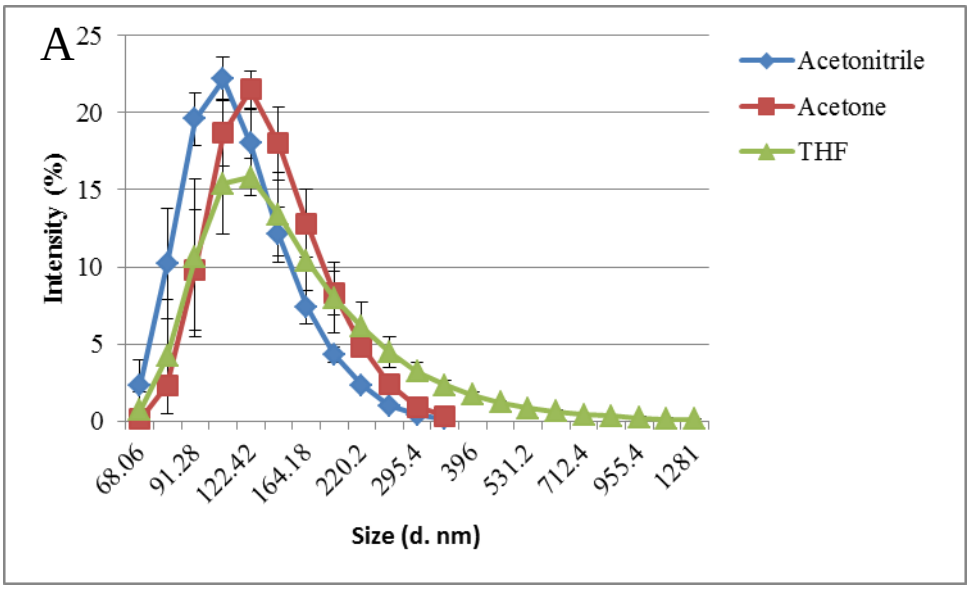

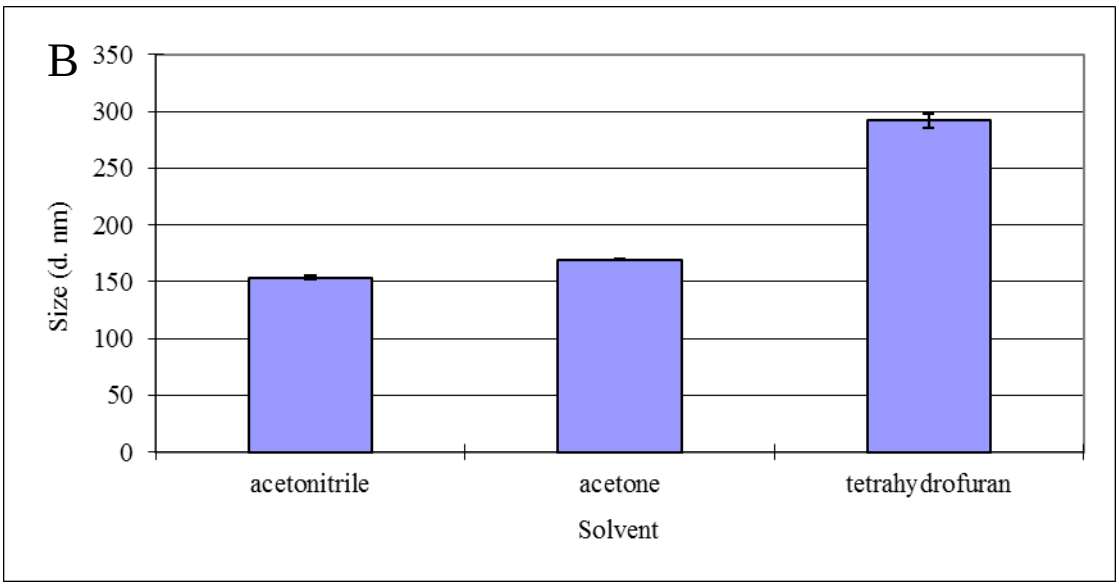

Figure (2) Size distribution vs. organic solvent.

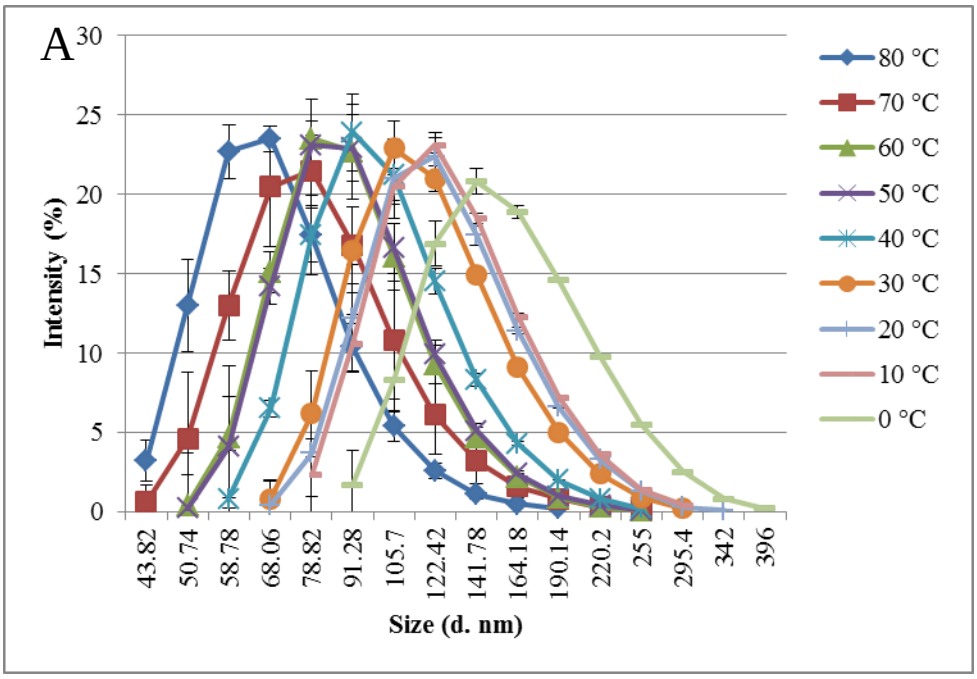

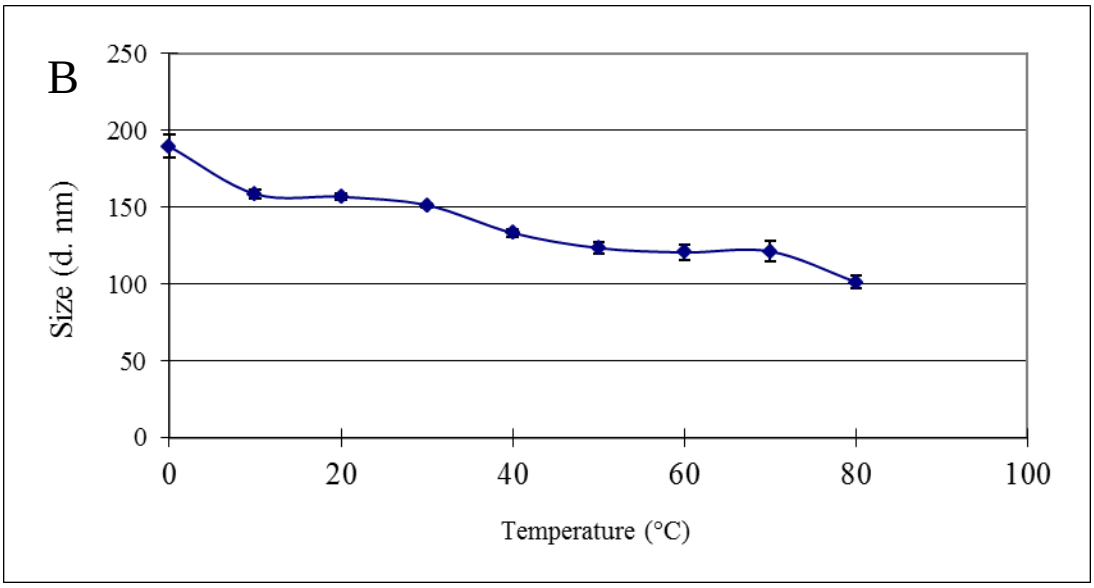

Figure (3) Size distribution vs. aqueous temperature.

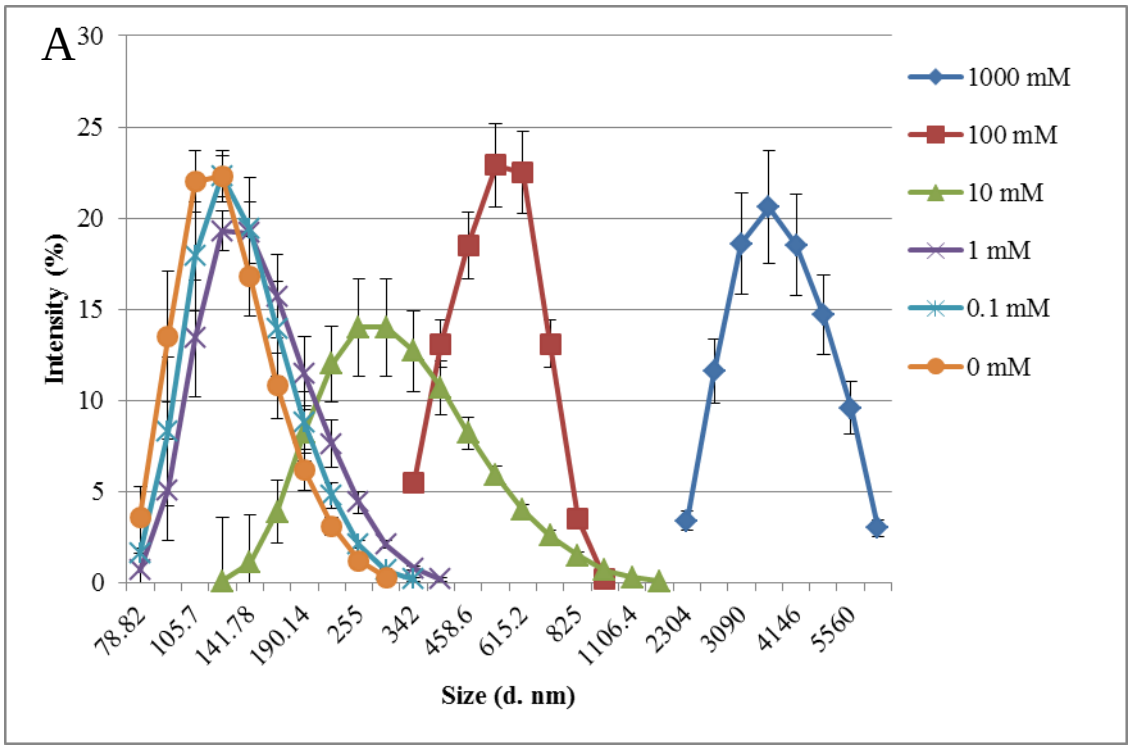
A
30
25
20
15
10
5
0
Intensity (%)
78.82
105.7
141.78
190.14
255
342
458.6
615.2
825
1106.4
2304
3090
4146
5560
Size (d. nm)
1000 mM
100 mM
10 mM
1 mM
0.1 mM
0 mM

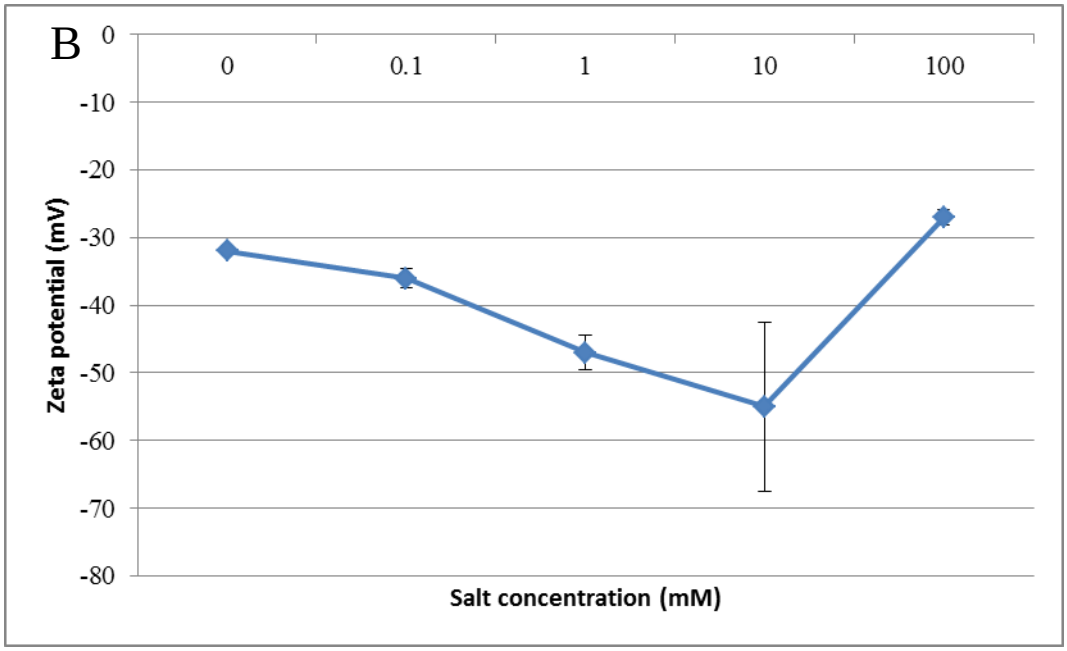
B
0
-10
-20
-30
-40
-50
-60
-70
-80
Zeta potential (mV)
0
0.1
1
10
100
Salt concentration (mM)

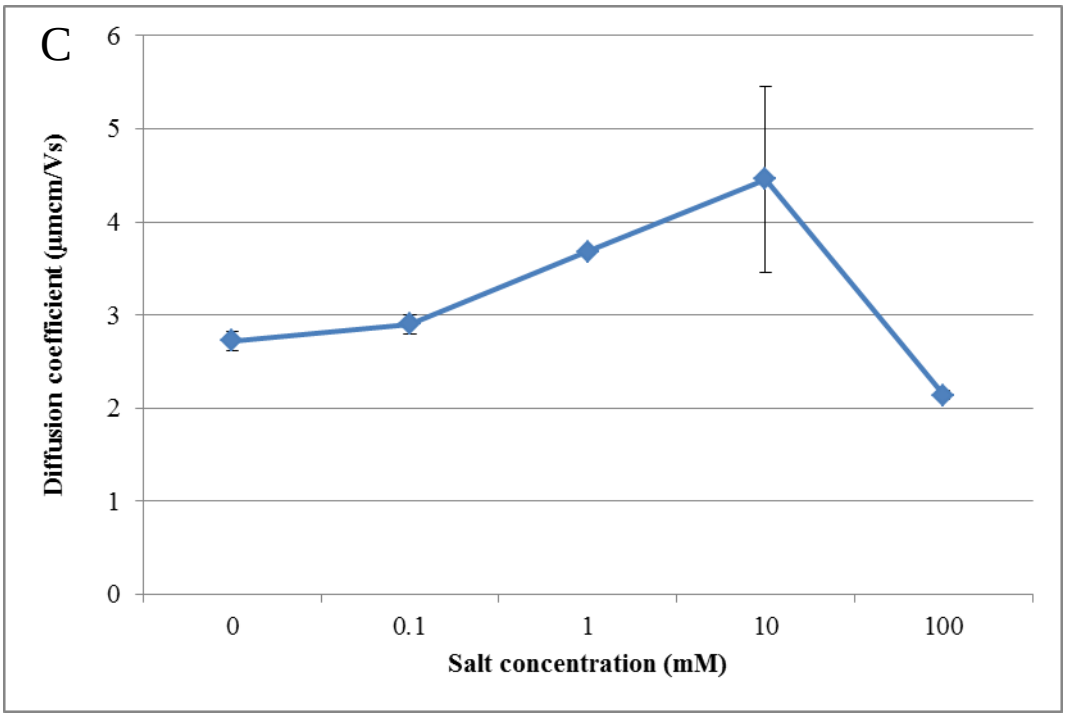

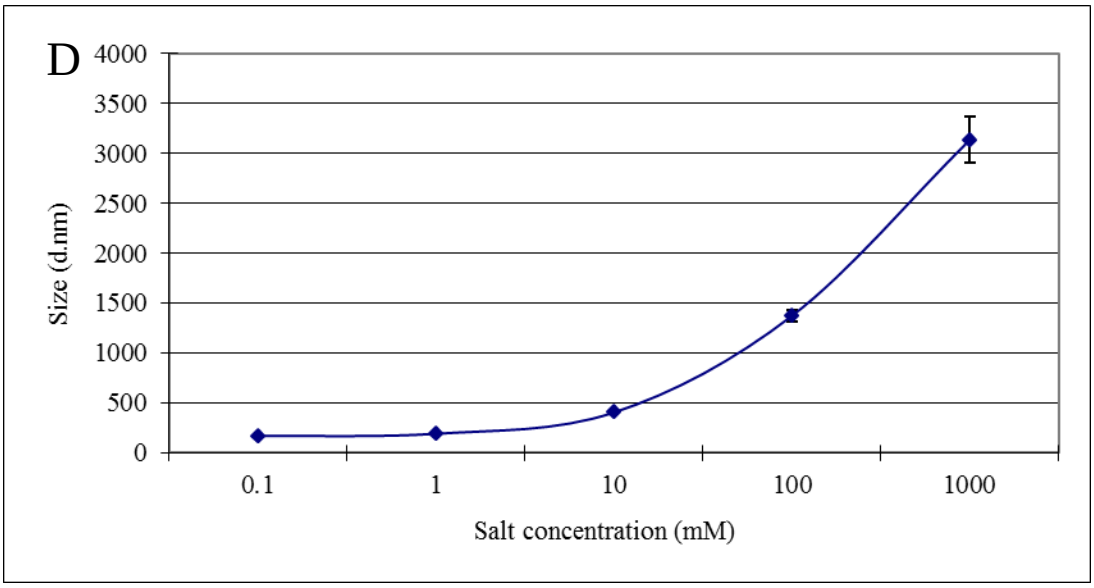

Figure (4) Influence of salt concentration on PNP size.

(A) Size vs. salt concentration, (B) zeta potential vs. salt concentration and (C) diffusion coefficient of PNP vs. salt concentration and (D) Mean size vs. salt concentration.

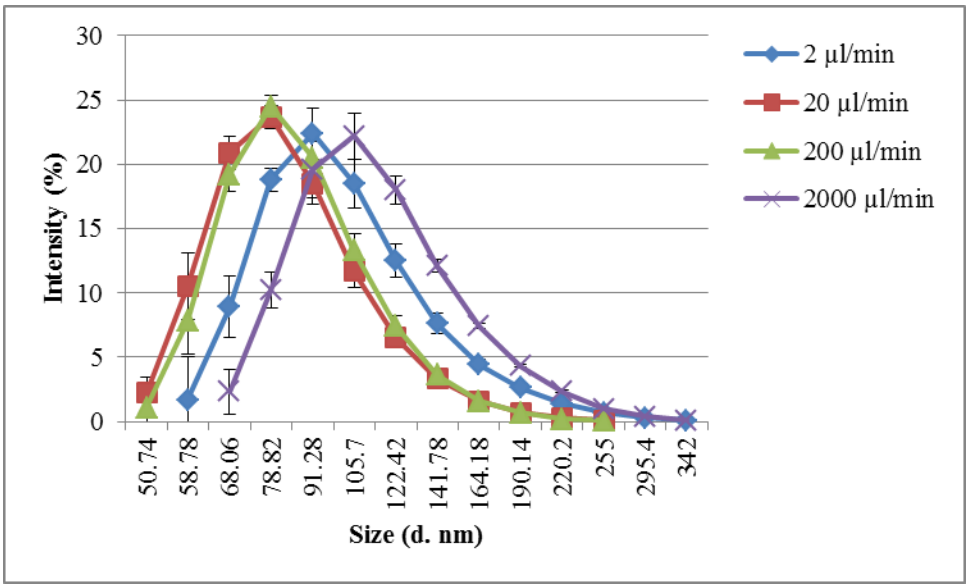

Figure (5) Size vs. flow rate of organic phase.

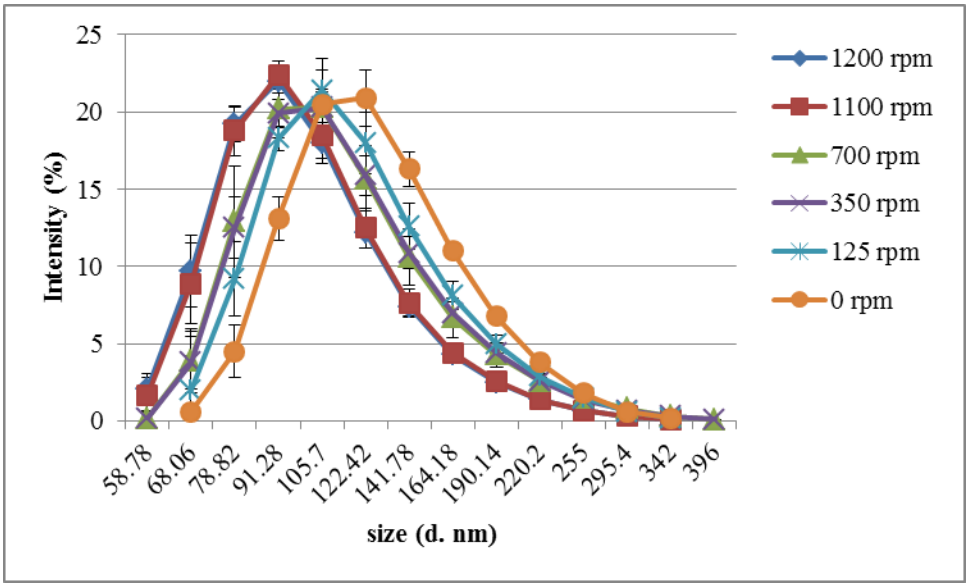

Figure (6) Size vs. agitation of aqueous phase.

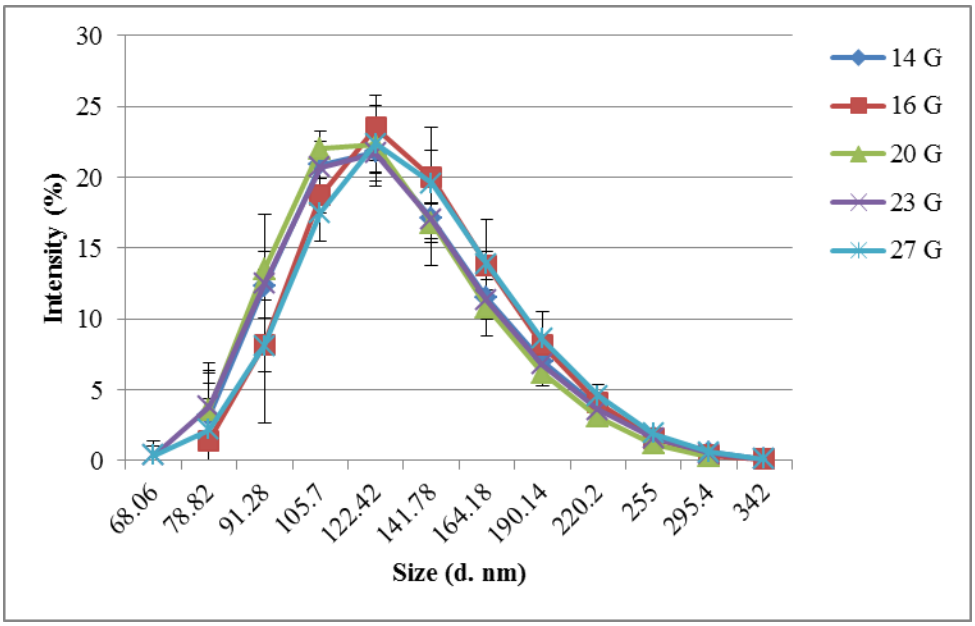

Figure (7) Size vs. gauge of the needle.

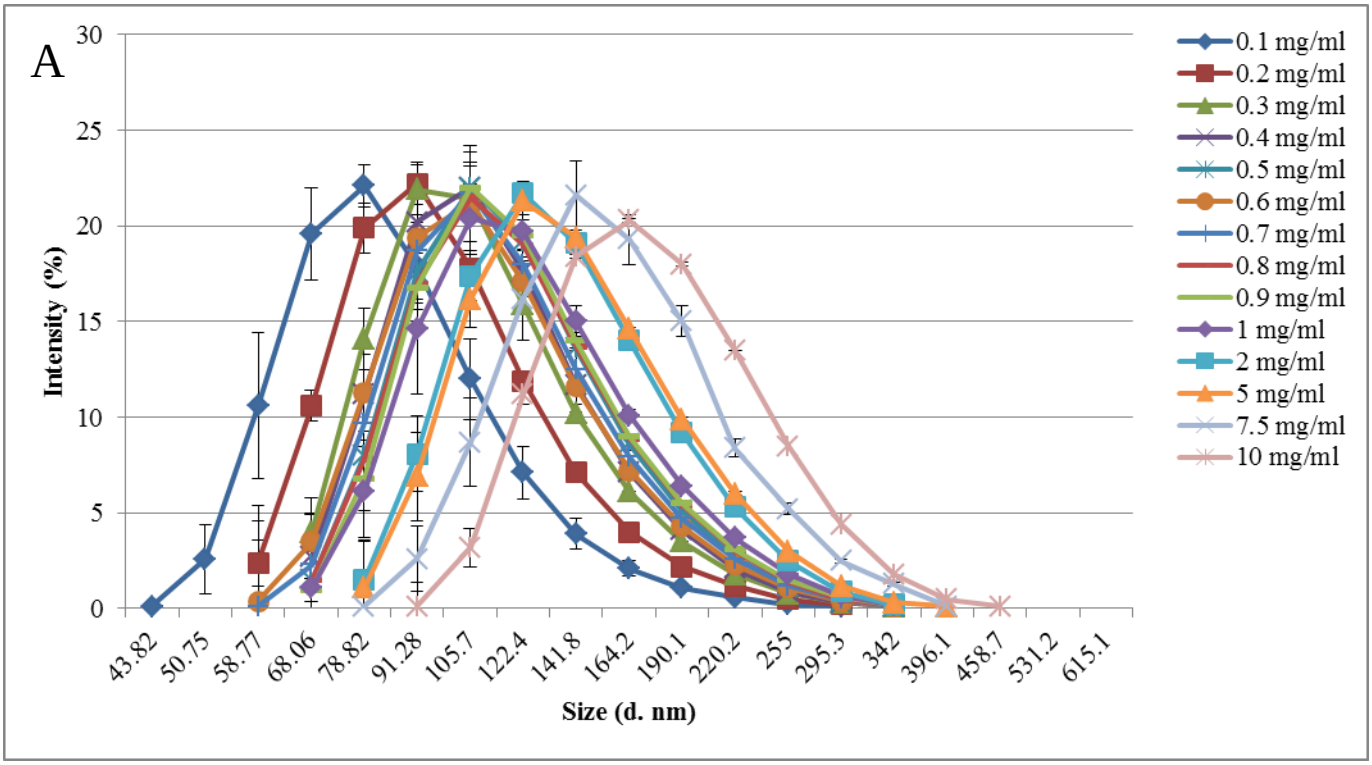
A
Intensity (%)
30
25
20
15
10
5
0
43.82
50.75
58.77
68.06
78.82
91.28
105.7
122.4
141.8
164.2
190.1
220.2
255
295.3
342
396.1
458.7
531.2
615.1
Size (d. nm)
0.1 mg/ml
0.2 mg/ml
0.3 mg/ml
0.4 mg/ml
0.5 mg/ml
0.6 mg/ml
0.7 mg/ml
0.8 mg/ml
0.9 mg/ml
1 mg/ml
2 mg/ml
5 mg/ml
7.5 mg/ml
10 mg/ml

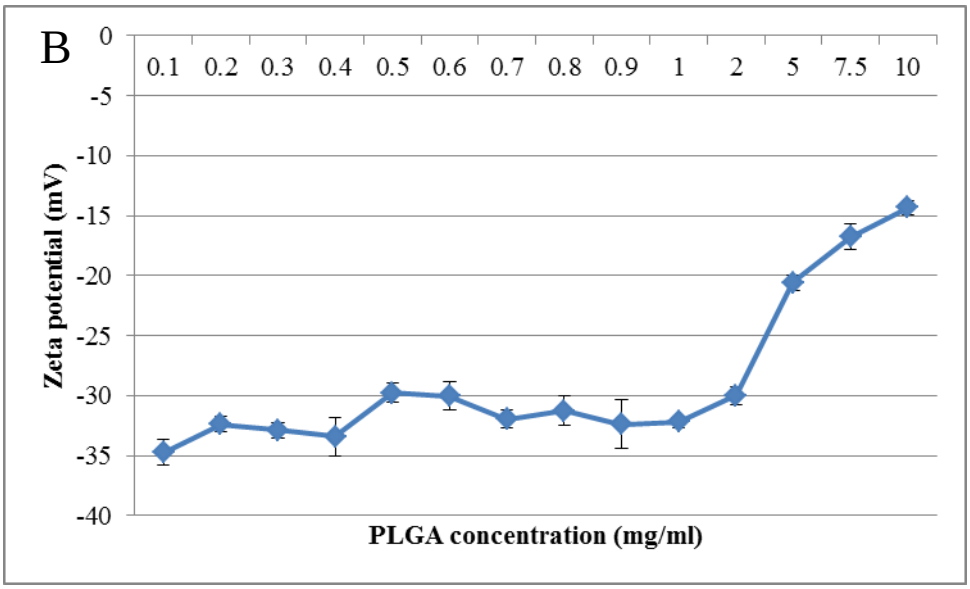
B
0
-5
-10
-15
-20
-25
-30
-35
-40
0.1
0.2
0.3
0.4
0.5
0.6
0.7
0.8
0.9
1
2
5
7.5
10
Zeta potential (mV)
PLGA concentration (mg/ml)

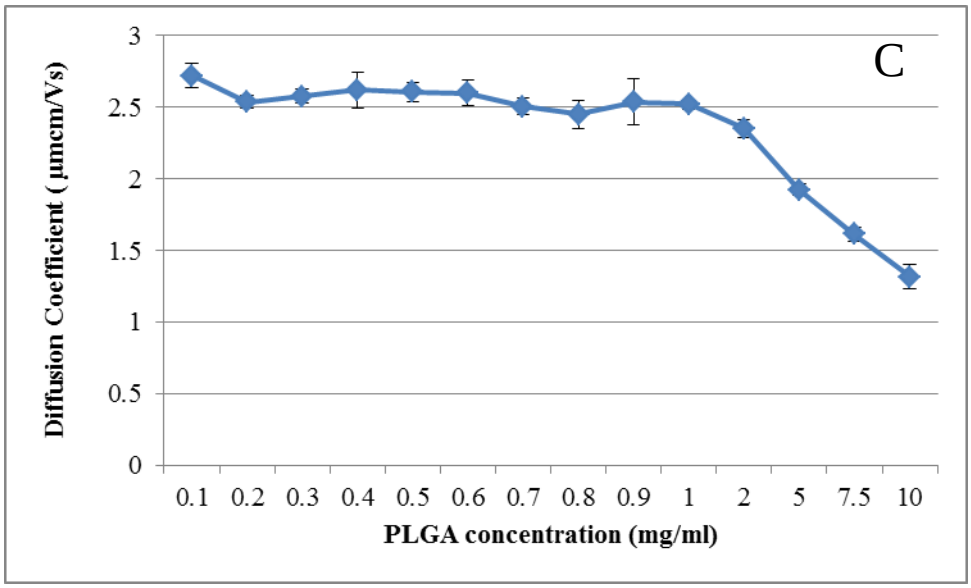

Figure (8) Influence of final concentration of PNP on the size.

(A) Size vs. final concentration, (B) zeta potential vs. final concentration and (C) diffusion coefficent of PNP vs. final concentration.

A

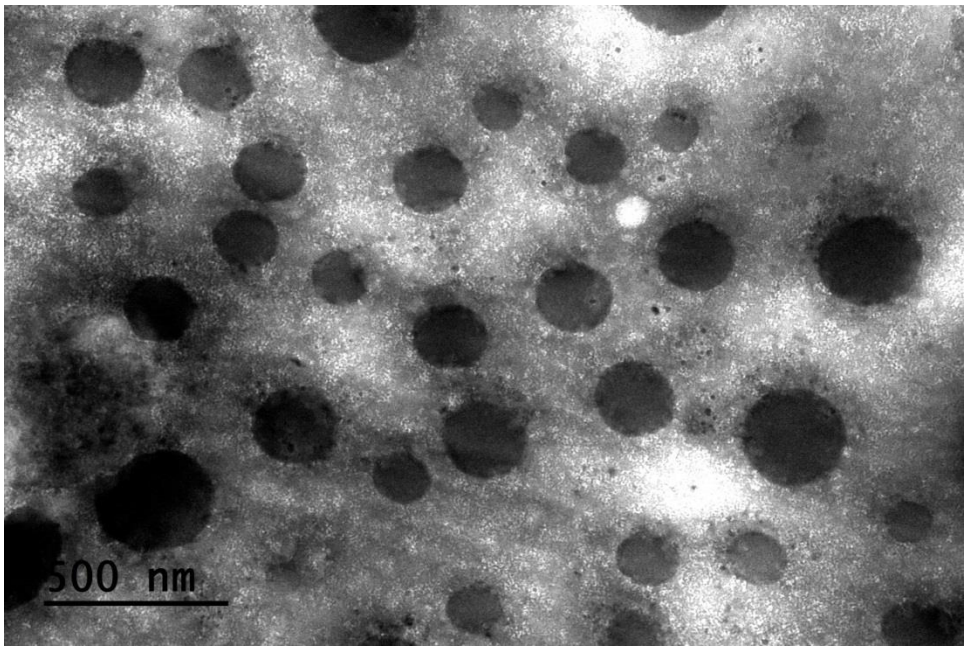

B

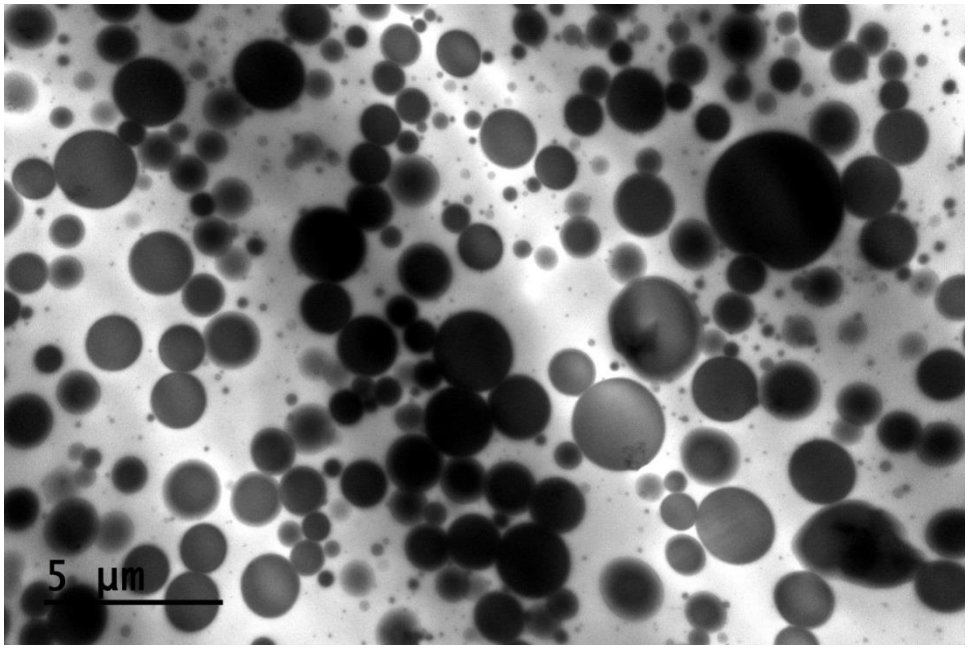

C

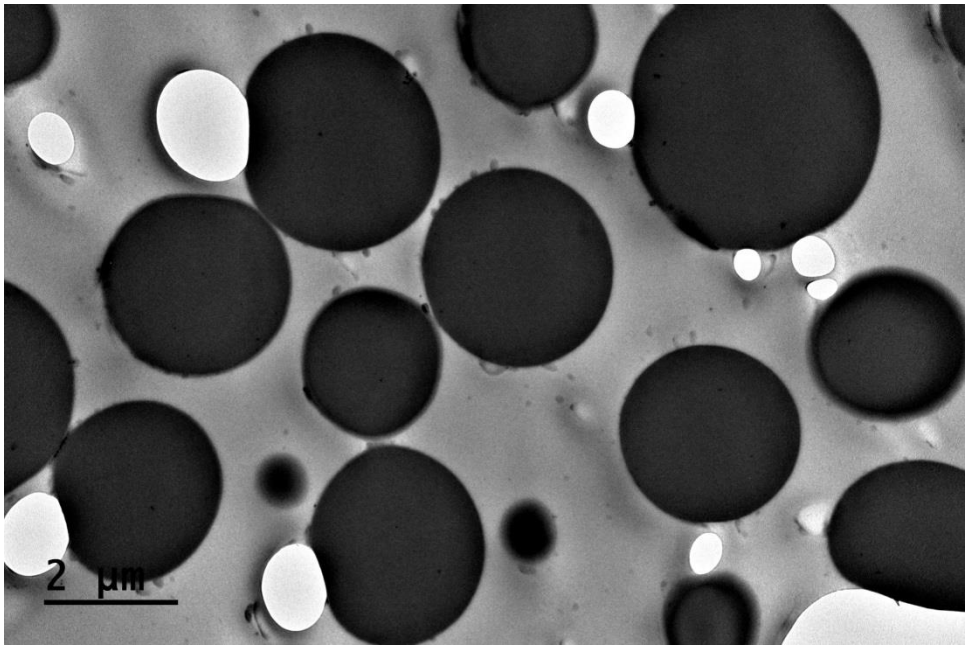

Figure (9) TEM images

of (A) small sized PNPs, (B) medium sized PNPs and (C) large sized PNPs.

Table [1] Diffusion coefficient of organic solvent with/without the presence of PLGA in water.

		Diffusion coefficient m^2/s	
		H2O	solvent
PLGA D_2O solution (1 mg/ml)	acetonitrile (10%)	2.042E-9	1.538E-9
	Acetone (10%)	2.151E-9	1.217E-9
	THF (10%)	2.125E-9	1.040E-9
D_2O	acetonitrile (10%)	2.101E-9	1.534E-9
	Acetone (10%)	2.014E-9	1.152E-9
	THF (10%)	2.054E-9	1.000E-9

Chapter VII: General Conclusions

The revolution on nanoparticle based drug carriers could potentially bring significant improvement to cancer treatment. The limited use of many conventional therapies due to insolubility, high toxicity, non-specificity could be overcome by incorporating into tumor targetable nanoparticles with controlled drug release. Currently, an optimal goal is described as (1) majority of the administrated particles reach, enter and spread into the tumor, (2) majority of the drug remain embedded when the carrier reach the tumor, (3) the drug and carrier are degradable *via* normal metabolize pathways and the degradation products bring no dire side effect to the patients.

So far, a number of improvements to the structure of nanoparticles have been made to achieve the goal. An increased targeting accuracy was seen based on the emphasis on both passive and active targeting. Briefly, PEG coatings can make the particles less visible to the mononuclear phagocyte system and thus prolong the circulation time [1]. Therefore, coated particles will have an enhanced EPR effect and distribute more at the tumor site. Grafting targeting ligand onto the particles was shown to increase the cell recognition and uptake rate [2]. However, they are also reported to add the chance of non-specific targeting [2], as also evidenced in our work. Targeting ligand with higher tumor specificity or chemical gradient driven targeting (pH, cytokines, growth factors) are possible solutions.

Basal drug leakage is another critical problem associated with conventional nanoparticles. Although claimed to fully release the drug in a duration of days or weeks, most nanoparticle lose more than 50% of the content with a burst release within in the first 5 hours of post-administration [3-5]. It remains as a big challenge for the particles to complete the delivery within 5-10 hours. Therefore, smart drug carriers with triggered release are needed. pH and

temperature sensitive nanoparticles were assembled for the purpose [6,7]. However, drug leakage from those particles was still observed under *in vivo* physiological conditions. Advanced particles with higher thermo stability and resistance to *in vivo* physical and chemical disturbance will help reduce the drug loss during the circulation.

We have developed a 3rd generation nanoparticle, single walled carbon nanohorn or PLGA supported immunoliposome, for anti-cancer drug delivery. The particle is consisted of a solid carbon nanohorn core for drug loading, and a surrounding immunoliposome for tumor targeting and pH triggered release.

A freeze thawing method for core particle encapsulation into immunoliposomes was established. The highest encapsulation rate was found for particles around 120 nm. A sucrose assisted centrifugation was used for nanohorn supported immunoliposome purification. A 90% purity of the suppoted immunoliposome was observed after one cycle of the centrifugation process.

Conjugation of targeting ligand to the surface of liposome was investigated. The surface ligand density was measured by a modified enzyme linked immune sorbent assay. Non-covalent binding of protein based ligand to the liposome showed a process and structure dependent manner. Proteins with membrane binding domain has higher conjugation rate than globular ones. Process wise, proteins added post-formation of the liposome at high temperature (above the transition temperature of the lipid component) showed the highest density of ligand at the liposome surface. On the other hand, covalently bind the ligand showed a 25 fold higher density than all non-covalent ones.

Nanohorn supported immunoliposomes were assembled using the optimized methods. Morphology study showed that 150 nm monodispersed particles with high structural

homogeneity were formed. The colloid stability was maintained over 30 days. Nanohorn supported immunoliposome showed a doubled paclitaxel (hydrophobic drug) loading capacity than conventional immunoliposomes. An *in vitro* drug release test showed minimum basal drug leakage under a normal blood circulation condition and a 7 days linear release inside the tumor cells. Herceptin® and anti Her2 monoclonal antibody grafted particles both showed high cell binding rate to SK-BR-3 cells (Her2 positive) than the other control groups. A lysosomal distribution of the particles after being uptake by the cells was visualized, indicating the drug will be released upon acidification as expected.

A biodegradable polymeric material PLGA was selected as an alternative core of particle for drug loading and immunoliposome supporting. To optimize size of the PLGA particles, a systematic study of a fabrication method, nano-precipitation, was conducted. The results showed that by tuning the polymer concentration in the organic phase, type of organic solvent used for PLGA solubilization, operation temperature and ionic strength of the aqueous solution, the resulting particle size could be accurately controlled.

In conclusion, the 3rd generation nanoparticle we assembled in this study showed a possibility of using combination of multiple types of conventional drug carriers to achieve improved drug delivery. The nanohorn supported immunoliposome showed high *in vitro* tumor cell specificity and elimination of basal drug leakage at physical conditions.

Reference

[1] S. Dufort, L. Sancey, J.L. Coll, Physico-chemical parameters that govern nanoparticles fate also dictate rules for their molecular evolution, Adv. Drug Deliv. Rev. 64 (2012) 179-189.

[2] M.S., Ehrenberg, A.E., Friedman, J.N., Finkelstein, G., Oberdorster, J.L., McGrath, The influence of protein adsorption on nanoparticle associate with cultured endothelial cells, Biomaterials 30 (2009) 603-610.

[3] T., Yang, M., Choi, F., Cui, J.S., Kim, S., Chung, C., Shim, D., Kim Preparation and evaluation of paclitaxel-loaded PEGylated immunoliposome, J. Control. Release 120 (2007) 169-177.

[4] S., Fredenberg, M., Wahlgren, M., Sekido, A. Axelsson, The mechanisms of drug release in poly(lactic-co-glycolic acid)-based drug delivery systems-A review, Int. J. Pharm. 415 (2011) 34-52.

[5] J., Xu, m., Yudasaka, S., Kourada, M., Sekido, Y., Yamamoto, S., Iijima, Single wall carbon nanohorn as a drug carrier for controlled release, Chem. Phys. Lett. 461 (2008) 189-192.

[6] S., Simoes, V., Slepushkin, N., Duzgunes, M.C.P., de Lima, On the mechanisms of internalization and intracellular delivery mediated by pH-sensitive liposomes, *Biochim. Biophys. Acta* 1515 (2001) 23-57.

[7] S.I. Kang, K. Na, Y.H., Bae, physicochemical characteristic and doxorubicin-release behaviors of pH/temperature-sensitive polymeric nanoparticles, Colloids Surf. A Physicochem. Eng. Asp. 231 (2003) 103-112.